AWARD NUMBER: W81XWH-14-1-0048

TITLE: Noninvasive in Vivo MRI Assessment of Prostate Cancer Using Hyperpolarized 15N Choline

PRINCIPAL INVESTIGATOR: LLOYD L. LUMATA, PH.D.

CONTRACTING ORGANIZATION: UNIVERSITY OF TEXAS AT DALLAS
                                                            Richardson, TX 75080

REPORT DATE: January 2017

TYPE OF REPORT: FINAL

PREPARED FOR: U.S. Army Medical Research and Materiel Command
                              Fort Detrick, Maryland 21702-5012

The views, opinions and/or findings contained in this report are those of the author(s) and should not be construed as an official Department of the Army position, policy or decision unless so designated by other documentation.

REPORT DOCUMENTATION PAGE

Form Approved
OMB No. 0704-0188

Public reporting burden for this collection of information is estimated to average 1 hour per response, including the time for reviewing instructions, searching existing data sources, gathering and maintaining the data needed, and completing and reviewing this collection of information. Send comments regarding this burden estimate or any other aspect of this collection of information, including suggestions for reducing this burden to Department of Defense, Washington Headquarters Services, Directorate for Information Operations and Reports (0704-0188), 1215 Jefferson Davis Highway, Suite 1204, Arlington, VA 22202-4302. Respondents should be aware that notwithstanding any other provision of law, no person shall be subject to any penalty for failing to comply with a collection of information if it does not display a currently valid OMB control number. **PLEASE DO NOT RETURN YOUR FORM TO THE ABOVE ADDRESS.**

1. REPORT DATE	2. REPORT TYPE	3. DATES COVERED
January 2017	Final	15 Mar 2014 – 20 Oct 2016

4. TITLE AND SUBTITLE	5a. CONTRACT NUMBER
Non-Invasive In Vivo MRI Assessment of Prostate Cancer Using Hyperpolarized 15N Choline	W81XWH-14-1-0048

5b. GRANT NUMBER
W81XWH-14-1-0048

5c. PROGRAM ELEMENT NUMBER

6. AUTHOR(S)	5d. PROJECT NUMBER
Lloyd Lumata	PC121415

5e. TASK NUMBER

5f. WORK UNIT NUMBER

E-Mail: lloyd.lumata@utdallas.edu

7. PERFORMING ORGANIZATION NAME(S) AND ADDRESS(ES)	8. PERFORMING ORGANIZATION REPORT NUMBER
University of Texas at Dallas 800 West Campbell Rd Richardson, TX 75080-1427	

9. SPONSORING / MONITORING AGENCY NAME(S) AND ADDRESS(ES)	10. SPONSOR/MONITOR'S ACRONYM(S)
U.S. Army Medical Research and Materiel Command Fort Detrick, Maryland 21702-5012	

11. SPONSOR/MONITOR'S REPORT NUMBER(S)

12. DISTRIBUTION / AVAILABILITY STATEMENT

Approved for Public Release; Distribution Unlimited

13. SUPPLEMENTARY NOTES

14. ABSTRACT

This study involved the use of hyperpolarized 15N choline as potential magnetic resonance imaging (MRI) metabolic agent for prostate cancer diagnostics. The main goal of this study was to monitor the anticipated high uptake of choline in tumors and the subsequent overproduction of phosphocholine due to overexpression of choline kinase. Using dissolution dynamic nuclear polarization (DNP) method, the MRI signal of 15N-enriched choline was amplified to about 48,000-fold measured in a 9.4 T magnet at 298 K. The 15N spin-lattice relaxation time of hyperpolarized choline in the liquid-state was found to be 240 s or 4 minutes. Hyperpolarized 15N choline was tested in vitro in PC-3 prostate cancer cells. We have found that choline metabolism is relatively slow in which it could take several hours to have substantial production of phosphocholine—a time scale which is outside the 8-10 minute observation window of hyperpolarized 15N MRI. The scientific efforts in this project have resulted in a number of research papers regarding optimization of hyperpolarized MRI signals and improvement of protocols for metabolic cell studies using hyperpolarization.

15. SUBJECT TERMS
MRI, NMR, cancer metabolism, DNP, hyperpolarization

16. SECURITY CLASSIFICATION OF:			17. LIMITATION OF ABSTRACT	18. NUMBER OF PAGES	19a. NAME OF RESPONSIBLE PERSON USAMRMC
a. REPORT	b. ABSTRACT	c. THIS PAGE	UU	89	19b. TELEPHONE NUMBER *(include area code)*
U	U	U			

Standard Form 298 (Rev. 8-98)
Prescribed by ANSI Std. Z39.18

Table of Contents

1. INTRODUCTION

As cancer cells proliferate, rapid production of new cell membranes is required and this is mainly provided by the biosynthesis of phospholipid components phosphatidylcholine (PtdCho) and phosphatidylethanolamine (PtdEtn) via the Kennedy pathway. Choline (Cho), an essential nutrient needed by the body, is a precursor substrate to the PtdCho branch of the Kennedy pathway. As a first step (see the Figure below), the enzyme choline kinase ChK-α catalyzes the phosphorylation of choline (Cho) into phosphocholine (pCho). The overexpression and increased activity of ChK-α and Cho transporters is implicated in the observation of elevated levels of Cho and its metabolites in a variety of human cancers including lung, colorectal, and prostate tumors. This upregulated choline uptake and the resulting increased phosphocholine production, taken together, is an emerging hallmark of cancer metabolism.

This study sought to utilize hyperpolarization technology via dynamic nuclear polarization (DNP) which would provide superb enhanced NMR sensitivity of ^{15}N nuclei on the order of at least 10,000-fold ^{15}N NMR signal enhancement. Due to the overexpression of CHK-α and increased choline transport in cancer cells, the expectation was that malignant prostate tumors would take in more exogenous hyperpolarized ^{15}N Cho *in vivo* and subsequently produce higher pCho levels than the normal prostate tissue. It was hypothesized therefore that the NMR intensity of pCho relative to Cho *in vivo* would correlate with the increased activity of CHK-α, thus aggressiveness of prostate tumors.

2. KEYWORDS

Nuclear magnetic resonance (NMR), magnetic resonance imaging (MRI), dynamic nuclear polarization (DNP), Kennedy pathway, hyperpolarization, choline, phosphocholine, choline kinase

3. ACCOMPLISHMENTS

What were the major goals of the project?

The major goals of this project were: (i) to obtain the best sample preparation method that yields the highest ^{15}N NMR signal enhancement of hyperpolarized ^{15}N-choline, (ii) to establish protocols for hyperpolarized ^{15}N NMR and MRI, and (iii) to evaluate the efficacy of using hyperpolarized ^{15}N choline as in vivo biomarker for prostate cancer.

What was accomplished under these goals?

GOAL 1. *to obtain the best sample preparation method that yields the highest ^{15}N NMR signal enhancement of hyperpolarized ^{15}N-choline.*

For this goal, five 50 µL samples containing 3 M ^{15}N-choline chloride in 1:1 vol/vol glycerol:water doped with 15 mM trityl OX063 were prepared. In addition, five 100 µL samples containing 1 M 15N-choline in 1:1 sulfolane:DMSO doped with 40 mM BDPA free radical were also prepared. Another pair of batches of trityl and BDPA-doped samples were also prepared but doped with 2 mM gadolinium complex ProHance or gadoteridol. These samples were individually inserted and polarized in the HyperSense commercial polarizer (UT Southwestern Medical Center) operating at 3.35
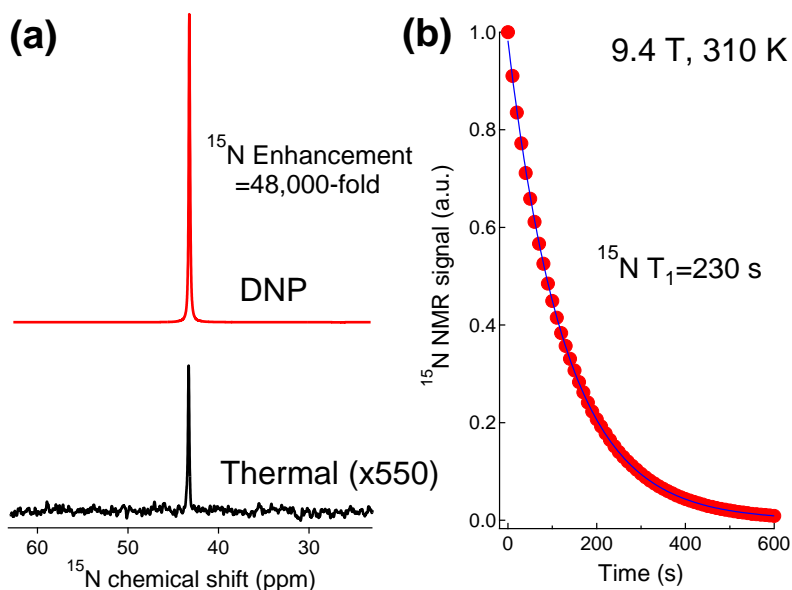

Figure 1. (a) Representative hyperpolarized (1 scan, 5-degree RF pulse) and thermal (4 scans, 90-degree pulse) ^{15}N NMR spectra of 36 mM ^{15}N-choline chloride in water taken at 9.4 T and 37 deg C. The calculated ^{15}N NMR signal enhancement of the hyperpolarized ^{15}N choline is 48,000-fold. (b) Decay of the hyperpolarized ^{15}N choline NMR signal taken by applying 15-degree RF pulse every 10 s. The calculated T_1 of ^{15}N choline at 9.4 T and 37 deg C is 230 s.

T and 1.2 K. After 2-3 hours of microwave irradiation, the samples were rapidly dissolved with 4 mL superheated water and the dissolution liquid were quickly transferred in a span of 8 s to a 10 mm NMR tube already placed in a 9.4 T NMR magnet with sample temperature at 37 deg C. The hyperpolarized ^{15}N NMR signal of choline was monitored by applying a 5-degree RF pulse every 10 s. Thermal or non-hyperpolarized ^{15}N NMR spectra of choline located at 43.3 ppm were also recorded for each sample using a 90-degree pulse with 4 scans as shown in Fig. 1a. Furthermore, the hyperpolarized ^{15}N T_1 decay data were also recorded as displayed in Fig. 1b. The average ^{15}N T_1 for choline is 230 s, which is 4-5 times longer than T_1 of the well-known hyperpolarized ^{13}C pyruvate—a staple metabolic agent in dissolution DNP. Based on these data, the ^{15}N NMR signal enhancements were calculated by getting the ratio of the integrated NMR spectral areas of the hyperpolarized over thermal signals, with corrections emanating from the RF flip angle used and the number of scans. *The highest hyperpolarized ^{15}N NMR signal enhancements recorded were from the trityl OX063-doped samples with 2 mM Gd-HP-DO3A or ProHance with <u>average enhancements (N=5 trials) of 48,000-fold</u> relative to thermal ^{15}N signal at 9.4 T and 310 K as displayed in Fig. 1a*. Without Gd-HP-DO3A, the average enhancement was only 15,000-fold. After several optimization steps, **<u>Goal 1 was successfully accomplished with 48,000-fold enhancement of the ^{15}N choline NMR signal</u>**. The DNP optimization studies in this project have resulted in four (4) peer-reviewed research papers regarding sample preparation methods on how to obtain the highest NMR signal enhancements in DNP.

GOAL 2. *to establish protocols for single voxel protocols for hyperpolarized ^{15}N magnetic resonance (MR) spectroscopy and MR spectroscopic imaging (MRSI) in phantom samples.*
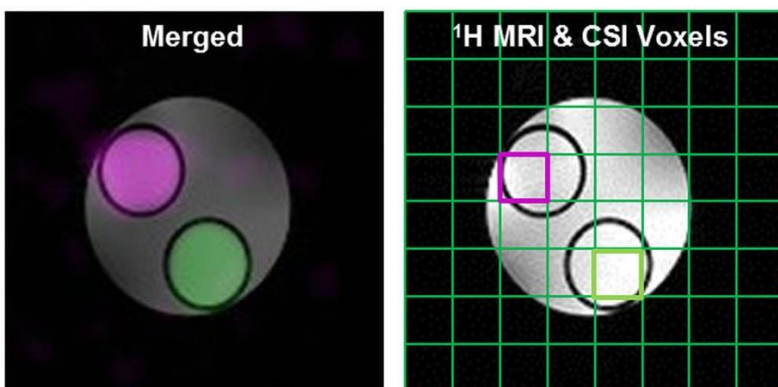
Figure 2. Hyperpolarized [15]N (purple and green smaller circles) magnetic resonance imaging (MRI) or chemical shift imaging (CSI) overlaid on ^{1}H MRI (big circle on left and right figures) on phantoms was successfully implemented in collaboration with Dr. Chalermchai Khemtong at UT Southwestern Medical Center. These HP ^{15}N CSI images are adapted from ^{15}N-labeled pyridine shown as examples (adapted from Jiang et al.., Scientific Reports 5, 9104 (2015)).

Using the optimized DNP sample preparation with 48,000-fold ^{15}N NMR signal enhancement obtained in Goal 1, optimization protocols for obtaining magnetic resonance spectroscopic imaging (MRSI) were established. Phantom set up was consisted of an outer 25 mm NMR tube with water with inner 10 mm NMR tube(s) to be filled with aqueous hyperpolarized 15N choline solutions. The phantom tube was set up inside a 25 mm ^{1}H/^{13}C/[15]N Varian probe in a 9.4 T vertical bore NMR magnet with microimaging capability. First, a reference sample of neat ^{15}N-enriched NH_4Cl in 5 mm NMR tube was used as a reference for verifying the 15N resonance. Next, 4 mL dissolution liquid containing 36 mM hyperpolarized ^{15}N choline was rapidly transferred from the hypersense using an automated process. The transit time of the dissolution liquid from the polarizer to the inner phantom tube was 8 s. Hyperpolarized ^{15}N MRSI using the CSI2D pulse sequence from Agilent VNMRJ software was performed with a 40 mm x 40 mm field of view (FOV). The optimum MRSI parameters that provided the best images were: RF flip angle=20 degrees, repetition time TR=200 ms, echo time TE=1.30 ms, and 1 scan (no signal averaging). A heat map of ^{15}N signals was generated in the inner 10 mm tube. After this step, a ^{1}H gradient echo MRI pulse sequence was initiated with the following optimum parameters: FOV=40 mm x 40 mm, TR=200 ms, TE=4 ms, RF flip angle=20 degrees with no signal averaging (1 scan). The hyperpolarized ^{15}N MRSI image was overlaid to the ^{1}H gradient echo image similar to the results displayed in Fig. 2. The hyperpolarized ^{15}N MRSI set up was done in collaboration with Dr. Chalermchai Khemtong at UTSW who published the very first MRI using a hyperpolarized ^{15}N compound (see Jiang et al.., Scientific Reports 5, 9104 (2015))—a project in which the PI is a collaborator. Thus, **Goal 2 which refers to the implementation of hyperpolarized ^{15}N MRSI and NMR protocols in phantom sample was successfully accomplished**.

GOAL 3. *to evaluate the efficacy of using hyperpolarized ^{15}N choline as in vivo biomarker for prostate cancer*.

For this Goal, the efficacy of hyperpolarized ^{15}N choline as biomarker for prostate cancer was first tested to monitor the first step of the Kennedy pathway in living PC-3 cancer cells. PC-3 cells were cultured and propagated in 25 cm petri dishes in standard CO_2 incubator at UTSW. The cells were harvested, pelletized, then resuspended in phosphate buffer at pH 7.4. 800 uL phosphate-buffered suspension containing approximately 50 million PC-3 prostate cancer cells was placed in a 1.5 mL microcentrifuge tube. Once the hyperpolarized ^{15}N choline sample was
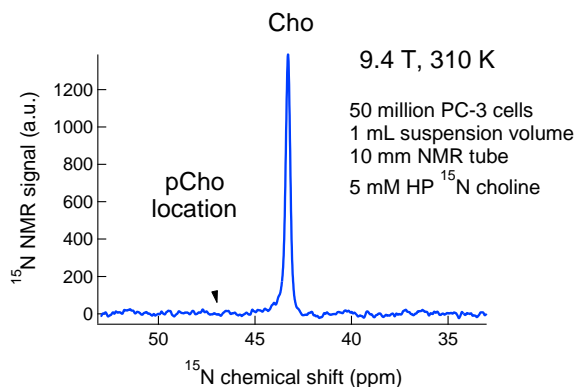
Figure 3. TOP: A photograph of a 10 mm NMR tube containing 1 mL suspension of 50 million living PC-3 cancer cells. 5 mM hyperpolarized 15N choline was administered to this cell suspension and signal detection was done every 5 s with a 10-degree RF pulse in a 9.4 T NMR magnet at 37 deg C. BOTTOM: Summation of the first 40 hyperpolarized ^{15}N spectra of the cell suspension study described above. [15]N choline (Cho) was detected at 43.3 ppm. However, ^{15}N phosphocholine (pCho) was not detected at the expected resonance of ~47 ppm.

ready for dissolution, a NMR set up was prepared in which the cell suspension was transferred to an air-bubbled 10 mL syringe tube with a 2-m long, 3 mm OD tygon tubing mounted on a 10 mm NMR tube. 4 mL hyperpolarized ^{15}N choline dissolution liquid was collected in a 50 mL beaker. An aliquot of 200 μL hyperpolarized liquid was rapidly injected into the bottom of the 10 mm NMR tube. The NMR tube was quickly lowered into the 9.4 T NMR magnet using the 2-m long tygon tubing attached to the tube. Once the NMR tube with HP ^{15}N choline was in place in the NMR coil, the 800 μL cell suspension was rapidly injected into the NMR tube. The rapid injection and the placement of the end of tygon tubing into the bottom of the tube created turbulence that assured homogeneous mixing of the cell suspension and the hyperpolarized ^{15}N choline solution. A photograph of the NMR setup after cell suspension injection is shown in Fig. 3. Next, an array of 10-degree RF pulses applied every 5 s was immediately started after the cell suspension injection using the VNMRJ software associated with the NMR spectrometer. ^{15}N NMR spectrum was recorded as the hyperpolarized ^{15}N signal decayed. As expected, hyperpolarized ^{15}N choline was detected at 43.3 ppm. *However, despite the roughly 8-minute time window of observation for hyperpolarized ^{15}N choline, the expected peak for ^{15}N phosphocholine at 46 ppm was not detected in a suspension of living PC-3 prostate cancer cells as shown in Fig. 3*. These experiments were repeated by varying of 15N choline concentration (2-10 mM), number of cells present in suspension (20-100 million cells), improvement of shimming conditions by switching to a smaller 5 mm NMR tube, and testing of phosphate buffer with DMEM medium. These changes in steps however did not result in the detection of ^{15}N phosphocholine in cells. Since it is well-known in the literature that the enzyme choline kinase (CK) is overexpressed in these prostate cancer cells, a question arose as to whether or not the CK-catalyzed conversion of choline into phosphocholine was fast enough to be observable within the time window of hyperpolarized ^{15}N NMR or MRI.

To answer this question, ^{13}C NMR measurement were performed on PC-3 extracts prepared with different incubation time of administered 5 mM ^{15}N choline in the cells: 8 minutes, 5 hours, and 24 hours.[1-^{13}C] choline was chosen for conventional NMR at 500 MHz NMR magnet because the [13]C T_1 at this labeling location is <5 s, thus ideal for signal averaging. On the other hand, ^{15}N choline has a T_1 of about 4 minutes, thus this would be prohibitively long for NMR signal averaging. 300 uL cell extract solutions in 99% D_2O were prepared in 5 mm NMR

tubes and inserted into a 500 MHz Bruker Ascend NMR magnet with temperature set at 37 deg C. The ^{13}C NMR spectra were taken with 2048 scans under Ernst angle conditions. [1-^{13}C] choline was detected at 57 ppm for all 3 samples. [1-^{13}C]phosphocholine, expected to appear at 66 ppm, was not detected in cell extracts prepared with 8-minute choline incubation time. This result corroborates with the in vitro hyperpolarized ^{15}N NMR results which implies that the production of phosphocholine from choline is relatively slow, that is outside the window of observation of hyperpolarized ^{15}N NMR. The ^{13}C phosphocholine NMR signal was slightly visible only after 24 hours of incubation time with choline as shown in Fig. 4. This is in contrast with pyruvate metabolism wherein
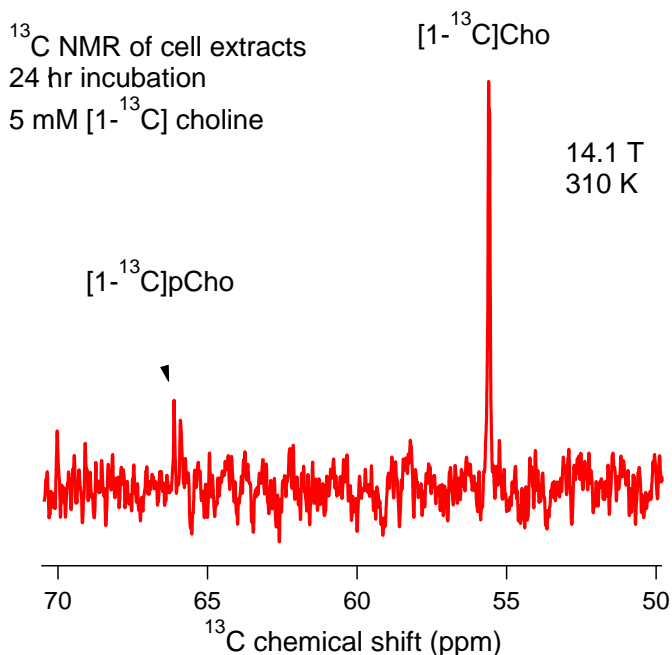

Figure 4. Representative ^{13}C NMR spectrum of PC-3 cell extract after administering the cells with 5 mM [1-^{13}C] choline over a 24-hour incubation time. [1-^{13}C]choline signal was detected at ~57 ppm while a small peak was seen at 66 ppm that corresponds to [1-^{13}C]phosphocholine. This NMR spectrum was taken at 14.1 T and 37 deg C with 2048 scans at Ernst angle conditions.

metabolic products such as lactate could be detected within a few seconds using hyperpolarized ^{13}C NMR/MRI. This slow metabolism of choline thus precluded the observation of phosphocholine production within the observational time scale of hyperpolarized ^{15}N NMR/MRI. Furthermore, a related study by Friesen-Waldner et al (*J Magn Reson Imaging. 2015 41(4):917-23*.) has shown that, despite excellent ^{13}C NMR enhancements, no phosphocholine production was observed *in vivo* in rat models with the administration of deuterated ^{13}C choline. This published result, in addition to the slow choline metabolism shown in the cell experiments, has precluded the need for additional *in vivo* studies with ^{15}N choline. **It is thus concluded based on these arguments that, despite the excellent ^{15}N NMR/MRI signal enhancements of hyperpolarized choline, <u>production of phosphocholine from choline is a relatively slow metabolic process that cannot be detected visibly within the time window of hyperpolarized ^{15}N NMR/MRI</u>. The <u>result of Goal 3</u> in this project was therefore <u>negative</u>.** It should be noted that aberrant choline metabolism can still be used as metabolic biomarker for prostate cancer using other techniques, however its slow metabolism is diagnostically incompatible with the time window of observation in hyperpolarization. Nevertheless, the experimental efforts in attempting to materialize Goal 3 have resulted in a comprehensive review article (*Lumata et al., Methods in Enzymology 561, 73-106 (2015)*) regarding the optimal methods/protocols in using hyperpolarization in monitoring metabolism *in vitro* and *in vivo*.

What opportunities for training and professional development has the project provided?
During the course of this project, my postdoctoral researcher and a graduate student in the lab were trained in using pertinent techniques for this research such as NMR spectroscopy, DNP or

hyperpolarization methods, MRI specialized for hyperpolarized agents, and cell/tissue culture techniques. These personnel in my lab have attended special training classes for NMR/DNP/MRI both at UT Dallas and at UT Southwestern Medical Center. Furthermore, this project has also provided these personnel and my research group in general exposure to conferences such as the Experimental NMR Conference (ENC), local and international meetings of the American Physical Society (APS) and American Chemical Society (ACS).

How were the results disseminated to communities of interest?

The results of this project were disseminated to the scientific community mainly by the publications (5 peer-reviewed papers that resulted in this project) and by presentations (11 research abstracts presented as talks or posters) in scientific conferences such as the ENC, APS, and ACS meetings. My research group has also showcased our research including this project to incoming freshmen students at UTD in outreach activities such as the UTD Scholars' Day, Eureka, and to the public at the Dallas Arboretum during the annual UTD physics outreach activity.

What do you plan to do during the next reporting period to accomplish the goals?

This is the final report.

4. IMPACT

What was the impact on the development of the principal discipline(s) of the project?

The results of this project have made significant advances on the optimization of the MRI signal-enhancing process of the DNP technology. We have reported in four research papers some newly discovered recipe on DNP sample preparation to obtain the highest MRI signal enhancements. The basic idea is that since this MRI signal-enhancing technology emanates from the interaction between electrons and nuclei, modification or addition of sample components that affects the properties of these entities could significantly contribute to changes in the DNP efficiency. We have detailed ways to further boost the DNP-enhanced MRI signals by a factor of 2-3 times of what can normally be achieved. Furthermore, this project also resulted in optimization protocols of using this technology when dealing with metabolic assessment of living cells or tissues.

What was the impact on other disciplines?

The optimization methods in DNP that resulted in this project can be used not only in metabolic assessment in cells and tissues using hyperpolarization, but also in liquid-state NMR characterization in chemistry in general. The optimization sample preparation for DNP that we have discovered can also be used for non-biological applications such as highly-sensitive detection of insensitive nuclei such as yttrium-89, silver-107,109, and other nuclei that are challenging to detect with conventional NMR spectroscopy.

What was the impact on technology transfer?

The field of DNP is still its nascent stage. The results of this project have led to development of proven protocols to achieve the highest NMR signals enhancements and suggested designs of in vitro and in vivo NMR/MRI metabolism set ups that may be adopted by other research groups.

What was the impact on society beyond science and technology?

We currently have no metric to evaluate that the results of this project has any significant impact on public awareness or behavior.

5. CHANGES/PROBLEMS

Changes in approach and reasons for change

The slow metabolism of choline has precluded detection of its metabolite phosphocholine. Other approaches such as NMR of ^{13}C-choline with short T1 were tested prostate cancer cells due to prohibitively long acquisition time when using ^{15}N choline in conventional NMR spectroscopy.

Actual or anticipated problems or delays and actions or plans to resolve them

During our NMR studies of hyperpolarized ^{15}N choline with prostate cancer cells, we have found that choline metabolism was relatively slow in our order of a few hours whereas the NMR/MRI detection time window was only on the order of several minutes. We have followed up with more studies using conventional NMR of prostate cancer cell extracts which revealed that the choline metabolite phosphocholine was only visibly produced when the parent compound was administered for at least 4 hours. This results confirmed that choline metabolism could be visibly detected by hyperpolarized NMR/MRI. We have further improved the enhancement levels of choline to up to 48,000-fold but no phosphocholine production was detected in our observation timescale. During the course of this project, other groups have reported to also try hyperpolarized choline in vivo but also confirmed that phosphocholine production was too slow to be detected by hyperpolarized NMR/MRI.

Changes that had a significant impact on expenditures

None.

Significant changes in use or care of human subjects. None

Significant changes in use or care of vertebrate animals. No vertebrate animal was used since we have discovered that phosphocholine production is too slow and could be detected on the timescale afforded by hyperperpolarized MRI.

Significant changes in use of biohazards and/or select agents. None

6. PRODUCTS

Publications (Total: 5)

1. Peter Niedbalski, Christopher Parish, Andhika Kiswandhi, Leila Fidelino, Chalermchai Khemtong, Zahra Hayati, Likai Song, Andre Martins, A. Dean Sherry, and Lloyd Lumata*, "Influence of Dy3+ and Tb3+-doping on 13C dynamic nuclear polarization" **Journal of Chemical Physics** 146, 014303 (2017).

2. Andhika Kiswandhi, Peter Niedbalski, Christopher Parish, Pavanjeet Kaur, Andre Martins, Leila Fidelino, Chalermchai Khemtong, Likai Song, A. Dean Sherry, and Lloyd Lumata*, "Impact of Ho3+-doping on 13C dynamic nuclear polarization using trityl OX063 free radical" **Physical Chemistry Chemical Physics** 18, 21351-21359 (2016).

3. Peter Niedbalski, Christopher Parish, Andhika Kiswandhi and Lloyd Lumata*, "13C dynamic nuclear polarization using isotopically-enriched 4-oxo-TEMPO free radicals" **Magnetic Resonance in Chemistry** 54, 962-967 (2016).

4. Andhika Kiswandhi, Bimala Lama, Peter Niedbalski, Mudrekh Goderya, Joanna Long and Lloyd Lumata*, "The effect of glassing solvent deuteration and Gd3+ doping on 13C DNP at 5 T ", **RSC Advances** 6, 38855-38860 (2016).

5. Lloyd Lumata*, Chendong Yang, Mukundan Ragavan, Nicholas Carpenter, Ralph J. DeBerardinis*and Matthew E. Merritt*, "Hyperpolarized 13C magnetic resonance and its use in metabolic assessment of cultured cells and perfused tissues", **Methods in Enzymology** 561, 73-106 (2015).

Conference Abstracts (Total: 11)

1. Construction and 13C NMR signal efficiency of a dynamic nuclear polarizer at 6.4 T and 1.4 K, Andhika Kiswandhi, Peter Niedbalski, Christopher Parish, Sarah Ferguson, David Taylor, George MacDonald, and Lloyd Lumata, **American Physical Society (APS) meeting**, Baltimore Convention Center, Baltimore, Maryland (March 14-18, 2016).

2. Optimization of 13C dynamic nuclear polarization: isotopic labeling of free radicals, Peter Niedbalski, Christopher Parish, Andhika Kiswandhi, and Lloyd Lumata, **American Physical Society (APS) meeting**, Baltimore Convention Center, Baltimore, Maryland (March 14-18, 2016).

3. Temperature dependence of proton NMR relaxation times at Earth's magnetic field, Peter Niedbalski, Christopher Parish, Andhika Kiswandhi, Sarah Ferguson, Eduardo Cervantes, Anisha Oomen, Anagha Khrishnan, Aayush Goyal, and Lloyd Lumata,

American Physical Society (APS) meeting, Baltimore Convention Center, Baltimore, Maryland (March 14-18, 2016).

4. Production and NMR signal optimization of hyperpolarized 13C-labelled amino acids, Christopher Parish, Peter Niedbalski, Sarah Ferguson, Andhika Kiswandhi, and Lloyd Lumata, **American Physical Society (APS) meeting**, Baltimore Convention Center, Baltimore, Maryland (March 14-18, 2016).

5. Impact of Gd3+ doping and glassing solvent deuteration on 13C DNP at 5 T, Andhika Kiswandhi, Bimala Lama, Peter Niedbalski, Mudrekh Goderya, Joanna Long, and Lloyd Lumata, **American Physical Society (APS) meeting**, Baltimore Convention Center, Baltimore, Maryland (March 14-18, 2016).

6. Real-time tracking of dissociation of hyperpolarized 89Y-DPTA: a model for degradation of open-chain Gd3+ MRI contrast agents, Sarah Ferguson, Peter Niedbalski, Christopher Parish, Andhika Kiswandhi, Zoltan Kovacs, and Lloyd Lumata, **American Physical Society (APS) meeting**, Baltimore Convention Center, Baltimore, Maryland (March 14-18, 2016).

7. Hyperpolarized 89Y NMR spectroscopic detection of Yttrium ion and DOTA macrocyclic ligand complexation: pH dependence and YDOTA intermediates, Sarah Ferguson, Peter Niedbalski, Christopher Parish, Andhika Kiswandhi, Zoltan Kovacs, and Lloyd Lumata, **American Physical Society (APS) meeting**, Baltimore Convention Center, Baltimore, Maryland (March 14-18, 2016).

8. Hyperpolarized 13C NMR lifetimes in the liquid-state: relating structures and T1 relaxation times, Christopher Parish, Peter Niedbalski, Zohreh Hashami, Leila Fidelino, Zoltan Kovacs, and Lloyd Lumata, **American Physical Society (APS) meeting**, Baltimore Convention Center, Baltimore, Maryland (March 14-18, 2016).

9. Hyperpolarized Magnetic Resonance: Enhancing MRI Signals by >10,000-fold for Non-Invasive Metabolic Assessment of Cancer, Lloyd Lumata, Invited Talk, **Joint Meeting of the Texas and Four Corners Sections of the American Physical Society (APS)**, New Mexico State University, Las Cruces, New Mexico (October 21-22, 2016).

10. Influence of Ho3+-doping on 13C dynamic nuclear polarization, Andhika Kiswandhi, Peter Niedbalski, Christopher Parish, Pavanjeet Kaur, Andre Martins, Leila Fidelino, Chalermchai Khemtong, Likai Song, A. Dean Sherry, and Lloyd Lumata, **Joint Meeting of the Texas and Four Corners Sections of the American Physical Society (APS)**, New Mexico State University, Las Cruces, New Mexico (October 21-22, 2016).

11. Hyperpolarized Magnetic Resonance in Medical Research, Lloyd Lumata, Invited Talk, **47th Winter Colloquium on the Physics of Quantum Electronics**, Cliff Lodge, Snowbird Resort, Snowbird, Utah (January 8-13, 2017)

7. PARTICIPANTS AND OTHER COLLABORATING ORGANIZATIONS

Individuals who worked on the project:

a) Name: Dr. Lloyd Lumata
   Project role: Principal Investigator
   Nearest person month worked: 12
   Contribution to the project: planned, supervised, and analyzed the research activities for this project.

b) Name: Dr. Andhika Kiswandhi
   Project Role: Postdoctoral Researcher
   Nearest person month worked: 3
   Contribution to the project: performed the hyperpolarized NMR and MRI experiments.
   Funding Support: UTD startup funding and in part by this grant award

c) Name: Peter Niedbalski
   Project role: Graduate student
   Nearest person month worked: 3
   Contribution to the project: performed cancer cell culture and hyperpolarized magnetic resonance experiments.
   Funding support: Welch Foundation

Partner Organization:

a) Name: University of Texas Southwestern Medical Center (UTSW)
   Partner's contribution to the project:
   Facilities: use of the commercial HyperSense DNP polarizer, 9.4 T Varian High resolution NMR system with MRI capability
   Personnel exchanges: UTSW technical staff assisted in cancer cell and MRI experiments

8. SPECIAL REPORTING REQUIREMENTS

Not applicable.

9. APPENDICES
Please find attached copies of the 5 peer-reviewed publications and 11 conference abstracts that have resulted from support of this grant award.

Influence of Dy^{3+} and Tb^{3+} doping on ^{13}C dynamic nuclear polarization

Peter Niedbalski, Christopher Parish, Andhika Kiswandhi, Leila Fidelino, Chalermchai Khemtong, Zahra Hayati, Likai Song, André Martins, A. Dean Sherry, and Lloyd Lumata

---

Articles you may be interested in

Accelerating two-dimensional nuclear magnetic resonance correlation spectroscopy via selective coherence transfer
The Journal of Chemical Physics **146**, 014202014202 (2017); 10.1063/1.4973547

On the generality of Michaelian kinetics
The Journal of Chemical Physics **146**, 014101014101 (2017); 10.1063/1.4973220

First principles calculation of the elasticity of ice VIII and X
The Journal of Chemical Physics **146**, 014501014501 (2017); 10.1063/1.4973339

Influence of Dy³⁺ and Tb³⁺ doping on ¹³C dynamic nuclear polarization

Peter Niedbalski,[1] Christopher Parish,[1] Andhika Kiswandhi,[1] Leila Fidelino,[2] Chalermchai Khemtong,[2] Zahra Hayati,[3] Likai Song,[3] André Martins,[2,4] A. Dean Sherry,[2,4] and Lloyd Lumata[1,a)]

[1]*Department of Physics, University of Texas at Dallas, 800 West Campbell Road, Richardson, Texas 75080, USA*
[2]*Advanced Imaging Research Center, University of Texas Southwestern Medical Center, 5323 Harry Hines Boulevard, Dallas, Texas 75390, USA*
[3]*National High Magnetic Field Laboratory, Florida State University, Tallahassee, Florida 32310, USA*
[4]*Department of Chemistry, University of Texas at Dallas, 800 West Campbell Road, Richardson, Texas 75080, USA*

Dynamic nuclear polarization (DNP) is a technique that uses a microwave-driven transfer of high spin alignment from electrons to nuclear spins. This is most effective at low temperature and high magnetic field, and with the invention of the dissolution method, the amplified nuclear magnetic resonance (NMR) signals in the frozen state in DNP can be harnessed in the liquid-state at physiologically acceptable temperature for *in vitro* and *in vivo* metabolic studies. A current optimization practice in dissolution DNP is to dope the sample with trace amounts of lanthanides such as Gd³⁺ or Ho³⁺, which further improves the polarization. While Gd³⁺ and Ho³⁺ have been optimized for use in dissolution DNP, other lanthanides have not been exhaustively studied for use in ¹³C DNP applications. In this work, two additional lanthanides with relatively high magnetic moments, Dy³⁺ and Tb³⁺, were extensively optimized and tested as doping additives for ¹³C DNP at 3.35 T and 1.2 K. We have found that both of these lanthanides are also beneficial additives, to a varying degree, for ¹³C DNP. The optimal concentrations of Dy³⁺ (1.5 mM) and Tb³⁺ (0.25 mM) for ¹³C DNP were found to be less than that of Gd³⁺ (2 mM). W-band electron paramagnetic resonance shows that these enhancements due to Dy³⁺ and Tb³⁺ doping are accompanied by shortening of electron T_1 of trityl OX063 free radical. Furthermore, when dissolution was employed, Tb³⁺-doped samples were found to have similar liquid-state ¹³C NMR signal enhancements compared to samples doped with Gd³⁺, and both Tb³⁺ and Dy³⁺ had a negligible liquid-state nuclear T_1 shortening effect which contrasts with the significant reduction in T_1 when using Gd³⁺. Our results show that Dy³⁺ doping and Tb³⁺ doping have a beneficial impact on ¹³C DNP both in the solid and liquid states, and that Tb³⁺ in particular could be used as a potential alternative to Gd³⁺ in ¹³C dissolution DNP experiments. *Published by AIP Publishing.*
[http://dx.doi.org/10.1063/1.4973317]

I. INTRODUCTION

Nuclear magnetic resonance (NMR) spectroscopy, especially of nuclei other than proton and at low concentrations, can be a challenging measurement owing to the inherently weak magnetic moments of nuclear spins.[1] As a result of relatively low gyromagnetic ratio γ of nuclear spins, the spin population difference between Zeeman energy states, quantified by the polarization, can be quite miniscule. This is particularly prominent in the case for low-γ nuclei such as ¹³C or ¹⁵N. Consequently, NMR under these conditions often requires a large number of scans in order to achieve adequate signal-to-noise. While NMR is relatively insensitive, electron paramagnetic resonance (EPR), a similar technology, does not suffer from this problem. This is a consequence of the relatively higher strength of the electron magnetic moment which is 3–4 orders of magnitude stronger than that of most nuclei. Thus, at similar magnetic fields and temperatures, EPR will have a significantly greater polarization, and hence, higher signal strength than NMR.[2]

Dynamic nuclear polarization (DNP) resolves the insensitivity problem of NMR by transferring the high thermal polarization of electrons to nuclei.[3] DNP was originally proposed as a method of increasing polarization in metals,[4] but was quickly expanded to diamagnetic solids.[5–7] The DNP process involves microwave irradiation of a sample of nuclear spins in a glassy solid doped with paramagnetic agents.[3] For most of its history, this technique was used to prepare polarized targets in particle physics experiments,[8] but has been revolutionized for chemical and biomedical applications with the invention of dissolution DNP in 2003.[9] In dissolution DNP, nuclear spins are polarized in the solid state and subsequently dissolved rapidly, resulting in a "hyperpolarized" room-temperature liquid yielding liquid-state signal enhancements of typically more than 10 000-fold.[9,10] Using this technology, samples containing low-γ nuclei such as ¹³C may be both highly polarized and physiologically compatible, allowing for biomedical applications such as ¹³C metabolic imaging in real-time.[11–15]

---

a)Author to whom correspondence should be addressed. Electronic mail: lloyd.lumata@utdallas.edu

The efficiency of DNP is highly dependent on the sample composition and physical conditions under which it takes place. Most commonly, high magnetic fields (typically >3 T) and low temperatures (close to 1 K) are used in order to ensure nearly complete electron polarization. Additionally, the DNP enhancement is contingent on the frequency of microwave irradiation used, which changes based on magnetic field and sample composition. One of the most important determining factors of the overall DNP signal enhancement is sample composition. The free radical used, the nuclei to be polarized, the substrate containing the nuclei, and the solvent in which the nuclei and free radical are dissolved all play an important role in the optimization of DNP. In dissolution DNP, organic free radicals including trityls and nitroxides are most commonly used as the polarizing agents.[16,17] Other radicals such as BDPA,[18] DPPH,[19] and galvinoxyl[20] have been used with some success as well as novel methods such as photoinduced radicals[21] and paramagnetic centers within nanoparticles.[22,23] Nitroxide free radicals have relatively wide EPR linewidths, which are better suited for DNP of high-γ nuclei such as ^{1}H spins and also provide decent polarization levels for low-γ nuclei such as ^{13}C.[24] This class of free radicals maintain their popularity by being comparatively inexpensive, highly water soluble, easily scavenged, and effective for cross polarization DNP.[25–30] Additionally, the DNP efficiency of these radicals may be increased through other means such as deuteration of the glassing matrix.[31–33] Meanwhile, the trityls, particularly OX063, which have some of the narrowest EPR linewidths among free radicals, were found to be excellent polarizing agents for low-γ nuclei like ^{13}C.[16,34] When using these radicals, DNP enhancements may be improved further by the addition of trace amounts of gadolinium.[34–37] Recently, it was found that the addition of holmium to a trityl-doped sample results in liquid state enhancement similar to that achieved by using gadolinium.[38] While the use of these lanthanides may lead to significant polarization gains, the free ion form of these lanthanides may lead to greater toxicity of the DNP sample, which must be considered prior to *in vivo* biomedical application.[39] One method used to combat the toxicity of rare earth metals is to encage these lanthanide ions with a chelating agent, thus rendering them relatively inert in the body.[40] Among the more prominent ligands used in gadolinium contrast agents are DTPA,[40,41] HP-DO3A,[42,43] and DOTA.[44] Of these, DOTA is considered to have high thermodynamic stability and kinetic inertness, and as such is an ideal gadolinium chelating ligand for use in *in vivo* studies.[41]

While a variety of Ln(III) complexes have numerous biomedical applications, particularly in contrast-enhanced MRI,[45] only Gd^{3+} and Ho^{3+} have been studied extensively as beneficial doping agents in ^{13}C dissolution DNP.[35–38] This in part takes precedent from a previous preliminary study which has shown that only Gd^{3+} and Ho^{3+} ions have beneficial effects on ^{13}C DNP, while the other Ln(III) ions appear to have no apparent effect on ^{13}C DNP enhancements for trityl-doped samples.[37] We would like to note that the measurements in the aforementioned previous DNP study on using lanthanide ions[37] were not really extensively optimized in terms of concentration dependence and the fact that the optimum DNP microwave frequency could shift with lanthanide doping.

Thus, in this work, we have revisited the question on whether Gd^{3+} and Ho^{3+} really stand alone among the lanthanides as beneficial additives in ^{13}C dissolution DNP samples. Due to the high cost of trityl OX063 free radical and DNP instrumental operation, we have selected only two lanthanides, Tb^{3+} and Dy^{3+}, for extensive ^{13}C DNP optimization studies. Tb^{3+} and Dy^{3+} have among the highest magnetic moments in the lanthanide series, on par with Gd^{3+} and Ho^{3+}. In fact, in terms of magnetic susceptibility (μ_{eff}) that is affected by many other physical properties mostly related to the ion anisotropy, Tb^{3+} and Dy^{3+} presented the highest and most promising parameters.[46] We have used Tb-DOTA and Dy-DOTA for the ^{13}C DNP study and carefully recorded the effects on DNP microwave sweeps, relative ^{13}C solid-state polarization buildup curves, liquid-state ^{13}C enhancement, and relaxation. The substrate used in these studies was [1-^{13}C] sodium acetate, which was chosen for its biological relevance and comparatively low cost. Furthermore, W-band EPR was used to elucidate the physical mechanisms of free electrons that are at play in ^{13}C DNP. With these optimized steps for measurements, the main goal of this work was to investigate whether these two selected lanthanides have any beneficial impact on ^{13}C DNP similar to the effects of Gd^{3+} and Ho^{3+} complexes.

II. EXPERIMENTAL

A. Sample preparation

Chemicals and reagents were acquired commercially and used without further purification. For each sample studied by DNP, 24.9 mg of [1-^{13}C] sodium acetate (Cambridge Isotope Lab, MA) was added to 100 μl of 1:1 v/v water:glycerol solution. This was prepared several hours prior to polarization and frozen at $-20\,^\circ$C until the experiment time. Immediately prior to the polarization, samples were thawed and 2.14 mg of trityl OX063 free radical was added to the solution. The final concentration in the solutions of sodium acetate and trityl OX063 was 3M and 15 mM, respectively. These DNP samples were prepared in 100 μl aliquots and doped with varying concentrations of Dy^{3+}-DOTA or Tb^{3+}-DOTA. The Dy-doped samples were prepared from an aqueous stock solution of 135.0 mM Dy^{3+}-DOTA (deionized water, pH 7.2) and Tb-doped samples from an aqueous stock solution of 124.5 mM Tb^{3+}-DOTA (deionized water, pH 7.2).

The Dy^{3+}-DOTA or Tb^{3+}-DOTA was prepared by adding to solutions free ligand (DOTA^{4-}) at M/l molar ratios of 1:1.05, and the resulting solutions were heated at 338 K under stirring for a least 12 h. The pH was kept close to 7 by periodic addition of aqueous KOH. The absence of free Dy^{3+} and Tb^{3+} ions in solution was verified by the xylenol orange test.[47,48] Final concentrations were checked by the Evans method.

The concentrations studied for Dy were 1.0, 1.5, 2.0, 3.0, and 4.0 mM and for Tb were 0.125, 0.25, 0.5, 1.0, 1.5, 2.0, 3.0, and 4.0 mM. Control samples and two additional samples, one containing 2 mM Ho^{3+}-DOTA and one containing 2 mM Gd^{3+}-DOTA, were also made for comparison. The holmium and gadolinium samples were prepared from aqueous stock solutions of 218 mM Ho^{3+}-DOTA (deionized water, pH 7.2) and 79.65 mM Gd^{3+}-DOTA (deionized water, pH 7.2),
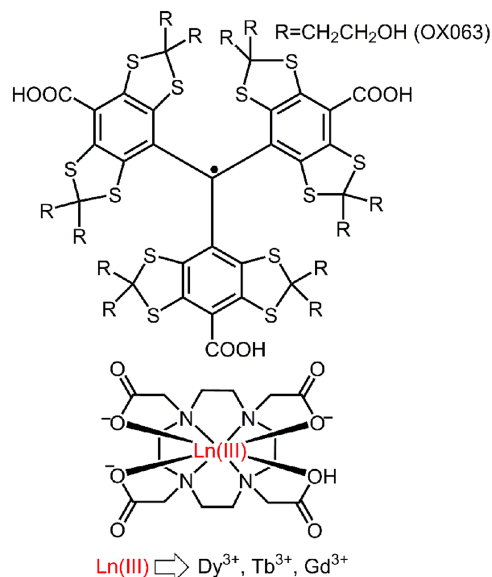
FIG. 1. The free radical polarizing agent and lanthanides complexes used in this work.

respectively. The free radical and DOTA ligand used in this work may be seen in Fig. 1.

B. EPR measurements

EPR measurements were conducted on a reference sample as well as samples doped with Tb, Gd, and Dy. The EPR experiments were performed prior to DNP experiments, and as such optimal concentrations had not yet been determined. Previous work has shown that the optimal concentration for both gadolinium and holmium is 2 mM,[34,35,38] so this was chosen to be the concentration of terbium and dysprosium studied in order to compare their electron T_1 under the same conditions. Measurements were performed at the National High Magnetic Field Laboratory (NHMFL) in Tallahassee, FL in the W-band (94 GHz) on a Bruker E680 EPR spectrometer (Bruker Biospin, Billerica, MA) using a Bruker TE$_{011}$ cylindrical cavity. The temperature of the sample was regulated using a CF1200 helium flow cryostat (Oxford Instruments, UK). Prior to insertion in the cylindrical cavity, samples were loaded in 0.15 mm ID thin quartz capillary tubes. Temperature dependent electronic T_1 data for trityl OX063 were recorded using saturation recovery, and the EPR spectra were monitored using the field-swept electron spin-echo method. Samples were studied at temperatures down to the low temperature limit of 5 K in order to most closely match DNP conditions.

C. Hyperpolarization and NMR measurements

All hyperpolarization experiments were conducted at the Advanced Imaging Research Center at the University of Texas Southwestern Medical Center (UTSW) using the commercial HyperSense polarizer (Oxford Instruments, UK). This polarizer uses a 3.35 T superconducting magnet, and the cryostat vacuum space has a base temperature of 1.2 K due to a roots blower pump vacuum system (Edwards Vacuum, UK). Irradiation of the sample in this polarizer is provided by a 100 mW ELVA microwave source (ELVA-1 millimeter

Wave Division, RU) with a 400 MHz sweepable frequency range.

^{13}C samples prepared as described above were inserted into the polarizer. Before running polarizing buildup experiments, microwave frequency sweeps were conducted for samples with various concentrations of Tb^{3+} and Dy^{3+} in order to determine the optimum polarization frequencies for DNP. The ^{13}C NMR signal of the sample was measured after 3 min of polarization at 5 MHz intervals over the range of the microwave source using a sweep program in the HyperSense. After each NMR scan, a series of hard pulses was applied to the sample to remove polarization built up at the previous frequency. In this manner, the positive P(+) and negative P(−) polarization peaks were found for different concentrations of the studied lanthanides. These were then normalized for comparison.

After the optimum irradiation frequencies were found, ^{13}C polarization buildup curves were measured for each sample. This was accomplished by irradiating each sample at the frequency determined by the positive polarization peak P(+) and measuring the ^{13}C NMR signal every 3 min until the curve had approximately reached a plateau. The actual percent polarization for samples was not found due to the prohibitively long acquisition times necessary to measure the thermal ^{13}C polarization. Rather, the relative polarization level was used to evaluate the efficacy of the lanthanide complexes on ^{13}C DNP. This is in line with previous studies which have used the same method to compare DNP performance.[32,35–38] Build-up curves were recorded and fit with single exponential equations, and using the fit, the relative polarization at 10 000 s was extrapolated.

Due to the large number of samples to be studied and limited access to the HyperSense polarizer, only single build-up curves were taken for samples with non-optimal concentrations of lanthanide. Meanwhile, the ^{13}C DNP samples doped with optimal lanthanide concentrations 1.5 mM Dy^{3+}-DOTA, 0.25 mM Tb^{3+}-DOTA, 2 mM Gd^{3+}-DOTA, and the control sample were each measured in triplicate. For each of the three trials, new samples were freshly made prior to polarization. One dissolution per lanthanide was carried out after these samples had reached maximum polarization. Upon dissolution, approximately 4 ml of aqueous solution of hyperpolarized [1-^{13}C] acetate was transferred through 0.125 in. OD PTFE tubing to a 10 mm NMR tube (Wilmad-LabGlass, NJ) which was already placed inside a 400 MHz Varian NMR magnet (Agilent Technologies, CA). This transfer was an automated process with a total shuttling time of 8 s from the Hyper-Sense to the high resolution NMR magnet. Once the liquid had been transferred, the decay of the hyperpolarized signal was monitored by applying 5° RF pulses at 2 s intervals. The first scan was taken immediately following the transfer of hyperpolarized liquid with a delay of 0.01 s. Following the array of scans, the sample was removed from the magnet for a specific time to ensure complete relaxation of the hyperpolarized signal. Subsequently, it was then returned to the magnet where a single NMR scan was taken using a 90° RF pulse in order to obtain the thermal equilibrium polarization from which liquid-state enhancements could be calculated.

D. Data analysis

All data were plotted and analyzed using Igor Pro version 6.2 (Wavemetrics, Lake Oswego, OR). Mean values and standard deviations were calculated for experiments with $N = 3$ trials. Liquid-state ^{13}C NMR data taken post dissolution in a Varian NMR spectrometer were processed using ACD labs version 12.0 (Advanced Chemistry Development, Toronto, Canada).

III. RESULTS AND DISCUSSION

One of the primary determining factors in total DNP enhancement of the NMR signal is the free radical that provides the electrons from which polarization is transferred to nuclei.[17,18,20,21,31,34,49] Trityl OX063, the stable organic radical used in this work, has a very narrow EPR linewidth that makes it ideal for polarizing low-γ nuclei such as ^{13}C. When using this free radical to polarize low-γ nuclei such as ^{13}C spins, DNP data at 3.35 T and temperatures close to 1 K have shown indications of thermal mixing (TM) as the predominant DNP mechanism.[24,50–53] Other DNP data at similar conditions suggested that the mechanism could be a combination of the solid effect (SE) and cross effect (CE).[54–56] Unlike the solid effect (SE)[57] and the cross effect (CE),[54,58] TM is a many-spin model for polarization that treats spin interactions as thermodynamic reservoirs.[24,59] Namely, these reservoirs are the nuclear Zeeman system (NZS) and electron Zeeman system (EZS), and the electron dipolar system (EDS). In terms of this model, the polarization method may be qualitatively understood as microwave irradiation cooling the EDS and subsequent thermal contact with the NZS (via the hyperfine interaction), leading to a decrease in the NZS spin temperature, i.e., an increase in nuclear polarization. Quantitatively, the maximum polarization achievable in this model is

$$ P_{max} = \mathscr{B}_I \left(I\beta_L \omega_e \frac{\omega_I}{2D} \frac{1}{\sqrt{\eta\,(1+f)}} \right), \tag{1} $$

where $\mathscr{B}_I$ is the Brillouin function, I the nuclear spin, $\beta_L = \hbar/kT_L$ the inverse lattice temperature, ω_e and ω_I the electron and nuclear Larmor frequencies, respectively, D the radical EPR linewidth, $\eta = t_Z/t_D$ the ratio of electron Zeeman to electron dipolar relaxation times, and f a general "leakage factor" that encompasses nuclear relaxation effects.[24]

A. EPR of trityl doped with Ln^{3+}

Because the free radical plays such a significant role in determining the overall polarization enhancement, it stands to reason that changing the electronic properties of the radical by addition of lanthanide complexes could change the maximum polarization.[34,60] In order to thoroughly investigate these changes, field swept EPR spectra (Fig. 2(a)) and the temperature dependence of electron T_1 were studied for the samples of interest. T_1 was determined by fitting the electron relaxation recovery curves using a double-exponential build-up $M(t) = M_a \exp\left(-t/T_{1,a}\right) + M_b \exp\left(-t/T_{1,b}\right) + C$. This equation results in two relaxation times, the longer of which ($T_{1,a}$)
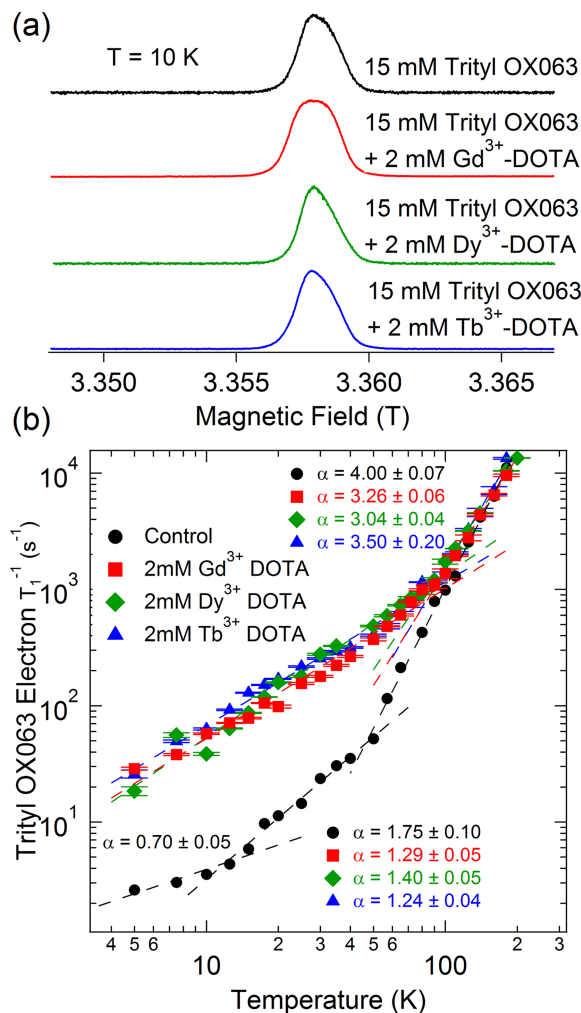

FIG. 2. (a) Field-swept W-band EPR spectra of trityl OX063 at 10 K in the absence or presence of trace amounts of lanthanides. (b) Temperature dependence of electron T_1 for trityl OX063 with and without lanthanide doping. The power law equation of best fit is shown for each data set with dashed lines and the power displayed for each sample.

corresponds to the electron T_1 while the shorter corresponds to the relaxation effects contributed by electron-electron cross relaxation effects.[61,62] Electron T_1^{-1} was plotted vs. temperature on a log-log plot (Fig. 2(b)), and a power law equation ($T_1^{-1} = AT^\alpha$) was fitted to the data.

At high temperatures, the electron T_1 of undoped trityl OX063 increases rapidly as the temperature is reduced, with a dependence of $\alpha \approx 4$. This suggests that at temperatures above about 50 K, electron relaxation is dominated by multiple-phonon processes such as the Orbach process.[63] Below 50 K to about 20 K, there is a decrease in the rate of change of T_1^{-1}, with temperature having $\alpha \approx 1.75$. Because this value is close to 2, it indicates that electron relaxation in this temperature regime is dominated by the Raman process.[63] Below 20 K, the dependence falls to $\alpha \approx 0.70$, which points to the one-phonon direct process as the primary means of electron relaxation.[63]

Samples doped with 2 mM Ln(III) complex gave nearly identical electron relaxation data. For each of the samples, there was only one major change in the power law fitting, which occurred at a higher temperature (90 K) than did

the shift in the reference data. Above 90 K, the electron relaxation rate is nearly identical to that of the reference sample, but is much more rapid below this temperature. In this low temperature regime, T_1^{-1} changes with temperature with an $\alpha \approx 1$ dependence, suggesting that below 90 K, the direct process dominates the electron relaxation behavior for the lanthanide doped samples. The lowest temperature studied for EPR was 5 K, but based on the trends of both the reference and lanthanide samples, it is likely that electron relaxation is dominated by the direct process at DNP temperatures near 1 K. This is corroborated by a previous study[34] which shows that the trityl electron relaxation of a reference sample close to 1 K falls reasonably close to a fit of relaxation data between 5 and 20 K extrapolated to 1 K.

B. ^{13}C solid state polarization

In order to ensure that samples were irradiated at the optimum frequency, microwave frequency sweeps were taken for all samples. Representative ^{13}C microwave frequency sweeps are shown in Fig. 3. Similar to previous studies of Gd^{3+} in DNP, Tb^{3+} and Dy^{3+} doped samples resulted in DNP spectra that had P(+) and P(−) shifted toward each other.[36,60] At the optimum concentration of Dy^{3+}-DOTA (1.5 mM), both positive and negative polarization peaks were shifted by 20 MHz from the reference sample. This shift was consistent over all concentrations of Dy studied, only increasing to 25 MHz for both peaks with 4 mM Dy. For the sample doped with the optimum concentration of Tb^{3+}-DOTA (0.25 mM), P(+) was shifted by 25 MHz, while P(−) was shifted only by 20 MHz. Decreasing the concentration of Tb^{3+} by half reduced the shift to 15 MHz from reference for both peaks, while increasing the concentration to 4 mM Tb^{3+} increased it to 30 MHz.

From a theoretical perspective, the locations of positive and negative polarization peaks can be approximated by Borghini's spin-temperature model.[3,64] Using this model, the DNP spectrum, including P(+) and P(−), depends almost entirely on the features of the EPR spectrum of the free radical used, with smaller contributions from electron and nuclear relaxation. In order to understand the microwave spectra, it is important to consider the EPR data gathered, which show minimal differences in EPR spectra and very significant differences in electron relaxation as discussed above. Though electron relaxation is a less dominant contributing factor in the microwave spectra based on the original Borghini model, it is possible that the magnitude change in relaxation time at low temperature is sufficient to cause a narrowing of the DNP spectrum.

On the other hand, other works have suggested that DNP under similar experimental conditions may be described by a combination of the solid effect and indirect cross effect that could be prevalent in samples having paramagnetic centers with inhomogeneously broadened EPR line shapes.[54–56] The change in DNP spectrum seen with lanthanide doping may be understood equally well by this model. The shortening of electronic T_1 induced by the lanthanide ion changes the level of contribution from the SE and CE, in this case accentuating the contributions from both mechanisms.[55] It is important to note

that full quantum mechanical models have been developed to explain this experimental DNP effect using these 2-spin and 3-spin processes.[54–56]

Once the polarization peaks were determined by way of microwave frequency sweeps, polarization build-up curves were taken by irradiating samples at the positive polarization peak P(+) while monitoring polarization at 3 min intervals. Initially, concentrations of 0 mM, 1 mM, 1.5 mM, 2 mM, 3 mM, and 4 mM of both Dy^{3+} and Tb^{3+} were studied. Samples were polarized for between 1.5 and 2 h and the data fit with a single exponential. For final comparison, data were extrapolated to 10 000 s. After these data were collected, it was found that Dy^{3+} had an optimum concentration of 1.5 mM. In addition, it was found that 0.25 mM Tb^{3+} doping resulted in the largest polarization gain. ^{13}C polarization enhancements relative to the reference sample are displayed in Fig. 4(a) for each of the concentrations of Tb and Dy studied. The polarization increases from 0 mM doping to the optimum concentration and decreases fairly rapidly at concentrations above the optimum. This is in contrast to the behavior of Gd^{3+}, which yields a "plateau" in polarization level improvement at concentrations between 2 and 8 mM,[37,60] but is quite similar to the "peak" behavior exhibited by Ho^{3+} doping.[37,38]

In Fig. 4(b), the build-up time constant is shown for each concentration of the two lanthanides. From these data, it is
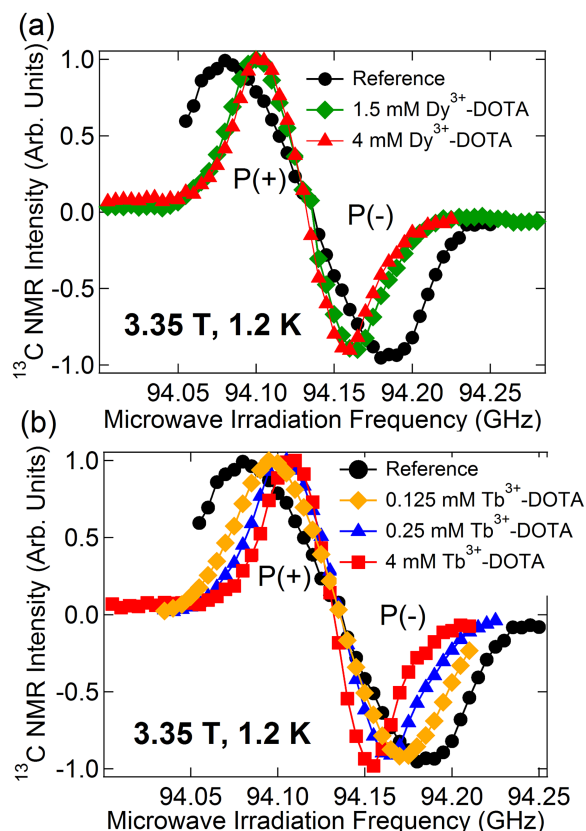
FIG. 3. Microwave frequency sweeps of ^{13}C DNP signals for 100 μl samples of 3M [1-^{13}C] sodium acetate in 1:1 v/v glycerol:water doped with 15 mM trityl OX063 and varying concentrations of (a) Dy-DOTA and (b) Tb-DOTA. All measurements were taken at 3.35 T and 1.2 K with a 100-mW sweepable microwave source.
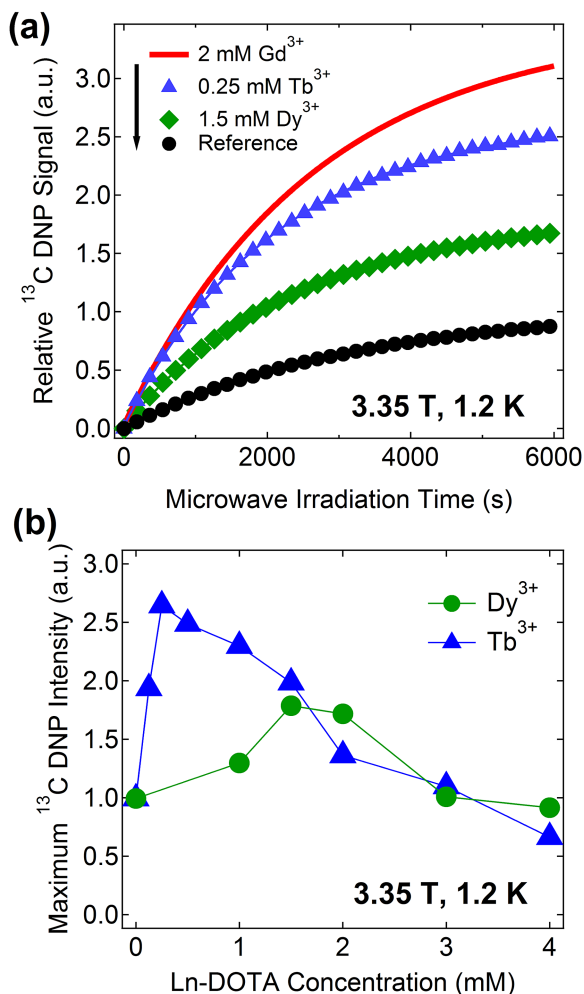
(a)

(b)

FIG. 4. (a) Relative ^{13}C DNP build-up curves for [1-^{13}C] acetate doped with 15 mM trityl OX063 and doped with the specified amount of Ln(III) complex. (b) The relative ^{13}C DNP enhancement of Tb^{3+}- and Dy^{3+}-doped samples as a function of their concentration. ^{13}C DNP intensities were normalized with respect to the DNP signal of the reference sample.

clear that, generally, a higher concentration of Tb or Dy leads to faster build-up. However, for Tb, even very small concentrations drastically reduce the polarization time, while for Dy, even high concentrations do not increase the polarization rate significantly. ^{13}C polarization build-up curves using optimal concentrations of each of the lanthanides studied are shown in Fig. 4(c). All curves are scaled such that the reference data are normalized. Dy was found to be the least effective of the lanthanides studied with a less than 2-fold enhancement. While ^{13}C DNP samples doping with Tb (~2.5-fold) and Ho (~3-fold) yielded significant improvements in DNP level with respect to that of the reference sample, it is apparent that Gd (~3.5-fold) doping in the sample results in the greatest solid-state ^{13}C polarization gain.

We would like to point out that the improved ^{13}C polarization level observed here with Tb^{3+} and Dy^{3+} doping is a combined result of determining the optimum doping concentration and optimum microwave irradiation frequency. Without carefully following the shifts in optimum microwave frequency with lanthanide doping, the advantage of Tb or Dy doping in ^{13}C DNP may not be as prominent as they were found to be here. For instance, the optimum microwave

frequencies for the reference (0 mM Tb-DOTA) and optimally Tb-doped (0.25 mM Tb-DOTA) ^{13}C DNP samples are approximately 25 MHz apart. Without the 25 MHz microwave shift correction for Tb doping, one could look at ^{13}C DNP spectra shown in Fig. 3(b) and predict that the polarization level will only be around 50% of the supposed maximum polarization. Furthermore, the achieved ^{13}C polarization levels are very dependent on the concentration of the lanthanides as can be seen in Fig. 4(b). The ^{13}C DNP enhancement effects of Dy^{3+} and Tb^{3+} doping reported here appear to be at odds with a previous study that showed that except for Gd^{3+} and Ho^{3+}, the other lanthanides including Tb^{3+} and Dy^{3+} had no apparent beneficial impact on ^{13}C DNP.[37] In terms of sample composition, the primary difference between the two studies is the use of Ln^{3+} chlorides by Gordon *et al.*,[37] whereas in this study each lanthanide was chelated in a DOTA complex. It is possible that the ligand to which the lanthanides are bound affects the magnetic properties in such a way as to increase ^{13}C polarization enhancement.[65–67] Moreover, the more probable reason for this difference in the results is that, unlike the aforementioned previous study,[37] the microwave frequency shift and lanthanide concentration dependence were carefully followed in this work.

The improvement of the ^{13}C DNP signal with lanthanide doping is attributed to the shortening of the electronic relaxation time of the free radical through interaction with the lanthanide dopant.[37,60,68] Under the thermal mixing model, this may be seen in Equation (1) in which η is reduced by a shortening of electronic T_1, leading to greater achievable polarization. It should be noted that the improvement of ^{13}C polarization may also be described using a combination of the cross and solid effects as presented by Ravera *et al.*[55] In either case, it is clear that there are a number of factors in addition to electronic T_1 that must contribute given that EPR shows that the trityl electron relaxation rate is similarly affected by each of the lanthanides studied. One possible explanation is the effect of a given lanthanide on the nuclear relaxation rate as discussed previously. Given this, though, it is difficult to pinpoint the origin of the significant polarization differences among the lanthanides. Of the four different lanthanides considered in this work, magnetic moment strength ranges from 7.94 μ_B for Gd^{3+} to 10.6 μ_B for Dy^{3+} and Ho^{3+} with Tb^{3+} intermediate at 9.7 μ_B.[65] Additionally, the electronic relaxation rates for Ho^{3+} and Tb^{3+} are nearly identical at room temperature, with Dy^{3+} having a slightly longer relaxation time and Gd^{3+} a relaxation time four orders of magnitude longer.[69,70] Of course, low temperatures could have a significant effect particularly on the relaxation behavior of lanthanide ions, but these values point to the difficulty of assigning a precise cause for the observed polarization behavior. It is currently unclear to us as to the exact cause of the drastic difference in optimal concentration for Tb^{3+} when compared to the other studied lanthanides. One possibility is that it might be related to the degenerate ground state present for this lanthanide. From all the lanthanides studied here presenting half-odd integer values, Tb^{3+} is the only one not belonging to the family of the Kramers ions. This is associated with non-constant magnetic moments in the absence (or presence) of an external magnetic field.[71,72]

C. Liquid state dissolution

After the optimal concentrations of Tb^{3+} and Dy^{3+} were determined, the liquid state properties of the samples with optimal concentrations were studied by rapidly dissolving the sample and monitoring the ^{13}C NMR signal in a 400 MHz high resolution magnet. We would like to note that the transfer of the dissolution liquid from the 3.35 T hyperpolarizer to the NMR tube in a 9.4 T NMR magnet takes 8 s to complete. All liquid-state ^{13}C NMR enhancements reported here were taken right after the dissolution transfer. In order to compare the liquid state enhancements of the Ln(III) doped samples, T_1 was determined by fitting the relaxation data to an exponential decay as previously described.[50,73] Nuclear relaxation due to both T_1 relaxation and RF pulse excitation was taken into account in this fitting. The data collected monitoring relaxation as well as the fitting is shown in Fig. 5(a). From this, it is clear that Gd^{3+}, despite being chelated in a DOTA complex, still has a significant shortening effect on the ^{13}C T_1 due to its strong paramagnetism.[74] Tb^{3+} and Dy^{3+}, on the other hand, have almost no effect on liquid-state T_1, with relaxation data essentially identical to the reference sample. This may be explained by the very rapid electronic relaxation times of the electrons of these lanthanides, which reduce the overall effect on nuclear relaxation.[37]

In order to quantify the overall liquid state enhancement achieved by each sample, the integrated area under each NMR peak was calculated for both the hyperpolarized (A_{HP}) and thermal (A_{Th}) signals. Then, the DNP enhancement was calculated as documented previously.[38] The hyperpolarized ^{13}C NMR spectra were taken approximately 8 s after the initial dissolution in order to accommodate the shuttling time from the polarizer to NMR magnet. A representative hyperpolarized and thermal signal, taken for the 0.25 mM Tb^{3+} sample, is shown in Fig. 5(b). The enhancements for Tb^{3+}, Dy^{3+}, Gd^{3+}, and the reference sample are shown in Fig. 5(c). Despite a solid state polarization about 3.5 times that of the reference, Gd^{3+} doping results in a liquid state enhancement just over twice that of the reference sample. Significantly, Tb^{3+} results in a nearly identical liquid state enhancement. This is a result of T_1 relaxation in the time interval between polarization and the start of the NMR scan. Because the relaxation rate with Gd^{3+} is increased, there is a greater amount of polarization lost during shuttling than for Tb^{3+} or Dy^{3+}, allowing for comparable liquid state enhancements for Tb^{3+} in spite of significantly lower solid state enhancement. The fact that Dy^{3+} and Tb^{3+} are less efficient relaxation agents compared to Gd^{3+} is advantageous for ^{13}C dissolution DNP since longer nuclear T_1 translates to longer hyperpolarization lifetime of ^{13}C spins.

IV. CONCLUSION

In summary, we have shown that in addition to Gd^{3+} and Ho^{3+} doping, Dy^{3+} and Tb^{3+} complexes are also beneficial additives to samples for ^{13}C DNP at 3.35 T and 1.2 K. Similar to the effects of Gd^{3+} and Ho^{3+} doping, the locations of the optimum microwave irradiation frequencies for ^{13}C samples doped with Dy^{3+} and Tb^{3+} are shifted depending upon the concentration, and thus it is important to carefully follow these shift corrections for optimized DNP results. The optimum concentrations for Tb-DOTA and Dy-DOTA doping were found to be 0.25 mM and 1.5 mM, respectively, which are relatively lower than the optimal DNP concentrations of Gd^{3+} (2 mM) and Ho^{3+} (2 mM) doping. At the optimum concentrations, Dy^{3+} and Tb^{3+} doping yielded significant improvements on the ^{13}C solid-state DNP signals, with enhancement factors of around 1.8 and 2.5-fold, respectively, relative to the ^{13}C DNP signal of a reference or undoped sample. W-band EPR results have shown that while the trityl OX063 free radical spectra are not significantly affected by lanthanide doping, the electron T_1 of the free radical is drastically reduced especially at low temperatures. The significant gain in ^{13}C DNP signal with lanthanide doping is ascribed to a thermal mixing model where shortened electron T_1 of the free radicals leads to dominant
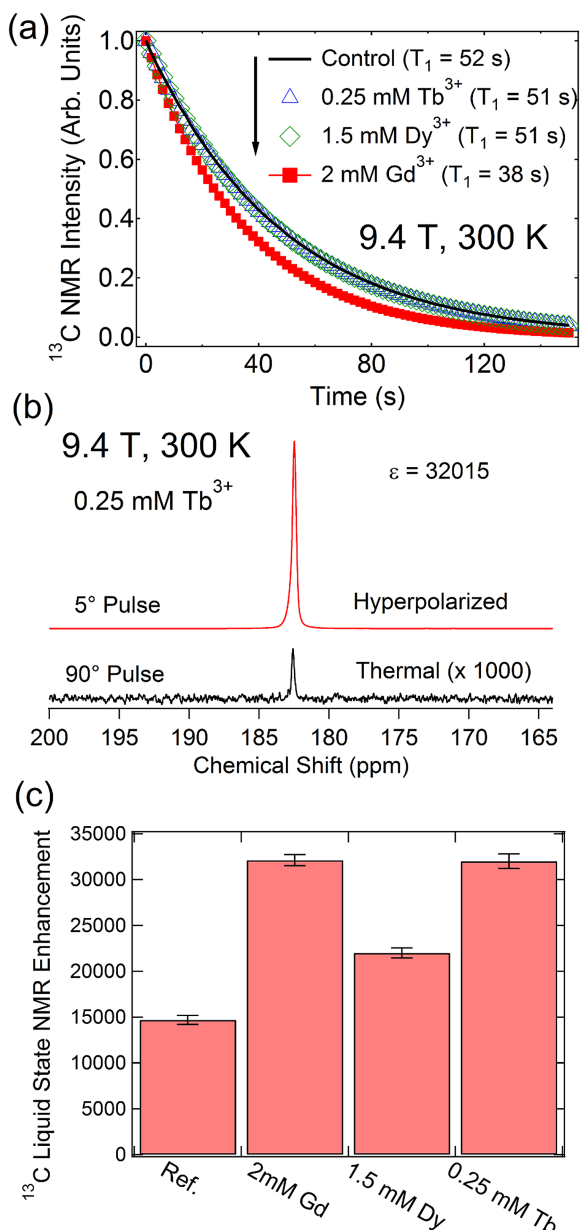

FIG. 5. (a) Decay of NMR signal intensity following dissolution of the polarized sample for a reference sample and samples doped with Tb^{3+}, Dy^{3+}, and Gd^{3+}. (b) Representative figure displaying the hyperpolarized and thermal ^{13}C NMR signal for a Tb^{3+}-doped sample. (c) Comparison of liquid state NMR enhancements for the Ln(III) complexes studied in this work.

electron cooling in DNP, thus resulting in lower spin temperature in electron dipolar system, and consequently higher nuclear polarization. Moreover, Tb^{3+} and Dy^{3+} are less effective relaxation agents compared to Gd^{3+}—an attribute that is advantageous in preserving the hyperpolarized state after the dissolution process.

ACKNOWLEDGMENTS

[1] A. Abragam, *The Principles of Nuclear Magnetism* (Clarendon Press, 1961).

[2] M. Brynda, in *Biomedical Applications of Biophysics*, edited by T. Jue (Humana Press, 2010), pp. 59–98.

[3] A. Abragam and M. Goldman, Rep. Prog. Phys. **41**, 395 (1978).

[4] A. W. Overhauser, Phys. Rev. **89**, 689 (1953).

[5] A. Abragam, Phys. Rev. **98**, 1729 (1955).

[6] C. D. Jeffries, Phys. Rev. **106**, 164 (1957).

[7] C. D. Jeffries, *Dynamic Nuclear Orientation* (Interscience Publishers, 1963).

[8] D. G. Crabb and W. Meyer, Annu. Rev. Nucl. Part. Sci. **47**, 67 (1997).

[9] J. H. Ardenkjær-Larsen, B. Fridlund, A. Gram, G. Hansson, L. Hansson, M. H. Lerche, R. Servin, M. Thaning, and K. Golman, Proc. Natl. Acad. Sci. U. S. A. **100**, 10158 (2003).

[10] J. H. Ardenkjaer-Larsen, J. Magn. Reson. **264**, 3 (2016).

[11] T. Prisner and W. Köckenberger, Appl. Magn. Reson. **34**, 213 (2008).

[12] F. A. Gallagher, M. I. Kettunen, and K. M. Brindle, Prog. Nucl. Magn. Reson. Spectrosc. **55**, 285 (2009).

[13] K. M. Brindle, S. E. Bohndiek, F. A. Gallagher, and M. I. Kettunen, Magn. Reson. Med. **66**, 505 (2011).

[14] K. Golman and J. S. Petersson, Acad. Radiol. **13**, 932 (2006).

[15] K. Golman, R. in 't Zandt, and M. Thaning, Proc. Natl. Acad. Sci. U. S. A. **103**, 11270 (2006).

[16] J. H. Ardenkjaer-Larsen, S. Macholl, and H. Jóhannesson, Appl. Magn. Reson. **34**, 509 (2008).

[17] U. L. Günther, in *Modern NMR Methodology*, edited by H. Heise and S. Matthews (Springer, Berlin, Heidelberg, 2011), pp. 23–69.

[18] L. Lumata, S. J. Ratnakar, A. Jindal, M. Merritt, A. Comment, C. Malloy, A. D. Sherry, and Z. Kovacs, Chem. - Eur. J. **17**, 10825 (2011).

[19] L. Lumata, M. Merritt, C. Khemtong, S. J. Ratnakar, J. van Tol, L. Yu, L. Song, and Z. Kovacs, RSC Adv. **2**, 12812 (2012).

[20] L. L. Lumata, M. E. Merritt, C. R. Malloy, A. D. Sherry, J. van Tol, L. Song, and Z. Kovacs, J. Magn. Reson. **227**, 14 (2013).

[21] A. Capozzi, J.-N. Hyacinthe, T. Cheng, T. R. Eichhorn, G. Boero, C. Roussel, J. J. van der Klink, and A. Comment, J. Phys. Chem. C **119**, 22632 (2015).

[22] P. Dutta, G. V. Martinez, and R. J. Gillies, J. Phys. Chem. Lett. **5**, 597 (2014).

[23] M. C. Cassidy, H. R. Chan, B. D. Ross, P. K. Bhattacharya, and C. M. Marcus, Nat. Nanotechnol. **8**, 363 (2013).

[24] J. Heckmann, W. Meyer, E. Radtke, G. Reicherz, and S. Goertz, Phys. Rev. B **74**, 134418 (2006).

[25] S. Jannin, A. Bornet, R. Melzi, and G. Bodenhausen, Chem. Phys. Lett. **549**, 99 (2012).

[26] S. Jannin, A. Comment, F. Kurdzesau, J. A. Konter, P. Hautle, B. van den Brandt, and J. J. van der Klink, J. Chem. Phys. **128**, 241102 (2008).

[27] A. Bornet, R. Melzi, A. J. Perez Linde, P. Hautle, B. van den Brandt, S. Jannin, and G. Bodenhausen, J. Phys. Chem. Lett. **4**, 111 (2013).

[28] M. Batel, M. Krajewski, A. Däpp, A. Hunkeler, B. H. Meier, S. Kozerke, and M. Ernst, Chem. Phys. Lett. **554**, 72 (2012).

[29] M. Batel, M. Krajewski, K. Weiss, O. With, A. Däpp, A. Hunkeler, M. Gimersky, K. P. Pruessmann, P. Boesiger, B. H. Meier, S. Kozerke, and M. Ernst, J. Magn. Reson. **214**, 166 (2012).

[30] B. Vuichoud, J. Milani, A. Bornet, R. Melzi, S. Jannin, and G. Bodenhausen, J. Phys. Chem. B **118**, 1411 (2014).

[31] P. Niedbalski, C. Parish, A. Kiswandhi, and L. Lumata, Magn. Reson. Chem. **54**, 962 (2016).

[32] L. Lumata, M. E. Merritt, and Z. Kovacs, Phys. Chem. Chem. Phys. **15**, 7032 (2013).

[33] F. Kurdzesau, B. van den Brandt, A. Comment, P. Hautle, S. Jannin, J. J. van der Klink, and J. A. Konter, J. Phys. D: Appl. Phys. **41**, 155506 (2008).

[34] L. Lumata, Z. Kovacs, A. D. Sherry, C. Malloy, S. Hill, J. van Tol, L. Yu, L. Song, and M. E. Merritt, Phys. Chem. Chem. Phys. **15**, 9800 (2013).

[35] L. Friesen-Waldner, A. Chen, W. Mander, T. J. Scholl, and C. A. McKenzie, J. Magn. Reson. **223**, 85 (2012).

[36] A. Kiswandhi, B. Lama, P. Niedbalski, M. Goderya, J. Long, and L. Lumata, RSC Adv. **6**, 38855 (2016).

[37] J. W. Gordon, S. B. Fain, and I. J. Rowland, Magn. Reson. Med. **68**, 1949 (2012).

[38] A. Kiswandhi, P. Niedbalski, C. Parish, P. Kaur, A. Martins, L. Fidelino, C. Khemtong, L. Song, A. D. Sherry, and L. Lumata, Phys. Chem. Chem. Phys. **18**, 21351 (2016).

[39] K. T. Rim, K. H. Koo, and J. S. Park, Saf. Health Work **4**, 12 (2013).

[40] X. Wang, T. Jin, V. Comblin, A. Lopez-Mut, E. Merciny, and J. F. Desreux, Inorg. Chem. **31**, 1095 (1992).

[41] L. D. Leon-Rodriguez and Z. Kovacs, Bioconjugate Chem. **19**, 391 (2008).

[42] G. W. White, W. A. Gibby, and M. F. Tweedle, Invest. Radiol. **41**, 272 (2006).

[43] K. T. Cheng, Molecular Imaging Contrast Agent Database MICAD, National Center for Biotechnology Information (US), Bethesda, MD, 2004.

[44] D. Meyer, M. Schaefer, and B. Bonnemain, Invest. Radiol. **23**(Suppl 1), S232 (1988).

[45] S. Aime, M. Botta, M. Fasano, and E. Terreno, Chem. Soc. Rev. **27**, 19 (1998).

[46] G. Pintacuda, M. John, X.-C. Su, and G. Otting, Acc. Chem. Res. **40**, 206 (2007).

[47] S. Aime, M. Botta, and G. Ermondi, Inorg. Chem. **31**, 4291 (1992).

[48] A. Barge, G. Cravotto, E. Gianolio, and F. Fedeli, Contrast Media Mol. Imaging **1**, 184 (2006).

[49] M. C. Cassidy, C. Ramanathan, D. G. Cory, J. W. Ager, and C. M. Marcus, Phys. Rev. B **87**, 161306 (2013).

[50] L. Lumata, A. K. Jindal, M. E. Merritt, C. R. Malloy, A. D. Sherry, and Z. Kovacs, J. Am. Chem. Soc. **133**, 8673 (2011).

[51] L. Lumata, M. E. Merritt, C. Malloy, A. D. Sherry, and Z. Kovacs, Appl. Magn. Reson. **43**, 69 (2012).

[52] J. Wolber, F. Ellner, B. Fridlund, A. Gram, H. Jóhannesson, G. Hansson, L. H. Hansson, M. H. Lerche, S. Månsson, R. Servin, M. Thaning, K. Golman, and J. H. Ardenkjaer-Larsen, Nucl. Instrum. Methods Phys. Res., Sect. A **526**, 173 (2004).

[53] S. Reynolds and H. Patel, Appl. Magn. Reson. **34**, 495 (2008).

[54] D. Banerjee, D. Shimon, A. Feintuch, S. Vega, and D. Goldfarb, J. Magn. Reson. **230**, 212 (2013).

[55] E. Ravera, D. Shimon, A. Feintuch, D. Goldfarb, S. Vega, A. Flori, C. Luchinat, L. Menichetti, and G. Parigi, Phys. Chem. Chem. Phys. **17**, 26969 (2015).

[56] D. Shimon, Y. Hovav, A. Feintuch, D. Goldfarb, and S. Vega, Phys. Chem. Chem. Phys. **14**, 5729 (2012).

[57] W. T. Wenckebach, Appl. Magn. Reson. **34**, 227 (2008).

[58] Y. Hovav, A. Feintuch, and S. Vega, J. Magn. Reson. **214**, 29 (2012).

[59] S. T. Goertz, Nucl. Instrum. Methods Phys. Res., Sect. A **526**, 28 (2004).

[60] L. Lumata, M. E. Merritt, C. R. Malloy, A. D. Sherry, and Z. Kovacs, J. Phys. Chem. A **116**, 5129 (2012).

[61] C. T. Farrar, D. A. Hall, G. J. Gerfen, S. J. Inati, and R. G. Griffin, J. Chem. Phys. **114**, 4922 (2001).

[62] T. A. Siaw, M. Fehr, A. Lund, A. Latimer, S. A. Walker, D. T. Edwards, and S.-I. Han, Phys. Chem. Chem. Phys. **16**, 18694 (2014).

[63] A. Abragam and B. Bleaney, *Electron Paramagnetic Resonance of Transition Ions* (Oxford University Press, Oxford, 2012).

[64] M. Borghini, Phys. Rev. Lett. **20**, 419 (1968).

[65] J. A. Peters, J. Huskens, and D. J. Raber, Prog. Nucl. Magn. Reson. Spectrosc. **28**, 283 (1996).

[66] K. Nwe, M. Bernardo, C. A. S. Regino, M. Williams, and M. W. Brechbiel, Bioorg. Med. Chem. **18**, 5925 (2010).

[67] N. Chatterton, C. Gateau, M. Mazzanti, J. Pécaut, A. Borel, L. Helm, and A. Merbach, Dalton Trans. **2005**, 1129.

[68] S. C. Serra, M. Filibian, P. Carretta, A. Rosso, and F. Tedoldi, Phys. Chem. Chem. Phys. **16**, 753 (2013).

[69] V. A. Atsarkin, V. V. Demidov, G. A. Vasneva, B. M. Odintsov, R. L. Belford, B. Radüchel, and R. B. Clarkson, J. Phys. Chem. A **105**, 9323 (2001).

[70] B. M. Alsaadi, F. J. C. Rossotti, and R. J. P. Williams, J. Chem. Soc., Dalton Trans. **1980**, 2151.

[71] E. D. T. de Lacheisserie, D. Gignoux, and M. Schlenker, *Magnetism* (Springer Science & Business Media, 2005).

[72] J. Solé, L. Bausa, and D. Jaque, *An Introduction to the Optical Spectroscopy of Inorganic Solids* (Wiley, 2005).

[73] B. R. Patyal, J.-H. Gao, R. F. Williams, J. Roby, B. Saam, B. A. Rockwell, R. J. Thomas, D. J. Stolarski, and P. T. Fox, J. Magn. Reson. **126**, 58 (1997).

[74] H. J. Weinmann, R. C. Brasch, W. R. Press, and G. E. Wesbey, Am. J. Roentgenol. **142**, 619 (1984).

CrossMark
← click for updates

Impact of Ho³⁺-doping on ¹³C dynamic nuclear polarization using trityl OX063 free radical

Andhika Kiswandhi,[a] Peter Niedbalski,[a] Christopher Parish,[a] Pavanjeet Kaur,[b] André Martins,[c] Leila Fidelino,[d] Chalermchai Khemtong,[d] Likai Song,[b] A. Dean Sherry[cd] and Lloyd Lumata*[a]

We have investigated the effects of Ho-DOTA doping on the dynamic nuclear polarization (DNP) of [1-¹³C] sodium acetate using trityl OX063 free radical at 3.35 T and 1.2 K. Our results indicate that addition of 2 mM Ho-DOTA on 3 M [1-¹³C] sodium acetate sample in 1 : 1 v/v glycerol : water with 15 mM trityl OX063 improves the DNP-enhanced ¹³C solid-state nuclear polarization by a factor of around 2.7-fold. Similar to the Gd³⁺ doping effect on ¹³C DNP, the locations of the positive and negative ¹³C maximum polarization peaks in the ¹³C microwave DNP sweep are shifted towards each other with the addition of Ho-DOTA on the DNP sample. W-band electron spin resonance (ESR) studies have revealed that while the shape and linewidth of the trityl OX063 ESR spectrum was not affected by Ho³⁺-doping, the electron spin–lattice relaxation time T_1 of trityl OX063 was prominently reduced at cryogenic temperatures. The reduction of trityl OX063 electron T_1 by Ho-doping is linked to the ¹³C DNP improvement in light of the thermodynamic picture of DNP. Moreover, the presence of Ho-DOTA in the dissolution liquid at room temperature has negligible reduction effect on liquid-state ¹³C T_1, in contrast to Gd³⁺-doping which drastically reduces the ¹³C T_1. The results here suggest that Ho³⁺-doping is advantageous over Gd³⁺ in terms of preservation of hyperpolarized state—an important aspect to consider for *in vitro* and *in vivo* NMR or imaging (MRI) experiments where a considerable preparation time is needed to administer the hyperpolarized ¹³C liquid.

1. Introduction

Due to its high specificity in molecular and structural elucidation of materials, nuclear magnetic resonance (NMR) is a valuable non-invasive analytical tool that is widely used in many areas of science and medicine. However, when compared to other spectroscopic methods, NMR is a rather insensitive technique especially when used on nuclei with low gyromagnetic ratio (γ) such as ¹³C spins. At ambient conditions and low concentrations, the time required for NMR data acquisition can become prohibitively long. This inherently low sensitivity in NMR emanates from the fact that nuclei have relatively low magnetic moments. As a consequence, the strength of the NMR signal which is proportional to polarization P or the nuclear spin population difference between the Zeeman energy

levels is relatively miniscule, with P on the order of only a few parts per million (ppm).[1,2]

On the other hand, electrons have a much larger magnetic moment than nuclei by about 3–4 orders of magnitude. Thus, electron spins can be easily polarized with P already approaching unity at low temperature close to 1 K and high magnetic field. By using slightly off-resonance microwave irradiation of samples doped with trace number of free electrons, a technique called dynamic nuclear polarization (DNP) can transfer this high electron spin alignment to nuclei with non-zero spin number.[1,2] This method consequently creates a large surplus of nuclear spins residing in one Zeeman energy level—a "hyperpolarized" state, which implies amplified NMR signals. The use of DNP can be traced back in the 1960s where highly polarized protons and deuterons were used as targets in nuclear scattering and particle physics experiments.[1,2]

The NMR signal amplification capability of DNP has find its practical application in chemistry and biomedicine with the invention of the dissolution DNP method by Ardenkjær-Larsen and co-workers in 2003.[3] Given that the spin–lattice relaxation time T_1 of nuclei of interest is sufficiently long, the amplified NMR signals of frozen polarized samples at cryogenic temperature can be mostly preserved in the liquid-state after rapid dissolution,

[a] *Department of Physics, University of Texas at Dallas, Richardson, TX 75080, USA. E-mail: lloyd.lumata@utdallas.edu*

[b] *National High Magnetic Field Laboratory, Florida State University, Tallahassee, FL 32310, USA*

[c] *Department of Chemistry, University of Texas at Dallas, Richardson, TX 75080, USA*

[d] *Advanced Imaging Research Center, University of Texas Southwestern Medical Center, Dallas, TX 75390, USA*

This journal is © the Owner Societies 2016

Phys. Chem. Chem. Phys., 2016, **18**, 21351–21359 | **21351**

translating to several thousand-fold NMR signal enhancements.[3] With the enhanced NMR sensitivity afforded by DNP, low-γ nuclei such as ^{13}C, ^{15}N, ^{6}Li, ^{89}Y, ^{107,109}Ag etc. can now be observed in 1 scan with excellent signal-to-noise ratio (SNR) even at millimolar (mM) concentrations.[3–8] The use of hyperpolarized ^{13}C-enriched biomolecules such as pyruvate, glucose, etc. has opened a new door to in vitro and in vivo metabolic NMR spectroscopy or imaging (MRI) that combines both excellent SNR and high chemical shift resolution.[9–16] Furthermore, this new technique also provides excellent temporal resolution, allowing for real-time analyses of metabolic activities in vitro in cells or in vivo in tissues of interest, which would be of great diagnostic and prognostic values for a variety of diseases.[9–16]

Due to the nature of this technology, the common theme in dissolution DNP is to achieve the highest polarization level in the solid-state and to preserve this polarization in the liquid-state. As such, optimization methods in sample preparation and DNP instrumentation are quite crucial to the success of in vitro or in vivo hyperpolarized ^{13}C NMR or MRI experiments. Different methods have been implemented in accordance to this theme. Among these optimization methods are the appropriate choice of free radical polarizing agents,[17–20] deuteration[21–23] and ^{13}C enrichment[24] of the glassing matrix, using polarizers operating at higher fields,[20,25–27] DNP cross polarization from ^{1}H spins to low-γ nuclei,[28] the use of trace amounts of lanthanides in the DNP sample,[29–32] the use of magnetic tunnel in shuttling of the liquid,[33] and dissolution in a fringe field area.[34] In this study, we have investigated the lanthanide doping method, in particular the effect of Ho^{3+}-doping on ^{13}C DNP. Previous studies have shown that lanthanides,[29–32] specifically Gd^{3+} complexes can significantly improve the DNP-enhanced polarization in the solid-state by a factor of 2–4 for samples doped with trityl OX063 free radical at 3.35 T. A previous study by Gordon et al. reported a set of DNP experiments on trityl-doped ^{13}C pyruvate samples in which the main finding was that only Ho^{3+}, in addition to Gd^{3+}, showed a beneficial improvement of DNP-enhanced ^{13}C polarization among the series of unchelated lanthanide ions used as dopants.[30] While Gd^{3+} complexes such as Gd-DOTA and Gd-HP-DO3A have been well studied and optimized as beneficial additives in DNP samples,[29–32] the use of Ho^{3+} doping has not been extensively investigated and optimized for DNP. Thus, the main goal of this research was to optimize the use of Ho^{3+} doping on ^{13}C DNP samples via extensive studies of its effects on the ^{13}C microwave DNP sweeps, relative ^{13}C polarization levels, and liquid-state ^{13}C enhancements and T_1. [1-^{13}C] sodium acetate, a biologically important substrate,[15,16] was chosen as the model ^{13}C compound in this study. It has a relatively lower cost and long liquid-state ^{13}C hyperpolarization lifetime comparable to that of the other popular DNP metabolic agents such as [1-^{13}C] pyruvate. The main DNP optimization data of this study were compared with ^{13}C DNP using the well-known DNP-enhancing Gd^{3+}-based dopant Gd-HP-DO3A. Furthermore, W-band electron spin resonance (ESR) was employed in this study to further elucidate the physical mechanisms behind the improvement of ^{13}C DNP signals with Ho^{3+}-doping.

2. Experimental

2.1 Sample preparation

All chemicals and reagents were acquired commercially and were used without further purification. 24.9 mg [1-^{13}C] sodium acetate (Cambridge Isotope Lab, MA) was added to a solution containing 1:1 v/v water:glycerol (Sigma-Aldrich, MO). 100 µL aliquots of these [1-^{13}C] acetate solutions were prepared a few hours before the experiment and subsequently frozen at −20 deg C. Each frozen solution was thawed and then mixed with 2.14 mg trityl OX063 free radical (Oxford Instruments Biotools, MA) right before the DNP experiment. The final concentrations of [1-^{13}C] acetate and trityl OX063 in the solution were 3 M and 15 mM, respectively. 100 µL aliquots of these DNP samples were prepared containing various concentrations of Ho-DOTA prepared from an aqueous stock solution of 218 mM Ho-DOTA (deionized water, pH = 7.2). Ho-DOTA was prepared by adding to Ho^{3+} solutions free ligand DOTA^{4+} (Macrocyclics, Dallas, TX) at M/L molar ratios of 1:1.05 and the resulting solutions were heated at 338 K under stirring for at least 12 h. The pH was maintained close to 7 by periodic addition of aqueous KOH. The absence of free Ho^{3+} ions in solution was verified by the xylenol orange test.[35–37] The Gd-HP-DO3A contrast agent or ProHance (Bracco Diagnostics, New Jersey) was purchased as a 0.5 M solution. The optimum DNP concentration of Gd-HP-DO3A (2 mM) in the ^{13}C DNP sample was prepared for use in comparative DNP studies with the Ho-doped samples. The structures of the trityl OX063 free radical and the two lanthanide complexes used in this study are displayed in Fig. 1.

2.2 Hyperpolarization and NMR measurements

The DNP experiments were performed at the Advanced Imaging Research Center at the University of Texas Southwestern Medical Center (UTSW) using a commercial polarizer HyperSense (Oxford Instruments, UK). This hyperpolarizer operates at 3.35 T and is equipped with a rootsblower pump vacuum system (Edwards Vacuum, UK) which provides a base temperature of 1.2 K for the cryostat sample space. A 100 mW ELVA microwave source (ELVA-1 millimeter Wave Division, RU) with 400 MHz sweepable frequency range was used to irradiate the samples.
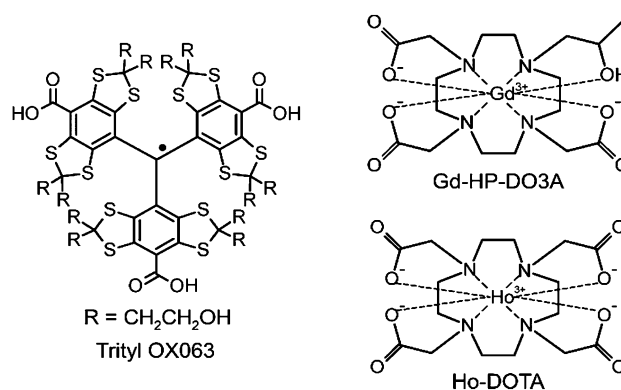

Fig. 1 Structures of the trityl OX063 free radical polarizing agent and the lanthanide complexes used in this work.

100 μL aliquots of ^{13}C DNP samples were inserted into the hyperpolarizer.

Prior to the polarization build-up experiments, ^{13}C microwave frequency sweeps were measured for ^{13}C samples with varying Ho^{3+} concentrations to determine their optimum microwave frequencies for the DNP, namely the positive P(+) and negative (P−) polarization peaks. For the DNP sweep, ^{13}C NMR signal was recorded after 3 minutes of microwave irradiation in 5 MHz steps using a DNP sweep program in the HyperSense. A train of hard pulses was applied after every ^{13}C NMR signal recording to avoid remnant polarization of a previous frequency step that may add up to the NMR signal of the next frequency step. The optimum P(+) and P(−) frequencies were located and normalized for comparison.

Once the optimum DNP frequencies were determined, ^{13}C polarization build-up curves were measured for each sample by recording the ^{13}C NMR signal every 3 minutes during irradiation of the sample at the P(+) microwave frequency. Due to instrumental difficulty and prohibitively long acquisition times needed in measuring the ^{13}C thermal NMR signals at cryogenic temperatures, we were not able to quantify the actual percent polarization levels for each sample in the frozen state. Instead, we have used relative polarization level as a method for evaluating the effect of this lanthanide complex on ^{13}C DNP. We note that such method has been nevertheless useful as a metric as demonstrated in previous DNP optimization studies.[22,23,30,32] The relative maximum ^{13}C DNP signal for each sample were recorded and normalized with respect to the ^{13}C DNP signal from the undoped reference sample. The solid-state ^{13}C polarization buildup curves for samples doped with 0 mM Ho (reference sample), 2 mM Ho (optimum concentration For Ho-DOTA), and 2 mM Gd (optimum concentration for Gd-HP-DO3A) were measured in triplicate. Three separate and freshly-made samples were used in the triplicate solid-state DNP build-up measurements. Relative bar graphs of mean values were plotted and normalized with respect to the reference sample. After the samples reached their maximum solid-state polarization, dissolution was carried out on these three aforementioned sets of samples to investigate the effects of Ho^{3+} and Gd^{3+} doping on ^{13}C NMR enhancement and ^{13}C T_1 in the liquid-state. Approximately 4 mL of aqueous dissolution liquid was rapidly transferred to a 10 mm NMR tube (Wilmad-LabGlass, NJ) inside a 400 MHz Varian NMR magnet (Agilent Technologies, CA) via a 0.125 in OD PTFE tubing (Cole-Parmer, IL). The dissolution transfer was done in an automated process and the total shuttling time of the hyperpolarized liquid from the HyperSense polarizer to the adjacent 9.4 T high resolution NMR magnet was 8 s. The liquid state T_1 decay of each sample was monitored by applying an array of 2-degree tip-angle RF pulse with 2-second repetition time. The first hyperpolarized ^{13}C NMR spectrum of this array was taken right after the 8-second dissolution transfer time with a time delay of 0.001 s. This hyperpolarized NMR spectrum, along with the subsequent thermal NMR measurement, was used in the liquid-state ^{13}C NMR enhancement calculation. The liquid-state T_1 values were calculated from the hyperpolarized ^{13}C NMR decay data using methods described previously.[6,38]

2.3 ESR measurements

ESR measurements were performed on the reference and samples doped with 2 mM Ho-DOTA to study the mechanism responsible for the DNP enhancement associated with Ho^{3+}-doping. The ESR measurements were carried out at the National High Magnetic Field Laboratory (NHMFL) in Tallahassee, FL. The W-band (94 GHz) measurements were performed on a Bruker E680 ESR spectrometer (Bruker Biospin, Billerica, MA) using a Bruker TE_{011} cylindrical cavity. The sample temperature was regulated using a CF1200 helium flow cryostat (Oxford Instruments, UK) down to 5 K to closely imitate the DNP polarization conditions. Samples were loaded in 0.15 mm I.D. thin quartz capillary tubes before inserting into the cylindrical cavity. The temperature-dependent trityl OX063 electron T_1 data were recorded by saturation recovery and the ESR spectra were collected using the field-swept electron spin-echo method.

2.4 Data analysis

The NMR, ESR, and DNP data were plotted and analyzed using Igor Pro version 6.2 (Wavemetrics, Lake Oswego, OR). The liquid-state ^{13}C NMR data gathered from Varian NMR spectrometer were processed using ACD labs version 12 (Advanced Chemistry Development, Toronto, Canada). Mean and standard values were calculated for samples done with $N = 3$ trials.

3. Results and discussion

The source of free electrons in DNP, mainly provided by stable organic free radicals, has a major impact in achieving the highest NMR signal enhancements.[17–20,39,40] The carbon-centered trityl OX063, the free radical used in this study, has a narrow ESR linewidth that is suited for polarizing low-γ nuclei such as ^{13}C. Numerous studies have shown that at least at $B_0 = 3.35$ T and temperatures close to 1 K, the predominant DNP process that allows for polarization transfer from trityl OX063 electrons to low-γ nuclei such as ^{13}C and ^{89}Y is the thermal mixing DNP mechanism.[6,7,41,42] Thermal mixing occurs when the source of free electrons has ESR linewidth D that is larger than or comparable to the Larmor frequency ω_n of the nucleus of interest.[1,2,40] In thermal mixing, a thermal contact is established between the electron dipolar system (EDS) and the nuclear Zeeman system (NZS) because of their compatible energies. Upon microwave irradiation, the spin temperature of EDS is lowered via dynamic cooling and due to the thermal link between the two reservoirs, the same low spin temperature is acquired by NZS.[1,2,40] This process translates to higher nuclear spin population difference or polarization, thus amplified NMR signals.

Since the free electrons are at the nexus of the polarization transfer process, perturbations to the electronic properties of the free radicals via addition of highly paramagnetic lanthanide complexes could contribute to changes in the maximum achievable nuclear polarization levels.[29,43] To extensively investigate the influence of Ho^{3+}-doping on ^{13}C DNP, we have first examined its effect on the ^{13}C microwave DNP sweeps as displayed in Fig. 2.
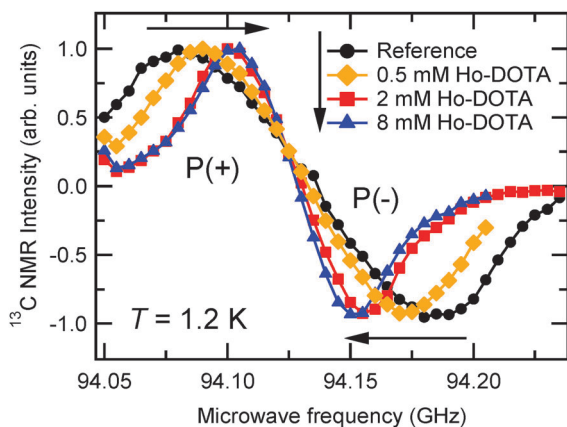
This journal is © the Owner Societies 2016

Phys. Chem. Chem. Phys., 2016, **18**, 21351–21359 | **21353**

Fig. 2 Normalized ^{13}C microwave DNP sweeps of 3 M [1-^{13}C] acetate in 1 : 1 v/v glycerol : water with 15 mM trityl OX063 and doped with varying concentrations of Ho-DOTA. These ^{13}C DNP data were taken at 3.35 T and 1.2 K. Two ^{13}C DNP maxima can be observed as denoted by P(+) and P(−). Note the shift in the locations of P(+) and P(−) with varying Ho-DOTA concentration. The arrows indicate the direction of increasing Ho-DOTA doping.

The ^{13}C microwave frequency sweeps, also known as ^{13}C microwave DNP spectra, are quite crucial since they provide the locations of the optimum microwave frequency peaks P(+) and P(−) for DNP.[23,29] It can be seen from Fig. 2 that the positions of the peaks vary with Ho-DOTA concentrations, where the separation between P(+) and P(−) become closer with increasing Ho-DOTA concentrations. Initially, the positions of both P(+) and P(−) peaks shift by approximately 10 MHz towards the center with an addition of 0.5 mM Ho-DOTA. Further increasing the Ho-DOTA concentration, the optimum microwave frequency shifts by another 10 MHz at 2 mM Ho-DOTA doping. However, at concentrations larger than 2 mM there is no significant shift in either P(+) or P(−) up to 8 mM. These optimum frequency shifts with Ho^{3+}-doping are reminiscent of similar behaviour with the effect of Gd^{3+}-doping on ^{13}C microwave DNP spectra.[29] Based on our data, we note that following the exact shift of P(+) or P(−) with Ho-doping could have a profound effect in achieving the highest ^{13}C DNP enhancement. For instance, it is estimated from the ^{13}C microwave spectra in Fig. 2 that ^{13}C DNP at 2 mM Ho^{3+}-doping without the corresponding 20 MHz P(+) peak shift correction from the reference sample will only yield about one-half of the maximum polarization that can be achieved if the sample was irradiated at the optimum frequency. Therefore, these peak shift corrections due to lanthanide doping are important considerations to achieve the highest NMR signal enhancements in DNP. On a separate but relevant theoretical note, the locations of P(+) and P(−) peaks can be approximately predicted by a spin-temperature model first put forth by Borghini.[1,44,45] In this model, the shape of the microwave DNP spectrum as well the maximum polarization values at P(+) and P(−) are almost exclusively dependent upon the shape and features of the ESR spectrum of the free radical polarizing agent used, and to a lesser extent, also upon the electron and nuclear relaxation rates.[1,44] Thus, an important question to answer is whether or not the presence of Ho^{3+} complex in the DNP samples affect the

electronic properties of the trityl OX063 free radical, leading to changes in the ^{13}C microwave DNP spectra. We will revisit this question in the subsequent discussion of relevant ESR data in this study.

With the optimum microwave frequencies for DNP identified, we then proceeded with the investigation of the growth of ^{13}C NMR signals as a function of microwave irradiation time for trityl-doped [1-^{13}C] acetate samples containing various concentrations of Ho-DOTA. Fig. 3a shows the representative ^{13}C solid-state polarization build-up curves of Ho^{3+}-doped ^{13}C samples as well as a sample doped with DNP optimum concentration of Gd-HP-DO3A. The ^{13}C DNP data were taken at the corresponding P(+) microwave frequency of each sample at 3.35 T and 1.2 K using a 100 mW microwave source. These ^{13}C DNP signal buildup curves were measured on the same volumes of DNP samples (100 µL) with the same [1-^{13}C] acetate (3 M) and trityl OX063 (15 mM) concentrations, type of glassing solvents (1 : 1 v/v glycerol : water), and DNP conditions (3.35 T and 1.2 K). Thus, their maximum ^{13}C NMR signals can be used as a polarimeter that reflect their relative ^{13}C polarization levels. Fig. 3b provides a summary of the relative ^{13}C DNP signals of all ^{13}C samples with varying Ho-DOTA concentrations; these data points correspond to the maximum ^{13}C NMR signals of the samples normalized with respect to the ^{13}C signal of the reference sample (0 mM Ho-DOTA). As can be seen from Fig. 3b, there seems to be a linear increase in the relative ^{13}C polarization as the Ho^{3+} concentration is increased from 0 mM to 2 mM. Then, a monotonic decrease of ^{13}C DNP signal can be observed with further increase of Ho^{3+} concentration from 2 mM to 8 mM. The optimum concentration of Ho-DOTA for ^{13}C DNP was found to be 2 mM. This result is similar to the optimum concentration reported for Gd^{3+}-doping on ^{13}C DNP.[29] However, the overall profile of Ho^{3+} concentration dependence of ^{13}C DNP signal has a subtle difference from that of previously reported Gd^{3+} doping DNP results. Ho^{3+}-doping exhibits a peak in maximum ^{13}C DNP signal at 2 mM then a steady decrease beyond this concentration, whereas in a previously published report,[29] Gd^{3+}-doping exhibits a plateau in maximum ^{13}C DNP signal from 2 mM to 5 mM then a monotonic decrease in DNP signal at higher concentrations. In Fig. 3c, the relative ^{13}C polarization levels achieved with optimum Ho-DOTA (2 mM) and Gd-HP-DO3A (2 mM) are compared as bar graphs normalized vis-à-vis the reference sample. The error bars are standard deviations for $N = 3$ trials. It can be readily observed from Fig. 3c that Ho-doping further enhanced the solid-state ^{13}C DNP signal of acetate by a factor of 2.7-fold, whereas Gd^{3+}-doping resulted in a 3.5-fold enhancement of the ^{13}C DNP signal of the reference sample. Thus, Gd^{3+}-doping, in this case, yielded slightly better ^{13}C solid-state polarization enhancement than Ho^{3+}-doping.

To further elucidate these ^{13}C DNP behaviour with Ho^{3+}-doping, ESR was performed on the reference sample and an optimally Ho-doped ^{13}C samples. Thus, we revisit that previous question on whether or not Ho^{3+}-doping affect the electronic properties of the free radical polarizing agent. First, inspection of Fig. 4a reveals that the shape and linewidth of the trityl OX063 W-band ESR spectrum at 10 K are essentially the same with or without Ho-DOTA. This finding is reminiscent of the
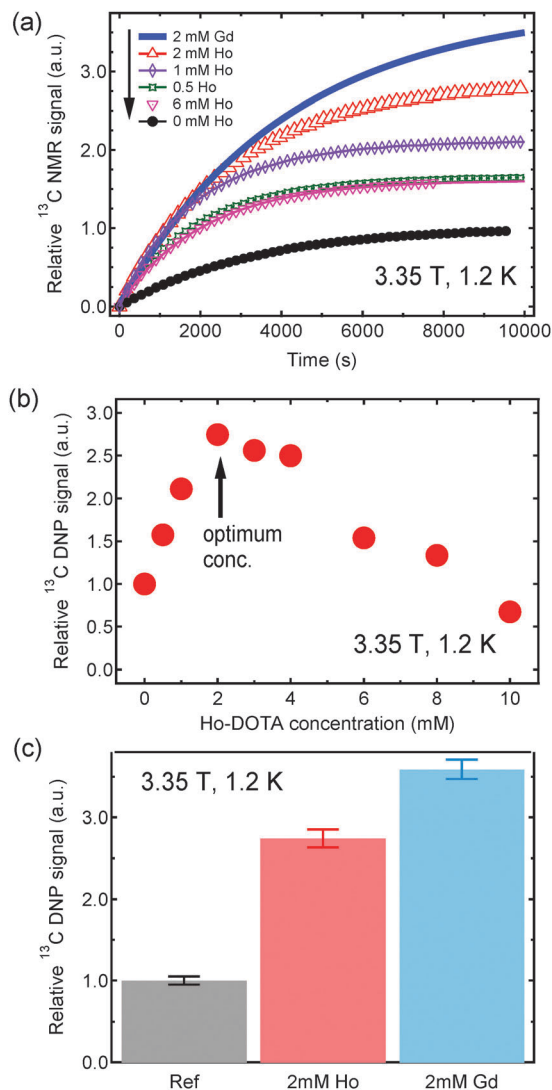
21354 | *Phys. Chem. Chem. Phys.*, 2016, **18**, 21351–21359

This journal is © the Owner Societies 2016

Fig. 3 (a) Representative normalized ^{13}C polarization build-up curves in the solid-state for 100 μL aliquots of 3 M [1-^{13}C] sodium acetate in 1 : 1 v/v glycerol : water with 15 mM trityl OX063 and doped with various concentrations of Ho-DOTA. For comparison, the build-up curve for the same ^{13}C sample doped with 2 mM Gd-HP-DO3A is included. (b) A summary of the relative ^{13}C maximum DNP signal for various concentrations of Ho-DOTA. The up arrow indicates the optimum Ho^{3+} concentration for DNP. (c) Comparative bar graph representations of the average relative ^{13}C DNP signals ($N = 3$) for the reference sample, and samples doped with 2 mM Ho-DOTA, and 2 mM Gd-HP-DO3A. All ^{13}C DNP data were taken at 3.35 T and 1.2 K.
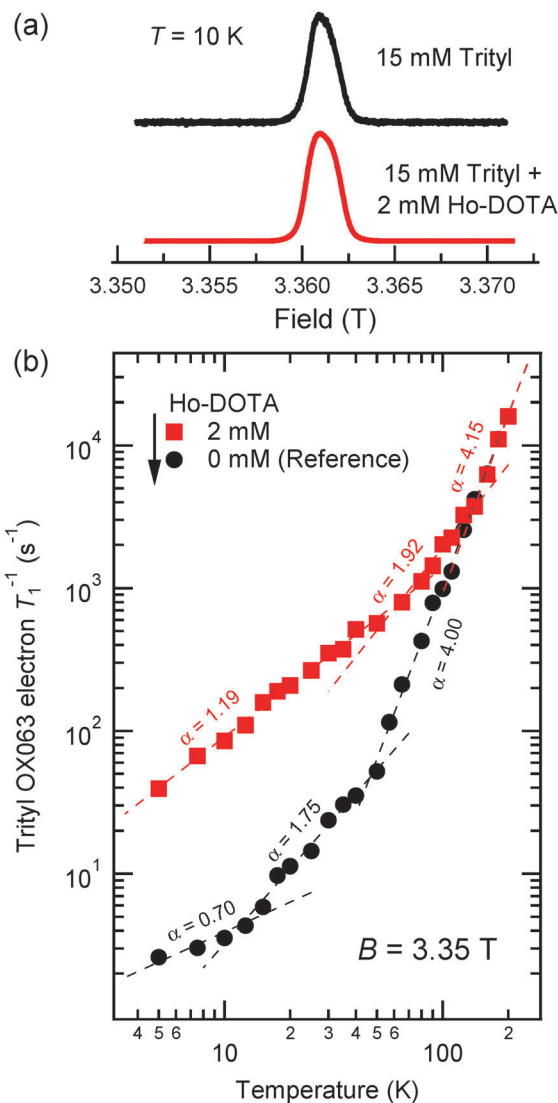

Fig. 4 (a) W-band ESR spectra of 15 mM trityl OX063 in 1 : 1 v/v glycerol : water with 3 M [1-^{13}C] sodium acetate in the presence and absence of 2 mM Ho-DOTA. Both spectra were measured at 10 K. (b) The temperature dependence of the trityl OX063 electron relaxation rate T_1^{-1} at W-band for the reference sample (solid circles) and the Ho^{3+}-doped sample (solid squares). The dashed lines are fits to a power-law equation mentioned in the text, with the approximate values of exponent α values given next to the fits.

previously reported ESR result for Gd-HP-DO3A in which the trityl OX063 spectrum was also not affected by the presence of an optimum DNP concentration of Gd^{3+} in the sample.[43] In addition, the W-band ESR signal of Ho^{3+} could not be detected, even in wider ESR spectral window. This behaviour is attributed to the very short relaxation times of Ho^{3+}, and lanthanides in general, even at this temperature which pose a challenge for direct ESR detection. Within the framework of the Borghini model for DNP,[1,44] the narrowing of the ^{13}C microwave DNP spectra with Ho^{3+}-doping shown in Fig. 2 does not seem to fit with the absence of visible changes in the trityl OX063 ESR

spectrum with Ho^{3+}-doping shown in Fig. 4a. As stipulated before, the Borghini prediction of microwave DNP spectrum is almost entirely dependent on the shape and size of the ESR spectrum of the polarizing agent in DNP.[44,45] There is, however, another term in the Borghini model equation that involves the ratio of the electron and nuclear relaxation times, which is often considered negligible since electron relaxation is still relatively small ranging from few μs to a second and nuclear relaxation is extremely long on the order of several-thousand seconds at cryogenic temperatures.[1] Qualitatively, it is thus suggested that the changes in the ^{13}C microwave DNP spectra due to Ho^{3+}-doping may be attributed to changes in the electron relaxation. A possible alternative explanation to microwave frequency shift with Ho-doping is that the DNP mechanism may be a combination

of solid effect and cross effect as suggested by previous studies that were done at relatively higher DNP temperatures of 6.5 K or above.[46,47] Based on this mechanism, it would seem that addition of lanthanide may cause the microwave DNP frequency shift by reducing the solid effect contribution and increasing the influence of cross effect, leading to a narrowing of the ^{13}C microwave DNP spectra. However, we note that it is also possible that the physics of DNP at 6.5 K or higher may be quite different for DNP done at $T \sim 1$ K. As mentioned before, mounting experimental evidence[6,7,41,42] suggest that thermal mixing is the predominant DNP mechanism for low-γ nuclei such as ^{13}C, ^{89}Y, *etc.*, at least at DNP conditions of 3.35 T and $T \sim 1$ K in which we have performed the experiments. Further combined DNP and ESR studies at these conditions may be needed to fully clarify these effects.

Next, we have also closely examined the effect of Ho^{3+}-doping on the trityl OX063 electron relaxation rate T_1^{-1} as shown in Fig. 4b. Before discussing the details and analysis of the relaxation data, we note that the electron T_1 data here were obtained by fitting the electron relaxation recovery curves at different temperatures with a double-exponential build-up function $M(t) = M_a \exp(-t/T_{1,a}) + M_b \exp(-t/T_{1,b}) + C$. In this equation, C is a constant, the longer time constant $T_{1,a}$ is the actual electron T_1 value of the free radical, and the smaller time constant $T_{1,b}$ corresponds to the contribution from electron-electron cross relaxation effects.[48,49] The electron T_1^{-1} *versus* temperature data shown in log–log scale in Fig. 4b were fitted to the power law equation $T_1^{-1} = AT^\alpha$, with the values of α given in Fig. 4b. For the reference sample, the trityl OX063 relaxation rate decreases rapidly with decreasing temperature, following $\alpha \approx 4$ dependence at high temperatures above 50 K. This result indicates that in this temperature regime, the predominant electron relaxation mechanism could be due to a combination of two-phonon Raman and other mechanisms such as three-phonon Orbach process.[50] As the temperature decreases further in the intermediate range from 50 K to around 20 K, the rate of change of T_1^{-1} for the reference sample slows down to $\alpha \approx 2$ dependence, indicating that the electronic relaxation mechanism is dominated by Raman process.[50] At lower temperatures, the relaxation rate further slows down to either $\alpha \approx 1$ or 0, indicative of the one-phonon direct process being the predominant electron relaxation mechanism.[50] Meanwhile, for the sample doped with 2 mM Ho^{3+}, the relaxation rate values almost overlap with those of the reference sample at higher temperature above 100 K. Below this temperature, it becomes apparent that the relaxation rates for the sample with Ho^{3+} is higher and this relaxation rate difference between the two samples becomes more prominent at lower temperatures. Below 60 K, the relaxation rate of the Ho^{3+}-doped sample appears to behave according to the direct process relaxation mechanism. At 5 K, which is the base temperature of the ESR cryostat, the presence of 2 mM Ho^{3+} in the sample resulted in a drastic reduction of the electron T_1 of trityl OX063 from 380 ms to about 25 ms. Following these low temperature power law trends, it seems likely that direct process would still be the dominant relaxation process for both samples at temperatures close to 1 K where DNP is performed.

Similar to the physical mechanism on DNP with Gd^{3+}-doping,[29] we qualitatively attribute the improvement of the ^{13}C DNP signal with Ho^{3+}-doping to the reduction in electron T_1 of trityl OX063 free radical. We invoke the thermodynamic model of DNP equation in which the theoretical maximum limit of polarization is given by the following equation:[29,40]

$$P_{\text{DNP,max}} = \tanh\left(\beta_{\text{L}} \frac{\omega_{\text{e}}\omega_{\text{I}}}{4D} \frac{1}{\sqrt{\eta(1+f)}}\right) \tag{1}$$

where $\beta_{\text{L}} = \hbar/k_{\text{B}}T_{\text{L}}$ (T_{L} is the lattice temperature), ω_{e} is the electron Larmor frequency, ω_{I} is the nuclear Larmor frequency, and D is the ESR linewidth of the electron system. The remaining factors in eqn (1) are $\eta = T_{1,Z}/T_{1,D}$, which is the ratio of the relaxation times of the electron Zeeman system to the electron dipolar spin–lattice system and f, which is the "leakage factor". The leakage factor f is caused by nuclear relaxation mechanisms other than the coupling of nuclei with the free electron spins involved in DNP.[1] In eqn (1), at a constant field and temperature, the factors β_{L}, ω_{e}, and ω_{I} in this study are the same between the reference and the Ho-doped samples. Based on the trityl ESR spectra, there is no significant change in D with Ho-doping. Therefore, assuming the "leakage factor" remains unchanged, the decrease of electron T_1 is the factor responsible for the improved DNP enhancement, similar to the effect of Gd-doping.[23,29,39] At this point, using eqn (1) as a guide, we can only provide qualitative explanation for linking the improved ^{13}C DNP efficiency with the reduction of trityl OX063 electron T_1 with Ho-doping, similar to the behaviour observed in ^{13}C DNP with Gd-doping.[29] Further experimental studies are needed to provide a more quantitative way of elucidating the relationship between these two aforementioned physical parameters in DNP.

Finally, we have also evaluated the effects of Ho-doping in dissolution DNP. Since the thermal and hyperpolarized NMR measurements were done on the same sample and with the same number of transients, the liquid-state enhancement relative to the thermal NMR signal was quantified using the following equation:[6]

$$\varepsilon = \frac{A_{\text{DNP}}}{A_{\text{Th}}} \frac{\sin \theta_{\text{Th}}}{\sin \theta_{\text{DNP}}} \tag{2}$$

where A_{DNP} and A_{Th} are the integrated areas of the hyperpolarized and the thermal signals, respectively and θ_{DNP} and θ_{Th} are their corresponding tip angles. In our experiment, the hyperpolarized and the thermal NMR signals were measured using 2° and 90° tip-angle pulses, respectively. Both thermal and DNP signal were measured with 1 transient. In addition, it should be noted that the values of liquid-state NMR enhancements reported were measured approximately 8 s after dissolution liquid transit time from polarizer to NMR magnet. Fig. 5a shows the representative ^{13}C thermal and hyperpolarized NMR spectra in the liquid-state at 9.4 T and 297 K are shown in Fig. 5a. A summary of the average ($N = 3$) ^{13}C NMR enhancements for the reference and ^{13}C DNP samples doped with 2 mM Ho-DOTA and 2 mM Gd-HP-DO3A is depicted on Fig. 5b. For the reference sample, the average liquid-state ε for [1-^{13}C] acetate DNP sample was

21356 | *Phys. Chem. Chem. Phys.,* 2016, **18**, 21351–21359
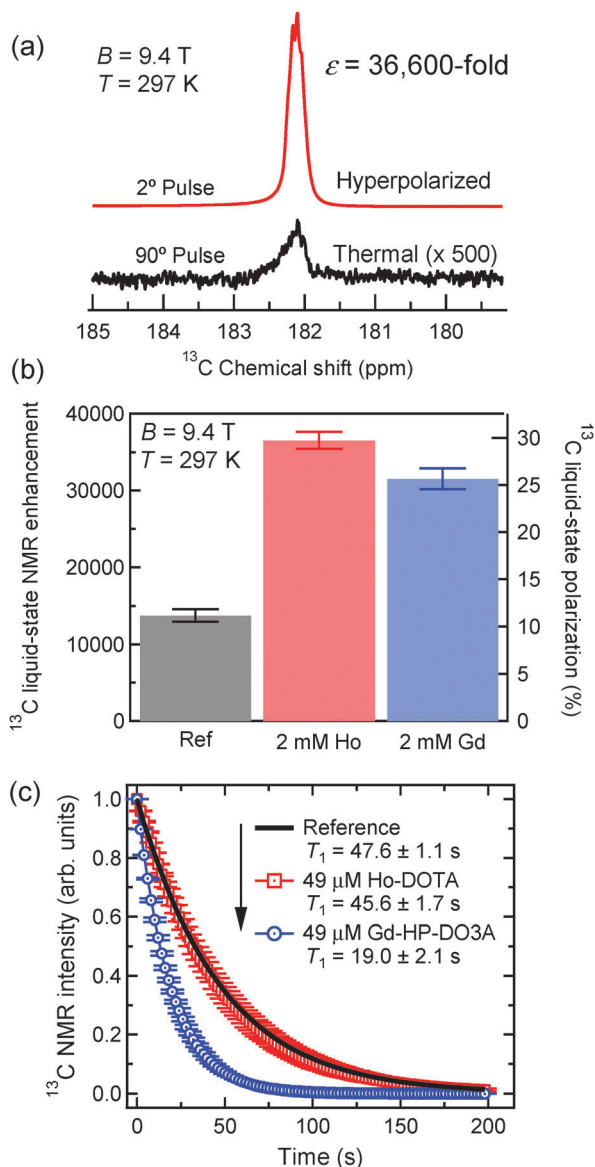
This journal is © the Owner Societies 2016

Fig. 5 (a) Representative thermal and hyperpolarized ^{13}C NMR signals of [1-^{13}C] sodium acetate in aqueous solutions after dissolution. The hyperpolarized signal was acquired using a 2° pulse at 9.4 T and 297 K. The thermal signal was taken using a 90° pulse with 1 transient and has been magnified by 500 times for clarity. (b) Average liquid-state ^{13}C NMR signal enhancements ($N = 3$) for the reference sample and for samples originally doped with 2 mM Ho-DOTA and 2 mM Gd-HP-DO3A in the polarizer. These enhancement values were measured 8 s after the dissolution transfer to the NMR magnet at 9.4 T and 297 K. The equivalent percent polarization level for the liquid-state ^{13}C NMR enhancement is displayed on the right axis. (c) Normalized ^{13}C hyperpolarization decay curves for the three aforementioned samples from which the corresponding liquid-state ^{13}C T_1 values were calculated.

found to be 13 700 ± 800 ($P = 11.2 ± 0.6\%$), while the sample doped with 2 mM Ho-DOTA gives an enhancement factor of 36 600 ± 1100 ($P = 29.7 ± 0.9\%$). These liquid-state ε values are roughly proportional to their relative solid-state ^{13}C DNP signals where the Ho-doped sample is about 2.7 times the DNP-enhanced polarization level of the reference sample. On the other hand,

the enhancement factor for the Gd-doped sample was only 31 500 ± 1350 ($P = 25.60 ± 1.1\%$), which is lower than the Ho-doped sample despite the fact that it has the highest relative ^{13}C solid-state DNP enhancement of about 3.5 times the DNP signal of the reference sample. This implies that the loss of liquid-state ^{13}C DNP signal due to T_1 relaxation during the dissolution liquid transit is more prominent in Gd-doped sample than the other 2 samples.

To determine the liquid-state ^{13}C T_1, the ^{13}C DNP relaxation decay curves were fitted to the following equation, which describes the polarization loss due to both the T_1 relaxation effect and radiofrequency (RF) pulsing:[6,38]

$$P(t) = P_0 \sin\theta (\cos\theta)^{t/\mathrm{TR}} e^{-t/T_1} \qquad (3)$$

where P, θ, t, TR, and T_1 are the polarization, the NMR tip angle, time, the repetition time, and the longitudinal relaxation time constant, respectively. In our setup, the RF tip angle θ for hyperpolarization was set as 2° with TR = 2 s. Fig. 5a shows the normalized ^{13}C polarization decay curves of the reference sample, and those doped with Ho^{3+} and Gd^{3+}. Based on these data, the calculated ^{13}C T_1 of trityl-doped [1-^{13}C] acetate reference sample is 47.6 ± 1.1 s. Meanwhile, addition of 2 mM Gd contrast agent in a 100 μL sample then dilution with 4 mL of water resulted in a reduction of liquid-state T_1 by nearly 60%, with $T_1 = 19.0 ± 2.1$ s in the presence of 49 μM Gd-HP-DO3A. On the other hand, Ho-DOTA doping of same amount as Gd-HP-DO3A did not lead to any significant difference in T_1 of ^{13}C, with liquid-state $T_1 = 45.9 ± 1.7$ s. This is apparent with the overlapping ^{13}C polarization decay curves of the reference sample and Ho^{3+}-doped sample shown in Fig. 5c. We note that if we assume that during the dissolution transfer of 8 s the predominant cause of DNP signal loss is T_1 decay, the calculated polarization levels at $t = 0$ s prior to dissolution are around 13%, 35%, and 40% for the reference, Ho-doped, and Gd-doped samples, respectively. These back-calculated polarization values are in close proportion to the relative ^{13}C solid-state polarization levels shown in Fig. 3c.

On a related note, we would like to point out that previous studies have shown that the type of chelation ligands can also affect both the polarization levels and T_1 relaxation times, at least for Gd^{3+} compounds.[30,32] The use of chelating ligands in lanthanide dopants is recommended in dissolution DNP to reduce the toxicity especially in *in vivo* experiments. In a previous study, Gd^{3+}-based contrast agents with macrocyclic ligands such as Gd-DOTA yielded less T_1 reduction effect and higher liquid-state NMR enhancements compared to samples doped with Gd^{3+} compounds with open-chain ligands such as Gd-EDTA.[32] On the other hand, T_1 reduction with Ho^{3+} is generally very minimal, regardless of the type of chelation ligand.[30] Overall, the use of lanthanide compounds with macrocyclic ligands is a preferred choice in dissolution DNP because of better stability, enhancement levels, and hyperpolarization lifetimes in the liquid-state.

The reduced T_1 effect observed upon addition of the Gd(III)-complexes is a well-known phenomenon. Gd^{3+} ions contain seven f-orbital unpaired electrons, a symmetric S-state, and its electronic relaxation is relatively slow. Gd-complexes are

This journal is © the Owner Societies 2016

Phys. Chem. Chem. Phys., 2016, **18**, 21351–21359 | **21357**

extensively used in contrast-enhanced MRI because these compounds are efficient nuclear T_1 relaxation agents.[51,52] Although its use has been mainly applied to reduce the T_1 of protons in water, similar effect can be observed in other nuclei, such as ^{13}C, ^{15}N, and ^6Li.[33–35] Curie relaxation is actually larger for Gd^{3+} than for Ho^{3+}, but dipolar relaxation is orders of magnitude larger for Gd than for Ho. As a result, Ho^{3+} is a less efficient T_1 relaxation agent compared to Gd^{3+}.[51,53] The strong relaxivity effect of Gd^{3+}, while beneficial for T_1-weighted conventional MRI, will present a problem when used in hyperpolarized ^{13}C experiments where longer preparation time (e.g. 15–30 s) is needed before administering the hyperpolarized ^{13}C liquid such as in in vivo hyperpolarized ^{13}C MRI. Furthermore, hyperpolarized ^{13}C experiments with bigger animal subjects may necessitate larger ^{13}C DNP sample volume (e.g. >100 μL) in which case the ^{13}C T_1 of the dissolution liquid will be reduced further in the presence of increased Gd^{3+} concentration, eventually negating the improved ^{13}C DNP polarization acquired in the solid-state due to Gd-doping. Based on our results, Ho-doping is advantageous over Gd-doping in terms of preservation of the usable enhanced liquid-state polarization in dissolution DNP.

4. Conclusion

In conclusion, we have found that inclusion of an optimum concentration of Ho-DOTA of around 2 mM in trityl-doped ^{13}C sample can significantly improve the ^{13}C solid-state polarization level, by about 2.7 times the ^{13}C DNP signal of the reference DNP sample at 3.35 T and 1.2 K. Ho^{3+}-doping resulted in the narrowing of the ^{13}C microwave DNP spectrum, so one must closely follow the shift in the optimum ^{13}C microwave frequencies to get the highest ^{13}C DNP signal. W-band ESR study has revealed that the shape and linewidth of the trityl OX063 ESR spectrum were not affected by Ho^{3+}-doping. However, the trityl OX063 electron T_1 was drastically reduced at cryogenic temperatures in the presence of 2 mM Ho-DOTA. Below 60 K, the electron relaxation rate versus temperature data for trityl OX063 in the presence of 2 mM Ho-DOTA appear to follow a power-law dependence indicative of the one-phonon direct process. Within the framework of the thermodynamic model for DNP, we ascribe the improvement of the ^{13}C DNP signal with Ho^{3+}-doping to the reduction of the electron T_1 of the trityl OX063 free radical. Similar to the DNP effect with Gd^{3+}-doping, the presence of Ho-DOTA in the trityl-doped ^{13}C sample lowers the spin temperature of the trityl OX063 electron dipolar system, which is in thermal contact with the nuclear Zeeman system, thus resulting in further enhancement of the ^{13}C DNP signal. Gd^{3+}-doping resulted in a slightly better ^{13}C solid-state DNP signal improvement than Ho^{3+}-doping, however this initial advantage of Gd^{3+} is negated by its strong reduction of ^{13}C T_1 of the hyperpolarized liquid. In comparison, the presence of Ho-DOTA in the hyperpolarized liquid, after dissolution of a typical ^{13}C DNP sample volume of 100 μL with 4 mL water, has a negligible or minimal reduction effect in liquid-state ^{13}C T_1. At least for the ^{13}C samples and DNP conditions described here, Ho^{3+}-doping consequently results in a

better ^{13}C NMR enhancements in the liquid-state than Gd^{3+}-doping right after the transit time of the dissolution liquid. It is anticipated that the reduction effect on polarization due to shorter ^{13}C T_1 with Gd-doping will become even more pronounced In hyperpolarized in vitro or in vivo ^{13}C NMR or MRI experiments where an extra preparation time and/or a larger DNP sample is needed. Therefore, especially in such cases, the use of Ho^{3+} complexes such as Ho-DOTA in a ^{13}C DNP sample may prove quite advantageous over Gd^{3+}-doping as it is expected to provide higher liquid-state ^{13}C NMR enhancement levels.

Notes and references

1 A. Abragam and M. Goldman, Rep. Prog. Phys., 1978, **41**, 395.
2 D. G. Crabb and W. Meyer, Annu. Rev. Nucl. Part. Sci., 1997, **47**, 67.
3 J. H. Ardenkjær-Larsen, B. Fridlund, A. Gram, G. Hansson, L. Hansson, M. H. Lerche, R. Servin, M. Thaning and K. Golman, Proc. Natl. Acad. Sci. U. S. A., 2003, **100**, 10158–10163.
4 W. Jiang, L. Lumata, W. Chen, S. Zhang, Z. Kovacs, A. D. Sherry and C. Khemtong, Sci. Rep., 2015, **5**, 9104.
5 R. Balzan, M. Mishkovsky, Y. Simonenko, R. B. van Heeswijk, R. Gruetter, U. Eliav, G. Navon and A. Comment, Contrast Media Mol. Imaging, 2016, **11**, 41–46.
6 L. Lumata, A. K. Jindal, M. E. Merritt, C. R. Malloy, A. D. Sherry and Z. Kovacs, J. Am. Chem. Soc., 2011, **133**, 8673–8680.
7 L. Lumata, M. E. Merritt, C. Malloy, A. D. Sherry and Z. Kovacs, Appl. Magn. Reson., 2012, **43**, 69–79.
8 L. Lumata, M. E. Merritt, Z. Hashami, S. J. Ratnakar and Z. Kovacs, Angew. Chem., Int. Ed., 2012, **51**, 525–527.
9 F. A. Gallagher, M. I. Kettunen and K. M. Brindle, Prog. Nucl. Magn. Reson. Spectrosc., 2009, **55**, 285–295.
10 K. M. Brindle, S. E. Bohndiek, F. A. Gallagher and M. I. Kettunen, Magn. Reson. Med., 2011, **66**, 505–519.
11 J. Kurhanewicz, D. B. Vigneron, K. Brindle, E. Y. Chekmenev, A. Comment, C. H. Cunningham, R. J. DeBerardinis, G. G. Green, M. O. Leach, S. S. Rajan, R. R. Rizi, B. D. Ross, W. S. Warren and C. R. Malloy, Neoplasia, 2011, **13**, 81–97.
12 C. Yang, B. Ko, C. Hensley, L. Jiang, A. Wasti, L. Lumata, M. Mitsche, M. Merritt and R. J. DeBerardinis, Mol. Cell, 2014, **56**, 414–424.

21358 | Phys. Chem. Chem. Phys., 2016, **18**, 21351–21359

This journal is © the Owner Societies 2016

13 L. Lumata, C. Yang, M. Ragavan, N. Carpenter, R. J. DeBerardinis and M. E. Merritt, *Methods Enzymol.*, 2015, **561**, 73–106.

14 C. Khemtong, N. R. Carpenter, L. L. Lumata, M. E. Merritt, K. X. Moreno, Z. Kovacs, C. R. Malloy and A. D. Sherry, *Magn. Reson. Med.*, 2015, **74**, 312–319.

15 M. Mishkovsky, A. Comment and R. Gruetter, *J. Cereb. Blood Flow Metab.*, 2012, **32**, 2108–2113.

16 A. Flori, M. Liserani, F. Frijia, G. Giovannetti, V. Lionetti, V. Casieri, V. Positano, G. D. Aquaro, F. A. Recchia, M. F. Santarelli, L. Landini, J. H. Ardenkjaer-Larsen and L. Menichetti, *Contrast Media Mol. Imaging*, 2015, **10**, 194–202.

17 L. Lumata, S. J. Ratnakar, A. Jindal, M. Merritt, A. Comment, C. Malloy, A. D. Sherry and Z. Kovacs, *Chem. – Eur. J.*, 2011, **17**, 10825–10827.

18 L. Lumata, M. Merritt, C. Malloy, A. D. Sherry, J. van Tol, L. Song and Z. Kovacs, *J. Magn. Reson.*, 2013, **227**, 14–19.

19 L. Lumata, M. Merritt, C. Khemtong, S. J. Ratnakar, J. van Tol, L. Yu, L. Song and Z. Kovacs, *RSC Adv.*, 2012, **2**, 12812–12817.

20 L. L. Lumata, R. Martin, A. K. Jindal, Z. Kovacs, M. S. Conradi and M. E. Merritt, *Magn. Reson. Mater. Phys., Biol. Med.*, 2015, **98**, 195–205.

21 F. Kurdzesau, B. van der Brandt, A. Comment, P. Hautle, S. Jannin, J. J. van der Klink and J. A. Konter, *J. Phys. D: Appl. Phys.*, 2008, **41**, 155506.

22 L. Lumata, M. E. Merritt and Z. Kovacs, *Phys. Chem. Chem. Phys.*, 2013, **15**, 7032–7035.

23 A. Kiswandhi, B. Lama, P. Niedbalski, M. Goderya, J. Long and L. Lumata, *RSC Adv.*, 2016, **6**, 38855–38860.

24 L. Lumata, Z. Kovacs, C. Malloy, A. D. Sherry and M. Merritt, *Phys. Med. Biol.*, 2011, **56**, N85–N92.

25 J. H. Ardenkjaer-Larsen, *J. Magn. Reson.*, 2016, **264**, 3–12.

26 S. Jannin, A. Comment, F. Kurdzesau, J. A. Konter, P. Hautle, B. van den Brandt and J. J. van der Klink, *J. Chem. Phys.*, 2008, **128**, 241102.

27 H. A. I. Yoshihara, E. Can, M. Karlsson, M. H. Lerche, J. Schwitterd and A. Comment, *Phys. Chem. Chem. Phys.*, 2016, **18**, 12409–12413.

28 A. Bornet and S. Jannin, *J. Magn. Reson.*, 2016, **264**, 13–21.

29 L. Lumata, M. E. Merritt, C. R. Malloy, A. D. Sherry and Z. Kovacs, *J. Phys. Chem. A*, 2012, **116**, 5129–5138.

30 J. W. Gordon, S. B. Fain and I. J. Rowland, *Magn. Reson. Med.*, 2012, **68**, 1949–1954.

31 A. Flori, M. Liserani, S. Bowen, J. H. Ardenkjaer-Larsen and L. Menichetti, *J. Phys. Chem. A*, 2015, **119**, 1885–1893.

32 L. F. Waldner, A. Chen, W. Mander, T. Scholl and C. McKenzie, *J. Magn. Reson.*, 2012, **223**, 85–89.

33 J. Milani, B. Vuichoud, A. Bornet, P. Miéville, R. Mottier, S. Jannin and G. Bodenhausen, *Rev. Sci. Instrum.*, 2015, **86**, 24101.

34 M. L. Hirsch, B. A. Smith, M. Mattingly, A. G. Goloshevsky, M. Rosay and J. G. Kempf, *J. Magn. Reson.*, 2015, **261**, 87–94.

35 A. F. Martins, S. V. Eliseeva, H. F. Carvalho, J. M. C. Teixeira, C. T. B. Paula, P. Hermann, C. Platas-Iglesias, S. Petoud, É. Tóth and C. F. G. C. Geraldes, *Chem. – Eur. J.*, 2014, **20**, 14834–14845.

36 A. Barge, G. Cravotto, E. Gianolio and F. Fedeli, *Contrast Media Mol. Imaging*, 2006, **1**, 184–188.

37 S. Aime, M. Botta and G. Ermondi, *Inorg. Chem.*, 1992, **31**, 4291–4299.

38 B. R. Patyal, J.-H. Gao, R. F. Williams, J. Roby, B. Saam, B. A. Rockwell, R. J. Thomas, D. J. Stolarski and P. T. Fox, *J. Magn. Reson.*, 1997, **126**, 58–65.

39 J. Heckmann, W. Meyer, E. Radtke, G. Reicherz and S. Goertz, *Phys. Rev. B: Condens. Matter Mater. Phys.*, 2006, **74**, 134418.

40 S. T. Goertz, *Nucl. Instrum. Methods Phys. Res., Sect. A*, 2004, **526**, 28–42.

41 J. Wolber, F. Ellner, B. Fridlund, A. Gram, H. Johannesson, G. Hansson, L. H. Hansson, M. H. Lerche, S. Mansson, R. Servin, M. Thaning, K. Golman and J. H. Ardenkjaer-Larsen, *Nucl. Instrum. Methods Phys. Res., Sect. A*, 2004, **526**, 173–181.

42 S. Reynolds and H. Patel, *Appl. Magn. Reson.*, 2008, **34**, 495–508.

43 L. Lumata, Z. Kovacs, A. D. Sherry, C. Malloy, S. Hill, J. van Tol, L. Yu, L. Song and M. Merritt, *Phys. Chem. Chem. Phys.*, 2013, **15**, 9800–9807.

44 M. Borghini, *Phys. Rev. Lett.*, 1968, **20**, 419–421.

45 M. Borghini and K. Scheffler, *Phys. Rev. Lett.*, 1971, **26**, 1362–1365.

46 E. Ravera, D. Shimon, A. Feintuch, D. Goldfarb, S. Vega, A. Flori, C. Luchinat, L. Menichetti and G. Parigi, *Phys. Chem. Chem. Phys.*, 2015, **17**, 26969–26978.

47 D. Banerjee, D. Shimon, A. Feintuch, S. Vega and D. Goldfarb, *J. Magn. Reson.*, 2013, **230**, 212–219.

48 T. A. Siaw, M. Fehr, A. Lund, A. Latimer, S. A. Walker, D. T. Edwards and S.-I. Han, *Phys. Chem. Chem. Phys.*, 2014, **16**, 18694–18706.

49 C. T. Farrar, D. A. Hall, G. J. Gerfen, S. J. Inati and R. G. Griffin, *J. Chem. Phys.*, 2001, **114**, 4922.

50 A. Abragam and B. Bleaney, *Electron paramagnetic resonance of transition ions*, Clarendon P., Oxford, 1970.

51 P. Caravan, J. J. Ellison, T. J. McMurry and R. B. Lauffer, *Chem. Rev.*, 1999, **99**, 2293–2352.

52 M. Norek and J. A. Peters, *Prog. Nucl. Magn. Reson. Spectrosc.*, 2011, **59**, 64–82.

53 C. F. G. C. Geraldes and C. Luchinat, in *Metal ions in biological systems: the lanthanides and their interrelations with biosystems*, ed. A. Sigel and H. Sigel, Marcel Dekker, New York, 2003, vol. 40, pp. 513–588.

^{13}C dynamic nuclear polarization using isotopically enriched 4-oxo-TEMPO free radicals

Peter Niedbalski, Christopher Parish, Andhika Kiswandhi and Lloyd Lumata*

The nitroxide-based free radical 2,2,6,6-tetramethyl-1-piperidinyloxy (TEMPO) is a widely used polarizing agent in NMR signal amplification via dissolution dynamic nuclear polarization (DNP). In this study, we have thoroughly investigated the effects of ^{15}N and/or ^{2}H isotopic labeling of 4-oxo-TEMPO free radical on ^{13}C DNP of 3 M [1-^{13}C] sodium acetate samples in 1 : 1 v/v glycerol : water at 3.35 T and 1.2 K. Four variants of this free radical were used for ^{13}C DNP: 4-oxo-TEMPO, 4-oxo-TEMPO-^{15}N, 4-oxo-TEMPO-d$_{16}$ and 4-oxo-TEMPO-^{15}N,d$_{16}$. Our results indicate that, despite the striking differences seen in the electron spin resonance (ESR) spectral features, the ^{13}C DNP efficiency of these ^{15}N and/or ^{2}H-enriched 4-oxo-TEMPO free radicals are relatively the same compared with ^{13}C DNP performance of the regular 4-oxo-TEMPO. Furthermore, when fully deuterated glassing solvents were used, the ^{13}C DNP signals of these samples all doubled in the same manner, and the ^{13}C polarization buildup was faster by a factor of 2 for all samples. The data here suggest that the hyperfine coupling contributions of these isotopically enriched 4-oxo-TEMPO free radicals have negligible effects on the ^{13}C DNP efficiency at 3.35 T and 1.2 K. These results are discussed in light of the spin temperature model of DNP. Copyright © 2016 John Wiley & Sons, Ltd.

Keywords: DNP; NMR; dynamic nuclear polarization; thermal mixing; TEMPO

Introduction

While nuclear magnetic resonance (NMR) is an incredibly valuable and widely used analytical tool in many fields of science, it is an inherently insensitive technology compared with other techniques such as electron spin resonance (ESR) under the same magnetic field. This low thermal NMR sensitivity arises from the small energy difference between the Zeeman energy levels for non-zero spin nuclei, leading to small spin population difference or nuclear polarization as dictated by Boltzmann law.[1] ESR works on the same principle as NMR. However, the electron has a much larger magnetic moment than any magnetically active nuclei, leading to much greater polarization, and thus signal strength, when used at the same magnetic field strength as NMR.[2] The NMR insensitivity problem can been addressed by the signal amplification technique known as dynamic nuclear polarization (DNP) that takes advantage of these fundamental properties of electron and nuclear spins. The use of DNP technique, which is a combination of ESR, NMR and cryogenic technologies, originated in the 1960s where highly polarized protons or deuterons were used as targets in nuclear scattering and particle physics experiments.[3,4] Through microwave irradiation of a diamagnetic sample containing the target nuclei and doped with trace amounts of free electrons from polarizing agents, the high degree of electron spin alignment or polarization can be transferred to the nuclear spins at high magnetic field and low temperature.[3,4]

It was not until 2003 with the invention of the dissolution method when the enhanced NMR signal in DNP is harnessed in the liquid state at room temperature.[5] In dissolution DNP, superheated solvent such as water is rapidly injected into the frozen polarized sample, and the end result is the production of injectable liquids containing highly polarized nuclear spins.[5] Using this technique, liquid-state NMR signal enhancements of typically three to four orders of magnitude can be readily achieved for nuclei with low gyromagnetic ratio γ such as ^{13}C, ^{15}N, ^{6}Li, ^{89}Y, ^{107,109}Ag and others.[5–11] With the advent of dissolution DNP, it has become feasible to use mainly hyperpolarized ^{13}C biomolecules as NMR and imaging (MRI) agents or tracers for in vitro and in vivo metabolic studies with excellent sensitivity and high specificity.[12–18]

Optimized sample preparation is a critical aspect in DNP to achieve the highest NMR signal enhancement levels both in the frozen and liquid states. It should be noted that central to the NMR amplification process in dissolution DNP is the source of free electrons that is primarily provided by stable, spin-1/2 organic free radicals.[19–23] In addition to the DNP conditions, the electronic properties of these free radicals, especially the ESR lineshapes and electron relaxation behavior, could significantly affect the level of nuclear polarization enhancements achieved via DNP.[23–25] For instance, shortening of electron spin–lattice relaxation time T_1 via addition of trace amounts of gadolinium and other lanthanides in DNP samples is linked to the significant improvement of ^{13}C DNP signals when trityl OX063 free radical is used as the polarizing agent.[25–29] In addition, previous DNP studies have shown that narrow ESR linewidth free radicals such as trityl OX063 and BDPA favor high DNP enhancements for low-γ nuclei such as ^{13}C and ^{2}H spins.[23,24] In this project, we have investigated the effects of ^{2}H and ^{15}N isotopic enrichment of the well-known nitroxide-based free radical 4-oxo-TEMPO on the ^{13}C DNP of [1-^{13}C]sodium acetate. A total of four variants of the 4-oxo-TEMPO free radical were examined: the unaltered 4-oxo-TEMPO, fully deuterated 4-oxo-TEMPO-d$_{16}$, ^{15}N-doped 4-oxo-TEMPO-^{15}N and ^{15}N-doped, fully

* Correspondence to: Lloyd Lumata, Department of Physics, University of Texas at Dallas, 800 West Campbell Road, Richardson, TX 75080, USA. E-mail: lloyd.lumata@utdallas.edu

Department of Physics, University of Texas at Dallas, Richardson, TX, USA

deuterated 4-oxo-TEMPO-^{15}N,d$_{16}$ (see structures in Fig. 1). This project follows along the lines of optimization methods in DNP in which certain isotopic enrichments in DNP sample components play significant roles in the improvement of the DNP signals. For example, deuteration of the glassing matrix has been shown to further improve the ^{13}C DNP signal by up to two or three times its base DNP enhancement for samples doped with wide ESR linewidth free radicals such as TEMPO.[30–32] Deuteration of the parent compound itself such as amino acids can lead to significantly longer nuclear T_1 and excellent NMR signal enhancements in the liquid state.[27,33] Furthermore, ^{13}C enrichment of the glassing matrix accelerates the ^{13}C polarization buildup process of ^{13}C biomolecules such as [1-^{13}C]pyruvate via faster nuclear spin diffusion, cutting the microwave DNP irradiation time to about a half.[34] The recent commercial availability of these 4-oxo-TEMPO free radical variants provides us an avenue to examine the effects on ^{13}C DNP by isotopic enrichment of another major component of DNP sample: the free radicals. In this work, the main goal is to evaluate the influence of the expected changes in the hyperfine coupling made by ^{2}H and ^{15}N isotopic enrichment of the 4-oxo-TEMPO free radical on ^{13}C DNP. We have chosen [1-^{13}C]acetate for this study because of its biochemical importance and its ^{13}C carbonyl location is ideal for DNP as a model for optimization of other hyperpolarized ^{13}C metabolic substrates such as [1-^{13}C]pyruvate. Furthermore, the ^{13}C DNP efficiency of these samples doped with 4-oxo-TEMPO variants were investigated in both non-deuterated and fully deuterated glassing matrices.

Experimental

Materials and DNP sample preparation

[1-^{13}C]Sodium acetate (Cambridge Isotope Laboratories, Tewksbury, MA), the four variants of 4-oxo-TEMPO free radical (Sigma-Aldrich, St. Louis, MO) as well as the deuterated and non-deuterated solvents (Sigma-Aldrich, St. Louis, MO) used in this study were all purchased from commercial sources and were used without further purification. The following 4-oxo-TEMPO free
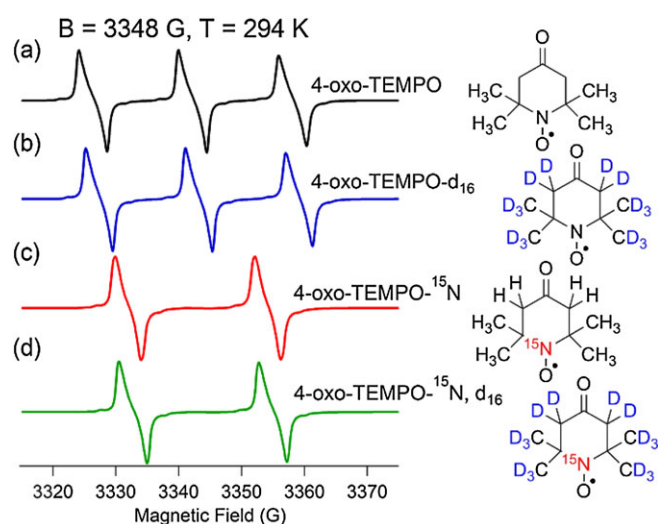

Figure 1. X-band ESR spectra in the liquid state at 294 K and the corresponding structures of the free radical polarizing agents used in this study: (a) 4-oxo-TEMPO, (b) 4-oxo-TEMPO-d$_{16}$, (c) 4-oxo-TEMPO-^{15}N and (d) 4-oxo-TEMPO-^{15}N, d$_{16}$. The concentration of each free radical used for ESR measurements was 5 mM in 1 : 1 v/v glycerol : water solution.

radical variants were used as polarizing agents in the ^{13}C DNP study: 4-oxo-TEMPO (4-oxo-2,2,6,6-tetramethyl-1-piperidinyloxy), deuterated 4-oxo-TEMPO (4-oxo-2,2,6,6-tetramethylpiperidine-d$_{16}$-1-oxyl), ^{15}N-enriched 4-oxo-TEMPO (4-oxo-2,2,6,6-tetramethylpiperidine-1-^{15}N-1-oxyl) and deuterated ^{15}N-enriched 4-oxo-TEMPO (4-oxo-2,2,6,6-tetramethylpiperidine-d$_{16}$,1-^{15}N-1-oxyl). The chemical structures of these free radicals are displayed in Fig. 1. For purposes of brevity of these free radical terms in labeling the x-axes of the bar graph figures, the free radical variants 4-oxo-TEMPO, 4-oxo-TEMPO-d$_{16}$, 4-oxo-TEMPO-^{15}N and 4oxo-TEMPO-^{15}N,d$_{16}$ are also hereafter abbreviated as 4OT, 4OT-d$_{16}$, 4OT-^{15}N and 4OT-^{15}N, d$_{16}$, respectively.

The ^{13}C acetate and 4-oxo-TEMPO free radical compounds were weighed out using Ohaus Discovery semi-micro analytical balance (Ohaus Corporation, Parsippany, NJ). Four 200 µl solutions each containing 49.8 mg of [1-^{13}C]sodium acetate in 1:1 v/v glycerol : water were prepared in graduated 1-ml polytetrafluoroethylene microcentrifuge tubes (USA Scientific, Ocala, FL) using vortex mixer and microcentrifuge (ThermoFisher Scientific, WI). These solutions were doped with either 1.36 mg 4-oxo-TEMPO, 1.49 mg 4-oxo-TEMPO-d$_{16}$, 1.37 mg 4-oxo-TEMPO-^{15}N or 1.50 mg 4-oxo-TEMPO-^{15}N,d$_{16}$. The final concentrations of ^{13}C acetate and free radical in each DNP sample were 3 M and 40 mM, respectively. In addition, the same set of ^{13}C DNP samples were prepared but in 1:1 v/v deuterated water and d$_8$-glycerol solutions. Thus, a total of eight 200 µl samples were prepared. These samples were then stored in a −80°F laboratory freezer (ThermoFisher Scientific, WI).

Electron spin resonance

To characterize the effects of ^{2}H and/or ^{15}N enrichment of 4-oxo-TEMPO, ESR measurements of these free radicals were performed at the Nanotech Institute at the University of Texas at Dallas using a Bruker EMX X-band ESR spectrometer (Bruker Biospin, Billerica, MA). Each of the 4-oxo-TEMPO variants was dissolved in 1:1 v/v water : glycerol solution to the concentration of 5 mM. A small aliquot of each 4-oxo-TEMPO variant was placed in 0.5-mm ID heparinized hematocrit capillary tubes, which were then placed in 4-mm thin wall quartz ESR tubes (Wilmad Lab-Glass, Vineland, NJ). Field-swept continuous wave (CW) ESR spectra in the liquid state were recorded at 294 K. Stacked plot of normalized X-band ESR spectra is shown in Fig. 1.

Dynamic nuclear polarization

All DNP hyperpolarization experiments were conducted at the Advanced Imaging Research Center at the University of Texas Southwestern Medical Center using the commercial HyperSense polarizer (Oxford Instruments, Abingdon, UK). This hyperpolarizer operates at 3.35 T and is equipped with a Edwards E40 roots blower pump (Edwards Vacuum, West Sussex, UK) that allows the cryostat to reach a base temperature of 1.2 K. Microwave irradiation of samples for DNP is provided by a 100 mW ELVA-1 W-band microwave source (ELVA-1 Millimeter Wave, RU) with a sweepable frequency range of 93.90–94.30 GHz.

^{13}C microwave frequency sweeps

The ^{13}C microwave frequency sweep data or DNP spectra, which indicate the optimum microwave frequencies to give the maximum DNP enhancement, were measured using a built-in NMR program in the HyperSense polarizer (Oxford Instruments, UK). Two hundred microliter aliquot of each of the ^{13}C acetate samples with

4-oxo-TEMPO variants was transferred to a PEEK cup using Rainin PR200 pipette (Mettler Toledo, Columbus, OH) and was quickly inserted into the polarizer. The microwave power was set at 100 mW, and the frequency was swept in the full sweepable range of 93.90–94.30 GHz with step interval of 5 MHz. The DNP sample was irradiated for 3 min at each frequency step, and the ^{13}C NMR signal was automatically recorded for each frequency. As described previously, a train of hard RF pulses is applied after every frequency step to ensure that the ^{13}C DNP signal at the next frequency step will have no residual ^{13}C DNP signal enhancement from the previous step.[8,29] After the microwave frequency sweep measurement, each of the ^{13}C DNP samples was retrieved from the polarizer and subsequently thawed out at room temperature. The samples were then stored in the −80°F laboratory freezer until the subsequent ^{13}C polarization buildup experiments.

^{13}C polarization buildup curves

Based on the ^{13}C microwave frequency sweep data, the optimum microwave irradiation frequency was found to be nearly the same for all samples at 94.15 GHz. This information was determined prior to performing the ^{13}C polarization buildup curve measurements. Two hundred microliter aliquot of each ^{13}C DNP sample was quickly inserted into the hyperpolarizer. The 3.35 T hyperpolarizer was conditioned to be at a temperature of 1.2 K before any polarization buildup points were taken. The microwave frequency was set to 94.15 GHz and turned on with 100 mW output power. Using the built-in NMR program in the HyperSense, a ^{13}C NMR spectrum at 3.35 T and 1.2 K was recorded every 3 min and plotted as a function of time until the ^{13}C polarization buildup curves reach their plateaus or maximum values. The ^{13}C polarization buildup curves for each sample were done in triplicate.

Data analysis

The ESR and ^{13}C DNP data were plotted and analyzed using Igor Pro version 6.4 (Wavemetrics, Lake Oswego, OR). Because the ^{13}C polarization buildup data were done in triplicate, mean values and standard deviations were calculated. The ^{13}C polarization buildup curves were fitted with a mono-exponential buildup equation with a buildup constant τ.[29] The relative maximum ^{13}C DNP signals and τ values for each ^{13}C DNP sample both in non-deuterated and deuterated glassing solvents were compared and analyzed in bar graph representations.

Results and Discussion

The nitroxide-based TEMPO free radical has become one of the popular polarizing agents for hyperpolarized NMR not only due to its ubiquity and relatively low cost but also because this free radical is very stable and highly efficient, especially in cross-polarization dissolution DNP.[35–40] The presence of nitroxides such as TEMPO in the dissolution liquid can shorten the liquid-state T_1 of the hyperpolarized nuclei. However, TEMPO free radicals can be easily quenched or neutralized with simple addition of trace amount of ascorbic acid prior to intravenous administration of hyperpolarized liquids. This is an important consideration especially during *in vivo* hyperpolarized NMR or imaging (MRI) experiments as this process leads to longer liquid-state T_1 and may reduce the toxicity of the sample to be administered.[41] Due to its hyperfine coupling with the nearby non-zero spin nuclei especially ^{14}N, non-symmetric structure and *g*-anisotropy, the ESR spectrum of TEMPO is known

to be relatively broad and has asymmetric spectral shape compared with other free radicals used in dissolution DNP such as the carbon-centered trityl OX063 and BDPA.[25] At W-band, the ESR linewidth of 4-oxo-TEMPO at 2% height is about 465 MHz, whereas the ESR linewidth for trityl OX063 based on this criterion is only around 60 MHz.[25] Due to its broad ESR lineshape, TEMPO can be used to hyperpolarize not only low-γ nuclei such as ^{13}C spins but also high-γ nuclei such as ^{1}H spins predominantly via the thermal mixing DNP process.[19,31,35–40]

In thermal mixing or the Borghini spin temperature model of DNP, the shape and size of the ESR spectrum are a crucial factor in identifying the locations of the optimum microwave irradiation frequencies and the maximum DNP enhancement levels.[3,4,42–44] As stated previously, hyperfine coupling or interaction between the free electron and the surrounding NMR-active nuclear spin is one of the major factors that affects the ESR spectral features of a free radical.[45] The effects of ^{2}H and/or ^{15}N isotopic enrichment of 4-oxo-TEMPO are visibly apparent on the liquid-state X-band ESR spectra 294 K displayed in Fig. 1. As can be expected from the structure of the regular 4-oxo-TEMPO, three peaks were visible in the dispersive X-band ESR spectrum in Fig. 1a that correspond to the hyperfine interaction of the electron with the adjacent ^{14}N spins (spin $I = 1$, $\gamma = 3.077$ MHz/T) and are consistent with previous reports.[46] In Fig. 1b, replacement of ^{1}H ($I = 1/2$, $\gamma = 42.58$ MHz/T) spins by ^{2}H ($I = 1$, $\gamma = 6.54$ MHz/T) spins within the free radical by using the variant 4-oxo-TEMPO-d$_{16}$ led to no noticeable difference in the field-swept CW ESR spectral features. This result is consistent with a previous ESR study of deuterated TEMPO free radical.[47] On the other hand, when the ^{14}N spins in the free radical are replaced by ^{15}N ($I = 1/2$, $\gamma = 4.316$ MHz/T) spins by using the variant 4-oxo-TEMPO-^{15}N, only two peaks were identified in the CW ESR spectrum as displayed in Fig. 1c. The reduction in the number of peaks when using the ^{15}N-enriched 4-oxo-TEMPO variant is consistent with the $n = (2I + 1)$ rule, where n is the number of peaks and I is the spin of the nucleus coupled to the free electron. In Fig. 1d, isotopic enrichment of both ^{2}H and ^{15}N spins within the free radical by using the variant 4-oxo-TEMPO-^{15}N,d$_{16}$ also led to two peaks in the CW ESR spectrum essentially identical to that of 4-oxo-TEMPO-^{15}N. Thus, these ESR results have shown that these isotopic enrichments within the 4-oxo-TEMPO free radical, particularly ^{15}N doping, have clearly modified the ESR spectral features via changes in the hyperfine coupling interaction.

To test whether these changes in the ESR spectral features have any impact on ^{13}C DNP, we have measured the ^{13}C microwave DNP spectra or microwave frequency sweep of ^{13}C DNP signals to identify the optimum frequency to polarize the samples. Due to the limited sweepable microwave frequency range (400 MHz) of the microwave source, only the first half of the ^{13}C DNP spectrum for each sample was plotted as shown in Fig. 2. Previous studies in homebuilt DNP hyperpolarizers with longer sweepable microwave frequency range have shown that it would take about twice this frequency range to completely display the full ^{13}C DNP spectra of TEMPO-doped DNP samples.[23,31,48] Nevertheless, despite this limitation, the ^{13}C DNP spectra measured here were sufficient to locate the positive polarization peak that conventionally refers to the polarization state where more ^{13}C spins are aligned with the applied magnetic field. The missing half of the ^{13}C DNP spectrum should contain the negative polarization peak where microwave irradiation at that frequency would cause the ^{13}C spins to populate the other Zeeman energy level. Close inspection of Fig. 2 shows that despite the differences seen in the room temperature X-band ESR spectra of these free radicals, the normalized ^{13}C DNP spectra
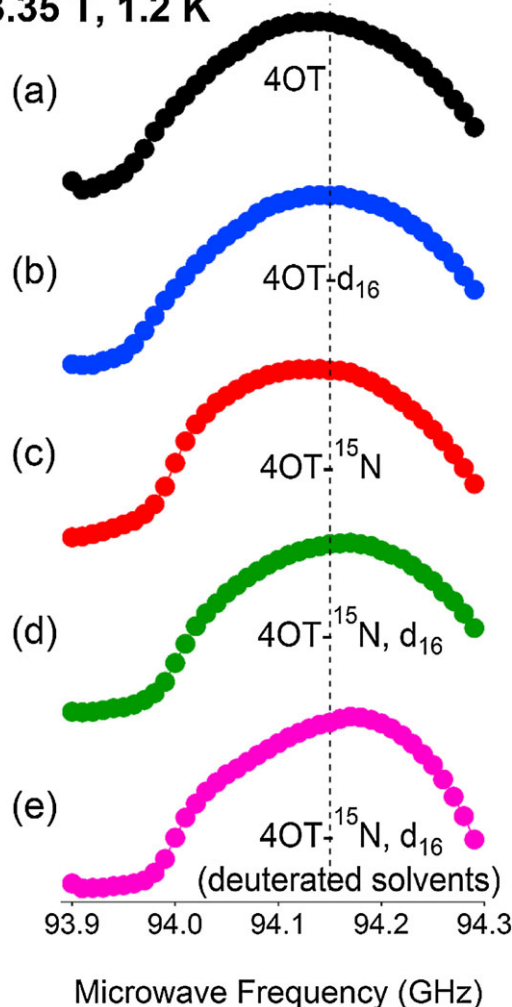
Figure 2. Normalized microwave frequency sweep data or ^{13}C DNP spectra of 3 M [1-^{13}C]sodium acetate in 1 : 1 v/v glycerol : water doped with 40 mM (a) 4-oxo-TEMPO, (b) 4-oxo-TEMPO-d$_{16}$, (c) 4-oxo-TEMPO-^{15}N, (d) 4-oxo-TEMPO-^{15}N,d$_{16}$ and (e) same as (d) but in 1 : 1 v/v D$_2$O : d$_8$-glycerol glassing solvent. The vertical line marks the chosen frequency for microwave irradiation. All ^{13}C DNP were taken at 3.35 T and 1.2 K. Note that only half of the ^{13}C DNP spectra of these samples were recorded due to the limited sweepable frequency range of the microwave source.

of ^{13}C acetate samples doped with these 4-oxo-TEMPO variants are nearly identical in spectral features at the polarizer conditions of 3.35 T and 1.2 K. There may be some very slight and subtle differences in the features of the ^{13}C DNP spectra among the different 4-oxo-TEMPO variants; however, the main observation here is that the location of the optimum microwave frequency is closely identical for all the variants that is at 94.15 GHz. Furthermore, we have also examined whether glassing solvent deuteration has any effect on ^{13}C microwave DNP spectrum of TEMPO-doped samples. In this light, we have opted to measure the ^{13}C DNP spectrum of 4-oxo-TEMPO-^{15}N,d$_{16}$ in fully deuterated glassing solvents (1 : 1 v/v d$_8$-glycerol : D$_2$O) to check whether ^{2}H and ^{15}N isotopic labeling in the free radical and ^{2}H enrichment in the solvent has any effect on the ^{13}C sweep data. As displayed in Fig. 2e, the ^{13}C DNP spectrum for this sample is also very identical to that of the other variants in non-deuterated glassing solvents. This is consistent with the results of previous study that reported that glassing solvent deuteration has no significant effect on the shape of the DNP

spectrum or location of the optimum DNP peaks.[30] It is expected that the other isotopic 4-oxo-TEMPO variants in deuterated glassing solvents will have very similar ^{13}C DNP spectra as well. One common prominent feature of ^{13}C DNP spectra of the ^{13}C samples doped with these 4-oxo-TEMPO variants is the relatively broad DNP maximum or polarization peak with a range of around 40–60 MHz, unlike the reported ^{13}C DNP spectra of narrow ESR linewidth free radicals such as trityl OX063 or BDPA in which each ^{13}C polarization peak is relatively sharp in the 5 MHz range.[23,30] It is possible that at 3.35 T and cryogenic temperature, the differences in the ESR spectral features due to hyperfine coupling may have already overlapped with the other contributions[45] to the inhomogeneous broadening of the ESR spectra such as g-anisotropy and homogeneous broadening due to strong electron dipole–dipole interactions. Thus, it is suggested that the effect of hyperfine coupling differences on the ^{13}C DNP spectra may be embedded somewhere in the subtle ^{13}C DNP spectral features but are not so visible due to the presence of other dominant ESR spectral broadening contributions.

Next, we have proceeded with the measurement of the ^{13}C polarization buildup curves after locating the nearly common optimum microwave irradiation frequency for all samples that is at 94.15 GHz. Figure 3a shows the growth of the relative ^{13}C DNP signals
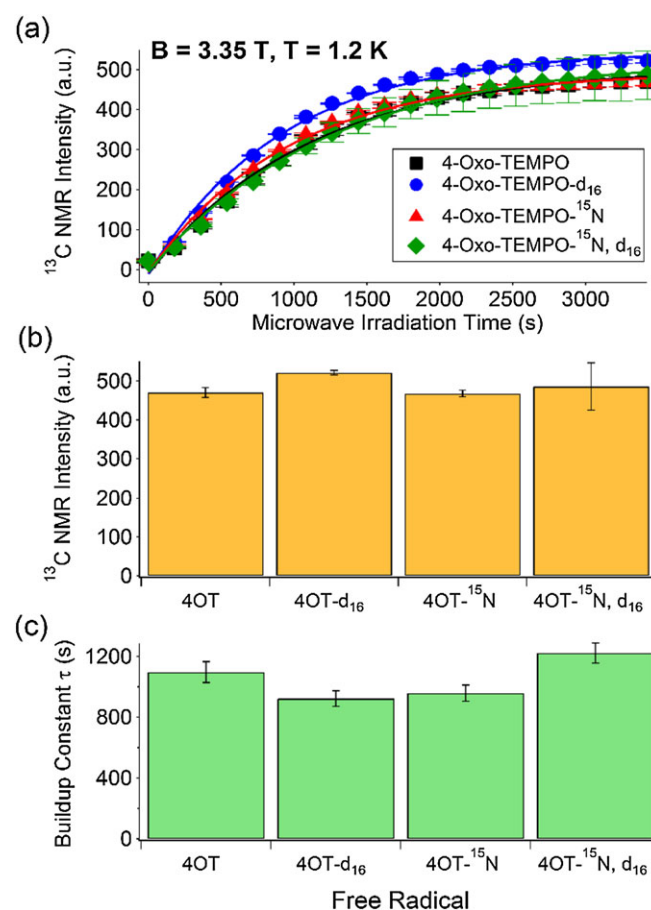

Figure 3. (a) ^{13}C polarization buildup curves for 3 M [1-^{13}C]acetate in non-deuterated glassing solvents (1 : 1 v/v glycerol : water) doped with 40 mM of each of the four variants of 4-oxo-TEMPO. These data were taken at 3.35 T and 1.2 K. The solid lines are fits to a mono-exponential buildup equation described in the text. (b) Bar graph representations of the relative maximum ^{13}C DNP signals obtained from each sample. (c) Comparison of ^{13}C polarization buildup time τ among the samples. The error bars in these graphs are from standard deviations with $N = 3$ trials for each sample.

as a function of microwave irradiation time at 3.35 T and 1.2 K for ^{13}C acetate samples doped with either of the four 4-oxo-TEMPO variants in non-deuterated glassing solvents (1 : 1 v/v glycerol : water). The growth of the ^{13}C DNP signals can be fitted with a single-exponential buildup equation with the buildup time constant τ.[29] The average values ($N = 3$ trials) of the relative maximum ^{13}C DNP signals and ^{13}C polarization buildup time constants τ extracted from the data in Fig. 3a are displayed in bar graph representations in Figs. 3b and 3c, respectively. The error bars in Fig. 3 are standard deviations with $N = 3$ trials. Due to the technical difficulty and prohibitively long acquisition times in getting a thermal ^{13}C NMR signal for each sample, we were not able to quantify the percent ^{13}C polarization for our ^{13}C acetate samples. However, we have employed the relative ^{13}C DNP-NMR signal level as a reliable metric for evaluating the effect of an optimization parameter, in this case, the isotopic labeling of a well-known polarizing agent, on the ^{13}C DNP efficiency. We note that the use of the relative ^{13}C DNP signals has been used extensively in previous DNP studies to examine the ^{13}C DNP performance of various sample preparation methods.[26,28,30,32] The main finding in the results displayed in Fig. 3 is that there was no significant difference in the ^{13}C DNP efficiency among the four 4-oxo-TEMPO variants. Furthermore, the kinetics of ^{13}C polarization signal growth with microwave irradiation time is also closely identical. These results further cement the finding hinted in Fig. 2 that the hyperfine coupling differences seen in ESR due to isotopic enrichment of 4-oxo-TEMPO have no significant impact on ^{13}C DNP efficiency for ^{13}C samples in non-deuterated glassing solvents at 3.35 T and 1.2 K.

Moreover, we have also tested the ^{13}C DNP efficiency of these free radicals on [1-^{13}C]acetate samples in fully deuterated glassing solvents at 3.35 T and 1.2 K as shown in Fig. 4. As mentioned previously, ^{2}H enrichment or deuteration of the glassing matrix has been shown to be beneficial for ^{13}C DNP using wide ESR linewidth free radicals such as 4-oxo-TEMPO.[30–32] This is mainly due to the fact that the predominant DNP mechanism using TEMPO at these conditions is thermal mixing that has implications on the microwave-driven cooling of nuclear spins via the electron dipolar system.[30–32] In thermal mixing or equal spin temperature model of DNP, a thermal contact is established between the electron dipolar system (EDS) and the nuclear Zeeman system (NZS) provided that the Larmor frequency of the target nuclei is less than or comparable with the ESR linewidth of the free radical.[3,4,45] The large ESR linewidth of 4-oxo-TEMPO or its isotopic variants allows simultaneous DNP cooling of all nuclei from ^{1}H spins to low-γ spins such as ^{13}C via thermal mixing. The NZS heat load that the EDS can cool is proportional to the number of nuclear spin N_s and the gyromagnetic ratio γ of nuclei involved, where specifically the specific heat capacity of NZS is $C_Z \sim N_s \omega_n^2$ where ω_n is the nuclear Larmor frequency γB_0.[45] When non-deuterated glassing solvent is used for ^{13}C DNP of samples doped with 4-oxo-TEMPO or its isotopic variants, the EDS cools down a NZS heat load that is composite of both ^{13}C ($\gamma = 10.705$ MHz/T) and ^{1}H ($\gamma = 42.58$ MHz/T) spins.[30–32,45] Glassing solvent deuteration leads to a composite NZS heat load of both ^{13}C and ^{2}H ($\gamma = 6.54$ MHz/T) spins, meaning (^{13}C + ^{2}H) spins is a lesser NZS heat load compared with (^{13}C + ^{1}H) spins for the EDS to cool down, therefore translating to lower ^{13}C nuclear spin temperature or higher ^{13}C polarization level when ^{2}H-enriched glassing solvent is used.[30–32,45] This DNP behavior explains the doubling of relative ^{13}C DNP signals of ^{13}C samples doped with 4-oxo-TEMPO variants when 1 : 1 v/v d$_8$-glycerol : D$_2$O glassing solvents are used. In addition to higher ^{13}C DNP signal intensity, the ^{13}C polarization buildup times are faster by a factor of 2 when ^{1}H spins are replaced by ^{2}H spins in the glassing matrix.
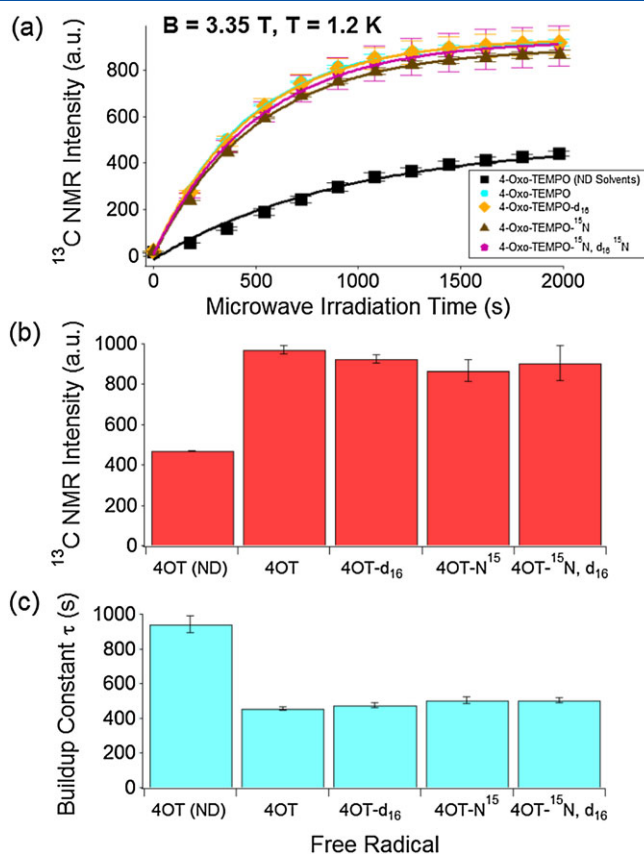

Figure 4. (a) ^{13}C polarization buildup curves for 3 M [1-^{13}C]acetate in deuterated glassing solvents (1 : 1 v/v d$_8$-glycerol : D$_2$O) doped with 40 mM of each of the four variants of 4-oxo-TEMPO. For comparison, a control 4-oxo-TEMPO-doped sample in non-deuterated (ND) glassing solvent was included. These data were taken at 3.35 T and 1.2 K. The solid lines are fits to a mono-exponential buildup equation described in the text. (b) Bar graph representations of the relative maximum ^{13}C DNP signals extracted from data in (a). (c) Comparison of ^{13}C polarization buildup time τ among the samples. The error bars in these graphs are from standard deviations with $N = 3$ trials for each sample.

The faster ^{13}C polarization buildup time when deuterated solvents are used may be ascribed to faster microwave-assisted DNP cooling due to lower NZS specific heat capacity of the (^{13}C + ^{2}H) spin bath, thus an easier nuclear system for the EDS to cool down.[45] Overall, the main finding of the data shown in Fig. 4 is that the ^{13}C DNP signals and ^{13}C polarization buildup times all improved in the same manner when ^{2}H-enriched glassing solvents are used for all the four 4-oxo-TEMPO variants.

Conclusion

In conclusion, we have investigated the effects of ^{2}H and/or ^{15}N isotopic enrichment of the free radical 4-oxo-TEMPO on ^{13}C DNP of [1-^{13}C]sodium acetate both in deuterated and non-deuterated glassing matrices. We have found that, despite the significant changes in the liquid-state ESR spectra brought about by the differences in hyperfine coupling, the ^{13}C DNP efficiency of the four 4-oxo-TEMPO free radical variants described here are essentially the same at the DNP conditions of 3.35 T and 1.2 K. The similarities in the ^{13}C microwave DNP spectra among the free radical variants suggest that the effect of the differences in hyperfine interactions may have been overlapped with the other factors affecting the ESR linewidth broadening such as g-anisotropy and electron

MRC

dipole–dipole interaction at these DNP conditions. Furthermore, when ^{1}H spins are replaced by ^{2}H spins in the glassing matrix, the ^{13}C polarization level doubled in a similar manner for all ^{13}C samples doped with the free radical variants and the ^{13}C polarization buildup time is faster by a about a factor of 2 for these samples. These behavior may be ascribed to the lower NZS heat load or specific heat capacity of ([2]H + [13]C) spin bath compared with ([1]H + [13]C) spin system for the EDS to cool down, leading to lower ^{13}C spin temperature and faster ^{13}C buildup time. For an economic point of view and at least for the DNP conditions described here, our results suggest that the regular 4-oxo-TEMPO is still the preferred choice for ^{13}C DNP among these free radicals considering the higher costs of ^{2}H and/or ^{15}N-enriched 4-oxo-TEMPO variants.

References

[1] A. Abragam, *The Principles of Nuclear Magnetism*, Clarendon Press, Oxford, **1961**.

[2] M. Brynda, Biomedical Applications of Biophysics(Series Ed: T. Jue), in *Handbook of Modern Biophysics Series*, Springer, New York City, USA, **2010**, pp. 59–98. ISBN:978-1-60327-233-9.

[3] A. Abragam, M. Goldman. *Rep. Prog. Phys.* **1978**, *41*, 395–467. doi:10.1088/0034-4885/41/3/002.

[4] D. G. Crabb, W. Meyer. *Annu. Rev. Nucl. Part. Sci.* **1997**, *47*, 67–109. doi:10.1146/annurev.nucl.47.1.67.

[5] J. H. Ardenkjaer-Larsen, B. Fridlund, A. Gram, G. Hansson, L. Hansson, M. H. Lerche, R. Servin, M. Thaning, K. Golman. *Proc. Natl. Acad. Sci. U. S. A.* **2003**, *100*, 10158–10163. doi:10.1073/pnas.1733835100.

[6] W. Jiang, L. Lumata, W. Chen, S. Zhang, Z. Kovacs, C. R. Malloy, A. D. Sherry, C. Khemtong. *Sci. Rep.* **2015**, *5*, 9104. doi:10.1038/srep09104.

[7] R. Balzan, M. Mishkovsky, Y. Simonenko, R. B. van Heeswijk, R. Gruetter, U. Eliav, G. Navon, A. Comment. *Contrast Media Mol. Imaging* **2016**, *11*, 41–46. doi:10.1002/cmmi.1656.

[8] L. Lumata, A. K. Jindal, M. E. Merritt, C. R. Malloy, A. D. Sherry, Z. Kovacs. *J. Am. Chem. Soc.* **2011**, *133*, 8673–8680. doi:10.1021/ja201880y.

[9] L. Lumata, M. E. Merritt, C. Malloy, A. D. Sherry, Z. Kovacs. *Appl. Magn. Reson.* **2012**, *43*, 69–79. doi:10.1007/s00723-012-0335-8.

[10] L. Lumata, M. E. Merritt, Z. Hashami, S. J. Ratnakar, Z. Kovacs. *Angew. Chem. Intl. Ed.* **2012**, *51*, 525–527. doi:10.1002/anie.201106073.

[11] S. Reynolds, H. Patel. *Appl. Magn. Reson.* **2008**, *34*, 495–508. doi:10.1007/s00723-008-0117-5.

[12] F. A. Gallagher, M. I. Kettunen, K. M. Brindle. *Prog. Nucl. Magn. Reson. Spectrosc.* **2009**, *55*, 285–295. doi:10.1016/j.pnmrs.2009.06.001.

[13] K. M. Brindle, S. E. Bohndiek, F. A. Gallagher, M. I. Kettunen. *Magn. Reson. Med.* **2011**, *66*, 505–519. doi:10.1002/mrm.22999.

[14] C. Yang, B. Ko, C. Hensley, L. Jiang, A. Wasti, L. Lumata, M. Mitsche, M. Merritt, R. J. DeBerardinis. *Mol. Cell* **2014**, *56*, 414–424. doi:10.1016/j.molcel.2014.09.025.

[15] L. Lumata, C. Yang, M. Ragavan, N. Carpenter, R. J. DeBerardinis, M. E. Merritt. *Methods Enzymol.* **2015**, *561*, 73–106. doi:10.1016/bs.mie.2015.04.006.

[16] C. Khemtong, N. R. Carpenter, L. L. Lumata, M. E. Merritt, K. X. Moreno, Z. Kovacs, C. R. Malloy, A. D. Sherry. *Magn. Reson. Med.* **2015**, *74*, 312–319. doi:10.1002/mrm.25419.

[17] J. Kurhanewicz, D. B. Vigneron, K. Brindle, E. Y. Chekmenev, A. Comment, C. H. Cunningham, R. J. Deberardinis, G. G. Green,

[18] K. Golman, J. S. Petersson. *Acad. Radiol.* **2006**, *13*, 932–942. doi:10.1016/j.acra.2006.06.001.

[19] A. Comment, B. van den Brandt, F. Uffmann, F. Kurdzesau, S. Jannin, J. A. Konter, P. Haulte, W. T. Wenckebach, R. Greutter, J. J. van der Klink. *Conc. Magn. Reson* **2007**, *31B*, 255–269. doi:10.1002/cmr.b.20099.

[20] L. Lumata, S. J. Ratnakar, A. Jindal, M. Merritt, A. Comment, C. Malloy, A. D. Sherry, Z. Kovacs. *Chem. Eur. J.* **2011**, *17*, 10825–10827. doi:10.1002/chem.201102037.

[21] L. Lumata, M. Merritt, C. Malloy, A. D. Sherry, J. van Tol, L. Song, Z. Kovacs. *J. Magn. Reson.* **2013**, *227*, 14–19. doi:10.1016/j.jmr.2012.11.006.

[22] L. Lumata, M. Merritt, C. Khemtong, S. J. Ratnakar, J. van Tol, L. Yu, L. Song, Z. Kovacs. *RSC Adv.* **2012**, *2*, 12812–12817. doi:10.1039/C2RA21853D.

[23] L. L. Lumata, R. Martin, A. K. Jindal, Z. Kovacs, M. S. Conradi, M. E. Merritt. *Magn. Reson. Mater. Phys., Biol., Med* **2015**, *98*, 195–205. doi:10.1007/s10334-014-0455-2.

[24] J. Heckmann, W. Meyer, E. Radtke, G. Reicherz, S. Goertz. *Phys. Rev. B* **2006**, *74*, 134418. doi:10.1103/PhysRevB.74.134418.

[25] L. Lumata, Z. Kovacs, A. D. Sherry, C. Malloy, S. Hill, J. van Tol, L. Yu, L. Song, M. Merritt. *Phys. Chem. Chem. Phys.* **2013**, *15*, 9800–9807. doi:10.1039/C3CP50186H.

[26] J. W. Gordon, S. B. Fain, I. J. Rowland. *Magn. Reson. Med.* **2012**, *68*, 1949–1954. doi:10.1002/mrm.24207.

[27] A. Flori, M. Liserani, S. Bowen, J. H. Ardenkjaer-Larsen, L. Menichetti. *J. Phys. Chem. A* **2015**, *119*, 1885–1893. doi:10.1021/jp511972g.

[28] L. F. Waldner, A. Chen, W. Mander, T. Scholl, C. McKenzie. *J. Magn. Reson.* **2012**, *223*, 85–89. doi:10.1016/j.jmr.2012.07.010.

[29] L. Lumata, M. E. Merritt, C. R. Malloy, A. D. Sherry, Z. Kovacs. *J. Phys. Chem. A* **2012**, *116*, 5129–5138. doi:10.1021/jp302399f.

[30] L. Lumata, M. E. Merritt, Z. Kovacs. *Phys. Chem. Chem. Phys.* **2013**, *15*, 7032–7035. doi:10.1039/C3CP50750E.

[31] F. Kurdzesau, B. van den Brandt, A. Comment, P. Hautle, S. Jannin, J. J. van der Klink, J. A. Konter. *J. Phys. D Appl. Phys.* **2008**, *41*, 155506. doi:10.1088/0022-3727/41/15/155506.

[32] A. Kiswandhi, B. Lama, P. Niedbalski, M. Goderya, J. Long, L. Lumata. *RSC Adv.* **2016**, *6*, 38855–38860. doi:10.1039/C6RA02864K.

[33] E. Chiavazza, A. Viale, M. Karlsson, S. Aime. *Contrast Media Mol. Imaging* **2013**, *8*, 417–421. doi:10.1002/cmmi.1538.

[34] L. Lumata, Z. Kovacs, C. Malloy, A. D. Sherry, M. Merritt. *Phys. Med. Biol.* **2011**, *56*, N85–N92. doi:10.1088/0031-9155/56/5/N01.

[35] S. Jannin, A. Bornet, R. Melzi, G. Bodenhausen. *Chem. Phys. Lett.* **2012**, *549*, 99–102. doi:10.1016/j.cplett.2012.08.017.

[36] S. Jannin, A. Bornet, S. Colombo, G. Bodenhausen. *Chem. Phys. Lett.* **2011**, *517*, 234–236. doi:10.1016/j.cplett.2011.10.042.

[37] A. Bornet, R. Melzi, A. J. Perez-Linde, P. Hautle, B. van den Brandt, S. Jannin, G. Bodenhausen. *J. Phys. Chem. Lett.* **2013**, *4*, 111–114. doi:10.1021/jz301781t.

[38] M. Batel, M. Krajewski, A. Däpp, A. Hunkeler, B. H. Meier, S. Kozerke, M. Ernst. *Chem. Phys. Lett.* **2012**, *554*, 72–76. doi:10.1016/j.cplett.2012.10.018.

[39] M. Batel, A. Däpp, A. Hunkeler, B. H. Meier, S. Kozerke, M. Ernst. *Phys. Chem. Chem. Phys.* **2014**, *16*, 21407–21416. doi:10.1039/c4cp02696a.

[40] B. Vuichoud, J. Milani, A. Bornet, R. Melzi, S. Jannin, G. Bodenhausen. *J. Phys. Chem. B* **2014**, *118*, 1411–1415. doi:10.1021/jp4118776.

[41] P. Miéville, P. Ahuja, R. Sarkar, S. Jannin, P. R. Vasos, S. Gerber-Lemaire, M. Mishkovsky, A. Comment, R. Gruetter, O. Ouari, P. Tordo, G. Bodenhausen. *Angew. Chem. Intl. Ed.* **2010**, *49*, 6182–6185. doi:10.1002/anie.201000934.

[42] M. Borghini, K. Scheffler. *Phys. Rev. Lett.* **1971**, *26*, 1362–1365. doi:10.1103/PhysRevLett.26.1362.

[43] M. Borghini. *Phys. Rev. Lett.* **1968**, *20*, 419–421. doi:10.1103/PhysRevLett.20.419.

[44] W. de Boer, M. Borghini, K. Morimoto, T. O. Niinikoski, F. J. Udo. *J. Low Temp. Phys.* **1974**, *15*, 249. doi:10.1007/BF00661185.

[45] S. T. Goertz. *Nucl. Instrum. Methods A* **2004**, *526*, 28–42. doi:10.1016/j.nima.2004.03.147.

[46] A. Okajo, K. Matsumoto, J. B. Mitchell, M. C. Krishna, K. Endo. *Magnet Reson. Med.* **2006**, *56*, 422–431. doi:10.1002/mrm.20958.

[47] B. van den Brandt, E. I. Bunyatova, P. Hautle, J. A. Konter. *Nucl.Instrum. Methods A* **2004**, *526*, 53–55. doi:10.1016/j.nima.2004.03.149.

[48] S. Jannin, A. Comment, F. Kurdzesau, J. A. Konter, P. Hautle, B. van den Brandt, J. J. van der Klink. *J. Chem. Phys.* **2008**, *128*, 241102.

The effect of glassing solvent deuteration and Gd^{3+} doping on ^{13}C DNP at 5 T

Andhika Kiswandhi,†[a] Bimala Lama,†[b] Peter Niedbalski,[a] Mudrekh Goderya,[a] Joanna Long[b] and Lloyd Lumata*[a]

We report the influence of glassing solvent deuteration and Gd^{3+} doping on ^{13}C dynamic nuclear polarization (DNP) nuclear magnetic resonance (NMR) performed on [1-^{13}C] sodium acetate at $B_0 = 5$ T and 1.2 K. Our data reveal that at 5 T, glassing solvent deuteration still results in a 40% improvement of the ^{13}C DNP signal when a large electron spin resonance (ESR) linewidth 4-oxo-TEMPO free radical is used, but results in a 60% decrease of the DNP signal in the case of a sample doped with small ESR linewidth trityl OX063. An addition of a trace amount of the Gd^{3+} complex Gd–HP–DO3A led to a negligible slight decrease on the ^{13}C polarization TEMPO-doped sample, but is still relatively beneficial for the trityl-doped sample with 30% improvement of the DNP-enhanced ^{13}C polarization. These findings indicate that while these DNP optimization steps are still valid at 5 T, the effects are not as pronounced as observed in ^{13}C DNP at $B_0 = 3.35$ T. These DNP results at 5 T are discussed thermodynamically within the framework of the thermal mixing model of DNP.

1. Introduction

Conventional nuclear magnetic resonance (NMR) spectroscopy, while very useful and widely used, lacks sensitivity due to the small difference in the spin populations between nuclear Zeeman spin states at ambient conditions, resulting in low polarization of the nuclei. In other words, this low polarization level stems from the energy difference between the two nuclear-spin states being low compared to the thermal energy.[1] In contrast, electron spins can be polarized rather easily, owing to their higher gyromagnetic ratio γ and thus a larger energy gap between the two spin states. In general, the γ of electrons is about three orders of magnitude higher than that of typically observed nuclei.

Dynamic nuclear polarization (DNP) is a method of amplifying nuclear polarization by transferring the high polarization of electrons to the nuclei *via* microwave radiation at low temperature and high magnetic field.[2] The resulting large enhancement in the nuclear polarization or NMR sensitivity leads to time savings in NMR measurements, especially on nuclei having low gyromagnetic ratios such ^{13}C, ^{15}N, ^{89}Y, or ^{107,109}Ag.[2–8] Furthermore, DNP-NMR has become a rapidly emerging technique in the biomedical research community, where it is used in probing metabolic anomalies in various

diseases such as cancer, with the combined superb sensitivity and high specificity provided by hyperpolarized ^{13}C NMR spectroscopy or imaging (MRI).[9–14]

In a typical dissolution DNP setup,[2] a sample containing the target nuclei is doped with a free radical at an optimum concentration and embedded uniformly in a glassing matrix. The whole solution is then cooled down to a cryogenic temperature (<4 K) in a high magnetic field (>1 T). The purpose of this step is to polarize the electrons provided by the free radicals by Boltzmann thermal polarization. Hyperpolarization is achieved by irradiating the frozen sample with a microwave frequency close to the electron spin resonance (ESR) frequency of the free radical. This process results in a transfer of the high spin alignment from the electrons to the target nuclei.[1,15,16] Taking advantage of the relatively long spin-lattice relaxation time T_1 of target nuclei, dissolution DNP is able to harness the amplified NMR signals in the liquid-state at physiologically tolerable temperatures.[2]

Based on the procedure above, for any nuclei, two factors contributing to the sensitivity enhancement can be identified: (i) instrumental setup (B_0/T ratio) and (ii) sample preparation. Factor (i) determines the polarization of the electrons in the free radical; B_0 also determines the energy difference between the nuclear Zeeman energy levels or the Larmor frequency of the nuclei (ω_I). B_0 and T also determine the relaxation constants of the electron and nuclear spins. Factor (ii), in particular the type of free radical used, determines whether the width (D) of the electron spin resonance (ESR) spectrum of the free radical is larger or smaller than ω_I. Together, these factors determine the way by which the predominant DNP mechanism proceeds: (a)

[a]*Department of Physics, University of Texas at Dallas, Richardson, Texas 75080, USA. E-mail: lloyd.lumata@utdallas.edu*

[b]*Department of Biochemistry and Molecular Biology, University of Florida, Gainesville, FL 32610, USA*

† These authors provided equal contribution.

via the solid effect when $D < \omega_I$ or (b) *via* the thermal mixing effect which occurs when $D > \omega_I$.[1,15,16] A study by Lumata *et al.* has shown the effects of deuteration of the glassing matrix in ^{13}C DNP at 3.35 T, which improves the nuclear polarization when galvinoxyl, DDPH, or 4-oxo-TEMPO is used.[17] However, the glassing solvent deuteration decreases the nuclear polarization when BDPA or trityl OX063 was used as the free radical dopant.[17] Similar studies on the effects of addition of trace amounts of lanthanides such as Gd^{3+} on DNP samples reported significant improvements in the DNP-enhanced polarization levels.[18–21] Many DNP optimization studies reported previously were performed at magnetic fields of 3.35 T, mainly due to the availability of commercial hyperpolarizer operating at 3.35 T (Hypersense, Oxford Instruments, UK) and W-band microwave source. Recent work has shown greater DNP-enhanced polarization levels can be gained at fields of 5–7 T[22–25] and a recent DNP hyperpolarizer for clinical purposes (SPINlab™, GE Healthcare, WI) has an operating field of 5 T.[26] Therefore, greater exploration of suitable sample conditions for optimal polarization properties at these fields are needed, especially as the electronic properties of free radicals change with field.[27] In this article, we have investigated the influence of glassing solvent deuteration and the inclusion of Gd^{3+} on ^{13}C DNP at a field of 5 T. Free radicals 4-oxo-TEMPO and trityl OX063 (Fig. 1) are used to represent free radicals with wide and narrow ESR linewidths, respectively.

2.   Experimental

2.1   Materials

The free radicals were obtained from commercial suppliers: (a) tris[8-carboxyl-2,2,6,6-benzo(1,2-*d*:5*d*)-bis(1,3)dithiole-4-yl]methyl-sodium salt (trityl OX063) [Oxford Instruments Molecular Bio-tools], (b) 4-oxo-2,2,6,6-tetramethylpiperidine-1-oxyl(4-oxo-TEMPO) [Sigma Aldrich]. [1-^{13}C] sodium acetate, glycerol, and deuterated

d_8-glycerol were purchased from Sigma Aldrich. ProHance Gd^{3+} contrast agent was purchased from Bracco Diagnostics, New Jersey as 0.5 M Gd–HP–DO3A solution in water. Deuterium used as a solvent in this study was obtained from Cambridge Isotope Laboratories (Tewksbury, Massachusetts). The samples are prepared by mixing the materials following a procedure described below and used without further purification.

Trityl-doped samples. The trityl samples were prepared to yield a volume of 100 μL each. [1-^{13}C] sodium acetate solution (3 M) in a 1 : 1 v/v glycerol/water glassing solvent was prepared and doped with trityl OX063 (15 mM) as a reference sample. For the deuterated sample, 1 : 1 v/v d_8-glycerol/D_2O was used in place of the glycerol/water glassing solvent. The sample doped with Gd^{3+} was prepared by adding a trace amount of ProHance contrast agent (2 mM). To ensure homogeneity, each sample was mixed using a vortex mixer for at least 3 minutes.

TEMPO-doped samples. The 4-oxo-TEMPO-doped samples were prepared to yield a total volume of 200 μL each. [1-^{13}C] sodium acetate solution (3 M) in a 1 : 1 v/v glycerol/water glassing solvent was prepared and doped with 4-oxo-TEMPO (40 mM) as a reference sample. For the deuterated sample, 1 : 1 v/v d_8-glycerol/D_2O was used in place of the glycerol/water glassing solvent. The sample doped with Gd^{3+} was prepared by adding a trace amount of ProHance contrast agent (2 mM). Each sample was mixed using a vortex mixer for at least 3 minutes.

2.2   Dynamic nuclear polarization and data analysis

The samples were polarized in a homebuilt DNP system at the University of Florida utilizing an 89 mm room-temperature bore superconducting Bruker magnet energized to 5 T as described before.[28] Samples were placed inside a cryostat and cooled down to $T = 1.2$ K. Due to the difficulty in obtaining the ^{13}C thermal NMR signal at cryogenic temperatures, only the relative ^{13}C polarization levels were plotted for each of the DNP samples. Relative ^{13}C DNP polarization levels were used in previous studies to evaluate the effectiveness of DNP optimization methods especially in sample preparation practices.[17,19,21] To ensure repeatability, all DNP measurements were done in triplicate. The mean values and standard deviations were calculated. The relative ^{13}C NMR intensity was measured using a Bruker Avance III console (Bruker Biospin, MA) connected to a four-turn NMR saddle coil with a 24 mm height and 18 mm diameter surrounding the sample in the cryostat. For the polarization build up measurements, relative polarization level was initially zeroed by a series of RF pulses. Each sample was then polarized for up to 4 hours with continuous 50 mW microwave irradiation at a frequency of 140.71 GHz (4-oxo-TEMPO) or 140.31 GHz (trityl OX063) using a microwave source from Virginia Diodes, Inc. ^{13}C NMR polarization build up was monitored every 200 s (4-oxo-TEMPO) or 300 s (trityl OX063) using a single, low-tip angle pulse (30 μs, 10 W). A signal acquisition time of 20 ms with 2048 data points was used followed by 1 kHz line broadening and Fast Fourier Transform (FFT). A linear baseline correction and zeroth order phase correction were applied to the Fourier transformed data. NMR
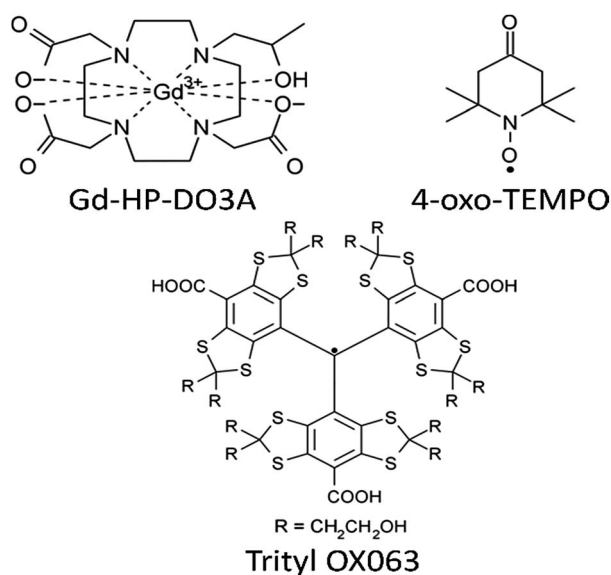

Fig. 1   Structures of ProHance Gd^{3+} contrast agent and free radical polarizing agents studied in this work.

signal intensity was measured by absolute integration. For determination of the optimal DNP microwave frequencies, similar signal acquisition and processing parameters were used, except polarization was monitored every 60 s for up to 12 minutes at each microwave frequency step. The DNP NMR data were plotted and analyzed using Igor Pro version 6.1 (Wave-metrics, OR).

3. Results and discussion

The results of the microwave frequency sweeps for reference samples doped with either 4-oxo-TEMPO or trityl OX063 radical are shown in Fig. 2. The optimum microwave frequencies for DNP are indicated by arrows, with both positive (P_+) and negative (P_-) maximum polarizations observed as expected. In trityl-doped samples, the addition of trace Gd^{3+} shifts the positive and negative maxima by approximately 12 MHz toward the center.

Fig. 3 and 4 show the relative ^{13}C polarization level of each of the trityl- and TEMPO-doped samples, normalized with respect to the reference samples which were set to unity. The data indicate that glassing solvent deuteration leads to a significant decrease, about 60%, in relative DNP-enhanced ^{13}C polarization in the case of trityl-containing sample. On the other hand, this sample preparation method leads to about 40% improvement in the relative ^{13}C polarization for the sample doped with TEMPO. These behavior with glassing solvent deuteration can

Fig. 3 The relative ^{13}C polarization for trityl (top) and TEMPO-doped samples (bottom) observed at $B = 5$ T, normalized with respect to the reference samples (see text). In both plots, reference samples are denoted by red circles, deuterated samples by blue triangles, and Gd^{3+} doped samples by green diamonds.

Fig. 2 The microwave frequency dependency of ^{13}C polarization for samples containing trityl (top) or TEMPO (bottom) electron spins. Arrows indicate the location of positive and negative polarization maxima.

be attributed to the differences in the nuclear Zeeman heat load, depending upon which type of free radical is used for DNP.[15,17]

As can be inferred from the structure, the nitroxide-based free radical 4-oxo-TEMPO has a large g-anisotropy and hyper-fine coupling contribution from the surrounding nuclei, thus a relatively broad ESR linewidth of about 465 MHz at 5% base was observed at 100 K using W-band ESR.[17] The ESR linewidth of TEMPO is larger than the Larmor frequencies of both protons ($\gamma = 42.58$ MHz T^{-1}) and ^{13}C ($\gamma = 10.7$ MHz T^{-1}) spins even at 5 T. Therefore, in the TEMPO-doped samples, the DNP process is expected to proceed predominantly *via* the thermal mixing process where both ^1H and ^{13}C spins are simultaneously polarized.[29] In thermal mixing, the nuclear Zeeman system (NZS) is being cooled down *via* thermal contact with the microwave-cooled electron dipolar system (EDS), with both systems eventually acquiring the same spin temperature.[15,30–33] The effectiveness of the DNP cooling process is affected by the heat capacity of each system. The specific heat capacity of NZS, C_Z, is proportional to ω_I^2, where ω_I is the Larmor frequencies of
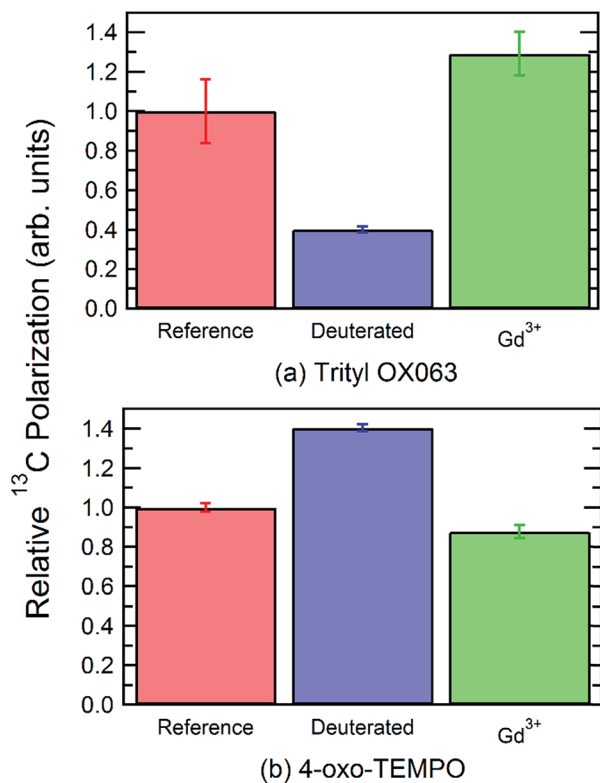
Fig. 4 The maximum polarization of the reference, deuterated, and Gd^{3+}-doped samples containing trityl (a) or TEMPO (b) free radicals.

the NMR-active nuclei present in the DNP sample.[15] Substitution of protons with deuterons (^{2}H $\gamma = 6.54$ MHz T^{-1}) in the DNP sample *via* deuteration of the glassing matrix lowers the specific heat capacity of NZS due to the lower γ or Larmor frequency of ^{2}H spins. Thermodynamically speaking, lower specific heat capacity of the deuterated sample means that the EDS can easily cool down the NZS, thus resulting in a lower nuclear spin temperature or a larger nuclear spin polarization.[17] Thus, glassing solvent deuteration is still recommended for ^{13}C DNP at 5 T when wide ESR linewidth free radical such as 4-oxo-TEMPO is used.

On the other hand, the case for the DNP with trityl OX063 is different. The carbon-centered free radical trityl OX063 has a narrow ESR spectrum with 5% base linewidth of 115 MHz at W-band due to its highly symmetrical structure and its free radical center is surrounded by mainly spin-less nuclei.[17] The ESR linewidth of trityl OX063 is comparable to the ^{13}C Larmor frequency so thermal mixing is the expected predominant DNP mechanism for ^{13}C and other low-γ nuclei using trityl. It has been shown in previous studies[3,5,18] that indeed trityl is more favorable for use in DNP of samples having low-γ spins such as ^{13}C. On the other hand, the Larmor frequencies of high-γ nuclei such as protons are much larger than the trityl ESR linewidth, thus ^{1}H DNP with trityl is expected to proceed mainly *via* solid effect.[34] This also means that, when trityl OX063 is used, the proton Zeeman system is essentially decoupled from EDS, thus EDS only has to cool down the ^{13}C spins. However, substitution of protons by deuterons in the glassing matrix leads to an

additional heat load for the EDS.[17,35] The ^{2}H Larmor frequency is less than or comparable to the trityl ESR D, thus the ^{2}H NZS is now thermally coupled to the trityl EDS. Microwave frequency sweep of ^{2}H-enriched compound doped with trityl revealed that its positive and negative polarization peaks almost overlap with the optimum microwave frequencies of trityl-doped ^{13}C samples at 3.35 T and 1.4 K as reported in a previous study.[8] This implies that EDS now has to cool down not only the ^{13}C spins but also the ^{2}H spins, eventually leading to slightly higher spin temperature or relatively lower ^{13}C DNP signal as shown in Fig. 3 and 4.[15,17] Therefore, glassing solvent deuteration is not beneficial for ^{13}C DNP at 5 T when trityl OX063 is used.

In the trityl-doped sample, it has to be emphasized that the addition of Gd^{3+} results in a significant shift in the optimum microwave frequency for polarization transfer.[18] Therefore, the frequency for the microwave irradiation must be retuned when Gd^{3+} is used. The addition of 2 mM Gd^{3+} in the trityl sample gives merely a modest enhancement of 30% in the polarization at a field of 5 T, in contrast to the 100–300% increase observed at $B_0 = 3.35$ T using [1-^{13}C] pyruvate as a target nuclei.[18–21] This result suggests that the polarization enhancement by an addition of Gd^{3+} decreases as the field increases. Interestingly, in the TEMPO-doped samples, the inclusion of Gd^{3+} results in a tiny decrease in the polarization. Such decrease was not observed at 3.35 T, unless the Gd^{3+} concentration exceeds the optimum value.[18] Both results indicate that the benefits of adding Gd^{3+} diminish at a higher field.

In order to explain the results of Gd^{3+} doping, we consider the theoretical maximum limit of thermal mixing process in DNP, which is given by[16,18]

$$P_{max} = \tanh\left(\beta_L \frac{\omega_e \omega_I}{4D} \frac{1}{\sqrt{\eta(1+f)}}\right) \quad (1)$$

where $\beta_L = \hbar/k_B T_L$ ($\hbar$, k_B, T_L are Planck's constant, the Boltzmann constant, and the lattice temperature, respectively). In eqn (1), ω_e, η ($=T_{1Z}/T_{1D}$), and f are the Larmor frequency of the electron spins, the ratio of the electronic Zeeman relaxation time (T_{1Z}) to the dipolar spin-lattice relaxation time (T_{1D}), and the "leakage factor", respectively. It has been reported that the addition of Gd^{3+} has negligible effect on ESR linewidth D.[27] The Larmor frequencies are the same for both the reference and Gd-doped samples thus, it leaves the factor $1/\sqrt{\eta(1+f)}$ as the potential source of enhancement. The Gd^{3+} ions affect the polarization mainly by lowering the relaxation time for the electronic Zeeman system T_{1Z} with no significant effect on the relaxation times of the nuclei.[18] Therefore, this suggests that the polarization enhancement due to Gd^{3+} doping is a result of decreasing η. As mentioned before, the improvement in ^{13}C DNP due to Gd-doping for trityl-doped samples is less pronounced at 5 T compared to the DNP optimization results observed at 3.35 T.[18–21] This behavior may be ascribed to the fact that the trityl electron T_1 are already shorter at higher magnetic fields,[27] thus it is likely the extent of electron T_1 reduction by Gd doping at higher fields is also less pronounced. Further ESR studies may be needed to elucidate this effect at higher magnetic fields. Nevertheless, Gd^{3+} doping is still advantageous for ^{13}C DNP at 5 T using trityl OX063 as the polarizing agent.

4. Conclusion

In conclusion, it has been shown that at $B_0 = 5$ T, glassing solvent deuteration is still beneficial for ^{13}C DNP when large ESR linewidth free radical such as 4-oxo-TEMPO is used. This effect results from the lowering of the heat capacity of the nuclear Zeeman system upon substitution of ^1H with ^2H spins, thus lowering the heat load for cooling by the electron dipolar system. Deuteration of the glassing matrix, however, is not recommended for ^{13}C DNP using trityl OX063 at 5 T. Deuteration in the case of trityl OX063 leads to a larger heat load to the nuclear Zeeman system, by creating an additional thermal link between the ^2H nuclear Zeeman system of the solvent and the electronic dipolar system, so ^{13}C polarization decreases. In addition, inclusion of trace amounts of Gd^{3+} shifts the optimum microwave frequency for ^{13}C DNP, so care must be taken when performing these experiments. A very slight decrease in ^{13}C DNP signal were observed when Gd^{3+} is added to TEMPO-doped samples. On the other hand, Gd^{3+} doping is still recommended for ^{13}C DNP at 5 T when trityl OX063 is used as the polarizing agent. The improvement, however, is relatively modest compared to the results at 3.35 T and this may be attributed to changes in electron relaxation behavior at higher fields. The optimization data obtained in this work may be useful in DNP sample preparation at higher fields, especially with the advent of the commercial clinical hyperpolarizer SPINlab™ which operates at a field of 5 T.

Acknowledgements

Notes and references

1 A. Abragam, *The principles of nuclear magnetism*, Oxford University Press, Oxford, 2004.
2 J. H. Ardenkjær-Larsen, B. Fridlund, A. Gram, G. Hansson, L. Hansson, M. H. Lerche, R. Servin, M. Thaning and K. Golman, *Proc. Natl. Acad. Sci. U. S. A.*, 2003, **100**, 10158–10163.
3 L. L. Lumata, R. Martin, A. K. Jindal, Z. Kovacs, M. S. Conradi and M. E. Merritt, *Magn. Reson. Mater. Phys., Biol. Med.*, 2014, **28**, 195–205.
4 W. Jiang, L. Lumata, W. Chen, S. Zhang, Z. Kovacs, A. D. Sherry and C. Khemtong, *Sci. Rep.*, 2015, **5**, 9104.
5 L. Lumata, A. K. Jindal, M. E. Merritt, C. R. Malloy, A. D. Sherry and Z. Kovacs, *J. Am. Chem. Soc.*, 2011, **133**, 8673–8680.
6 L. Lumata, M. E. Merritt, C. Malloy, A. D. Sherry and Z. Kovacs, *Appl. Magn. Reson.*, 2012, **43**, 69–79.
7 L. Lumata, M. E. Merritt, Z. Hashami, S. J. Ratnakar and Z. Kovacs, *Angew. Chem., Int. Ed.*, 2012, **51**, 525–527.
8 S. Reynolds and H. Patel, *Appl. Magn. Reson.*, 2008, **34**, 495–508.
9 L. Lumata, C. Yang, M. Ragavan, N. Carpenter, R. J. DeBerardinis and M. E. Merritt, *Methods Enzymol.*, 2015, **561**, 73–106.
10 A. Comment and M. E. Merritt, *Biochemistry*, 2014, **53**, 7333–7357.
11 J. Kurhanewicz, D. B. Vigneron, K. Brindle, E. Y. Chekmenev, A. Comment, C. H. Cunningham, R. J. DeBerardinis, G. G. Green, M. O. Leach, S. S. Rajan, R. R. Rizi, B. D. Ross, W. S. Warren and C. R. Malloy, *Neoplasia*, 2011, **13**, 81–97.
12 K. Golman and J. S. Petersson, *Acad. Radiol.*, 2006, **13**, 932–942.
13 K. M. Brindle, S. E. Bohndiek, F. A. Gallagher and M. I. Kettunen, *Magn. Reson. Med.*, 2011, **66**, 505–519.
14 S. J. Nelson, D. Vigneron, J. Kurhanewicz, A. Chen, R. Bok and R. Hurd, *Appl. Magn. Reson.*, 2008, **34**, 533–544.
15 S. T. Goertz, *Nucl. Instrum. Methods Phys. Res., Sect. A*, 2004, **526**, 28–42.
16 J. Heckmann, W. Meyer, E. Radtke, G. Reicherz and S. Goertz, *Phys. Rev. B: Condens. Matter Mater. Phys.*, 2006, **74**, 134418.
17 L. Lumata, M. E. Merritt and Z. Kovacs, *Phys. Chem. Chem. Phys.*, 2013, **15**, 7032–7035.
18 L. Lumata, M. E. Merritt, C. R. Malloy, A. D. Sherry and Z. Kovacs, *J. Phys. Chem. A*, 2012, **116**, 5129–5138.
19 J. W. Gordon, S. B. Fain and I. J. Rowland, *Magn. Reson. Med.*, 2012, **68**, 1949–1954.
20 A. Flori, M. Liserani, S. Bowen, J. H. Ardenkjaer-Larsen and L. Menichetti, *J. Phys. Chem. A*, 2015, **119**, 1885–1893.
21 L. F. Waldner, A. Chen, W. Mander, T. Scholl and C. McKenzie, *J. Magn. Reson.*, 2012, **223**, 85–89.
22 J. H. Ardenkjaer-Larsen, S. Macholl and H. Jóhannesson, *Appl. Magn. Reson.*, 2008, **34**, 509–522.
23 H. Jóhannesson, S. Macholl and J. H. Ardenkjaer-Larsen, *J. Magn. Reson.*, 2009, **197**, 167–175.
24 S. Jannin, A. Comment, F. Kurdzesau, J. A. Konter, P. Hautle, B. van den Brandt and J. J. van der Klink, *J. Chem. Phys.*, 2008, **128**, 241102.
25 S. Jannin, A. Bornet, R. Melzi and G. Bodenhausen, *Chem. Phys. Lett.*, 2012, **549**, 99–102.
26 J. H. Ardenkjaer-Larsen, *J. Magn. Reson.*, 2016, **264**, 3–12.
27 L. Lumata, Z. Kovacs, A. D. Sherry, C. Malloy, S. Hill, J. van Tol, L. Yu, L. Song and M. E. Merritt, *Phys. Chem. Chem. Phys.*, 2013, **15**, 9800–9807.
28 B. Lama, J. H. P. Collins, D. Downes, A. N. Smith and J. R. Long, *NMR Biomed.*, 2016, **29**, 226–231.
29 A. Comment, B. van der Brandt, K. Uffman, F. Kurdzesau, S. Jannin, J. A. Konter, P. Hautle, W. T. Wenkebach, R. Gruetter and J. J. van der Klink, *Concepts Magn. Reson., Part B*, 2007, **31**, 255–269.
30 M. Borghini and K. Scheffler, *Phys. Rev. Lett.*, 1971, **26**, 1362–1365.
31 M. Borghini, W. de Boer and K. Morimoto, *Phys. Lett. A*, 1974, **48**, 244–246.

32 M. Borghini, *Phys. Rev. Lett.*, 1968, **20**, 419–421.

33 W. de Boer, M. Borghini, K. Morimoto, T. O. Niinikoski and F. J. Udo, *J. Low Temp. Phys.*, 1974, **15**, 249.

34 J. Wolber, F. Ellner, B. Fridlund, A. Gram, H. Johannesson, G. Hansson, L. H. Hansson, M. H. Lerche, S. Mansson, R. Servin, M. Thaning, K. Golman and J. H. Ardenkjaer-Larsen, *Nucl. Instrum. Methods Phys. Res., Sect. A*, 2004, **526**, 173–181.

35 F. Kurdzesau, B. van der Brandt, A. Comment, P. Hautle, S. Jannin, J. J. van der Klink and J. A. Konter, *J. Phys. D: Appl. Phys.*, 2008, **41**, 155506.
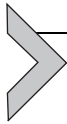
Hyperpolarized ^{13}C Magnetic Resonance and Its Use in Metabolic Assessment of Cultured Cells and Perfused Organs

Lloyd Lumata[*,1], **Chendong Yang**[†], **Mukundan Ragavan**[‡],
Nicholas Carpenter[‡], **Ralph J. DeBerardinis**[†,1], **Matthew E. Merritt**[‡,1]

[*]Department of Physics, University of Texas at Dallas, Richardson, Texas, USA
[†]Children's Medical Center Research Institute, University of Texas Southwestern Medical Center, Dallas, Texas, USA
[‡]Advanced Imaging Research Center, University of Texas Southwestern Medical Center, Dallas, Texas, USA
[1]Corresponding authors: e-mail address: lloyd.lumata@utdallas.edu; ralph.deberardinis@utsouthwestern.edu; matthew.merritt@utsouthwestern.edu

Contents

Abstract

Diseased tissue is often characterized by abnormalities in intermediary metabolism. Observing these alterations *in situ* may lead to an improved understanding of pathological processes and novel ways to monitor these processes noninvasively in human patients. Although ^{13}C is a stable isotope safe for use in animal models of disease as well as human subjects, its utility as a metabolic tracer has largely been limited to *ex vivo* analyses employing analytical techniques like mass spectrometry or nuclear magnetic resonance spectroscopy. Neither of these techniques is suitable for noninvasive metabolic monitoring, and the low abundance and poor gyromagnetic ratio of conventional ^{13}C make it a poor nucleus for imaging. However, the recent advent of hyperpolarization methods, particularly dynamic nuclear polarization (DNP), makes it possible to enhance the spin polarization state of ^{13}C by many orders of magnitude, resulting in a temporary amplification of the signal sufficient for monitoring kinetics of enzyme-catalyzed reactions in living tissue through magnetic resonance spectroscopy or magnetic resonance imaging. Here, we review DNP techniques to monitor metabolism in cultured cells, perfused hearts, and perfused livers, focusing on our experiences with hyperpolarized [1-^{13}C]pyruvate. We present detailed approaches to optimize the DNP procedure, streamline biological sample preparation, and maximize detection of specific metabolic activities. We also discuss practical aspects in the choice of metabolic substrates for hyperpolarization studies and outline some of the current technical and conceptual challenges in the field, including efforts to use hyperpolarization to quantify metabolic rates *in vivo*.

1. INTRODUCTION: IMPORTANCE OF DEVELOPING METHODS TO OBSERVE METABOLIC FLUX IN DISEASE STATES

Metabolism is at the root of essentially all physiological processes (DeBerardinis & Thompson, 2012). The production and expenditure of energy, storage and breakdown of macromolecules, disposal of waste, and many other processes are subserved by thousands of enzymatic reactions at work in human cells. Recent work has produced insights that greatly extend the influence of metabolism and metabolites to include such seemingly disparate processes as signal transduction, posttranslational modification of proteins, and epigenetic effects on gene expression (Choudhary, Weinert, Nishida, Verdin, & Mann, 2014; Kaelin & McKnight, 2013; Ward & Thompson, 2012). These observations further emphasize the principle that metabolism is inexorably intertwined with cellular function and tissue homeostasis. In short, normal tissue function cannot occur unless metabolism is properly regulated.

For most of the past century, metabolism research has been dominated by studies in organs like the liver, one of whose major functions is to maintain metabolic homeostasis for the entire body, and the skeletal muscle, heart, and brain, whose normal function involves energetically demanding processes. However, many other tissues are equally dependent on a broad complement of metabolic activities. As an example, an emerging theme in cell biology research is the importance of acute metabolic changes for enabling physiological cell growth and proliferation (Metallo & Vander Heiden, 2013; Plas & Thompson, 2005). Because growth and proliferation are viewed as metabolically demanding in terms of the need for energy and macromolecular synthesis, there has been interest in understanding how the signals that stimulate punctuated bursts of cell proliferation engage the metabolic network to satisfy these demands. T-cell activation is one of the many processes now known to require several specific metabolic activities to support cell growth and proliferation (Gerriets et al., 2015).

Given the many links between metabolism and cellular function, it is unsurprising that most diseases feature abnormal metabolism at the cellular level (DeBerardinis & Thompson, 2012). Of the hundreds of monogenic diseases caused by mutations in single enzymes (the so-called inborn errors of metabolism), a high fraction affects the liver, heart, muscle, and brain. Many other monogenic metabolic diseases involve poorly defined effects on growth, either because of systemic metabolic imbalances or perhaps effects on specific populations of cells whose function is required for normal growth. Importantly, common diseases also involve altered metabolism. Among the most common causes of death in the United States, heart disease, cancer, stroke, and diabetes can all be viewed as involving altered metabolism at the level of the cell and/or organ. Thus, we need better tools to understand metabolic regulation in diseased tissues. Preferably, some of these tools will support metabolic analysis in intact tissue.

Metabolic dysregulation is a prominent and clinically relevant feature of cancer biology. As early as the 1920s, Warburg demonstrated that malignant cells have a propensity to take up excess amounts of glucose and convert it into lactate, even when oxygen availability was sufficient to oxidize glucose completely to carbon dioxide (Warburg, 1956b). The successful use of [18]fluoro-2-deoxyglucose (FDG) as a radiotracer for positron emission tomography (PET) studies in cancer patients has validated the clinical importance of glucose uptake in human tumors (Gallamini, Zwarthoed, & Borra, 2014). FDG–PET is commonly used to image the distribution of malignant tissue and to monitor the effects of therapy. Other

imaging techniques have also been employed to observe altered metabolic states in tumors. Proton magnetic resonance spectroscopy (^{1}H MRS) enables the detection and quantitation of abundant metabolites, some of which have prognostic or diagnostic value. To date, this technique has been used most extensively in brain tumors and other central nervous system diseases (Oz et al., 2014). An example of a recent technical development is the use of ^{1}H MRS to detect 2-hydroxyglutarate, an "oncometabolite" produced by mutant forms of the metabolic enzymes isocitrate dehydrogenase-1 and -2 in brain tumors (Andronesi et al., 2012; Choi et al., 2012; Elkhaled et al., 2012; Pope et al., 2012). After a considerable amount of research over the past decade, metabolic reprogramming as a consequence of tumorigenic mutations in oncogenes or tumor suppressor genes is now considered to be one of the major biological hallmarks of cancer (Hanahan & Weinberg, 2011).

Stable isotope tracers like ^{13}C are widely used to investigate metabolism in living systems. Transfer of ^{13}C from a parent molecule (e.g., glucose) into downstream metabolites reports the activity of metabolic pathways, providing an important complement to measurements of steady-state metabolite levels. Because ^{13}C is a nonradioactive tracer that is effectively monitored using analytical techniques like nuclear magnetic resonance or mass spectrometry, administering ^{13}C to animals or human subjects is safe. A typical experiment involves the administration of one or more isotope-labeled nutrients to the subject, followed by periodic or endpoint acquisition of tissues of interest (e.g., blood, urine, tumor), extraction of informative metabolites, and analysis of isotope enrichment patterns to infer metabolic pathway activity. This type of approach has been used successfully in mice and humans to probe metabolic alterations in cancer and other metabolic disorders (Busch, Neese, Awada, Hayes, & Hellerstein, 2007; Maher et al., 2012; Marin-Valencia et al., 2012; Sunny, Parks, Browning, & Burgess, 2011; Ying et al., 2012; Yuneva et al., 2012).

Each of these methods has only a limited ability to report on the metabolic network. Stable isotope approaches are invasive and destructive; that is, they require tissue sampling and metabolite extraction in order to obtain information about metabolism. In addition, metabolic activity is inferred from ^{13}C enrichment rather than by observing metabolism directly through an imaging technique. On the other hand, while PET supports direct, noninvasive detection of a labeled metabolic probe, the resulting information is limited to anatomic localization of probe uptake and accumulation, with essentially no information about downstream metabolic

activities. ^{1}H MRS quantifies metabolite pools but provides no information about flux and is somewhat limited by the narrow chemical shift range of the ^{1}H spectrum.

Methods to image ^{13}C would be powerful tools to probe disease-associated metabolic changes because they would enable direct visualization of metabolic activity and in principle could be repeated multiple times in the same subject. The wide chemical shift range of the ^{13}C NMR spectrum means that a very large number of individual carbon positions from intermediary metabolites could be monitored simultaneously. The major challenges associated with carbon imaging involve the low *in vivo* abundance and poor gyromagnetic ratio of the ^{13}C nucleus; these factors, combined with the low level of spin polarization, result in a very small signal detectable by magnetic resonance. However, using a process termed hyperpolarization, the spin polarization can be greatly enhanced, thereby enhancing the magnetic resonance signal (Ardenkjaer-Larsen et al., 2003; Kurhanewicz et al., 2011). Hyperpolarization techniques temporarily redistribute the population of energy levels of ^{13}C nuclei into a nonequilibrium state. This state is highly unstable, with a T_1 varying with the chemical environment of the nucleus but typically lasting less than 60 s. However, the signal gain during this period of time can routinely exceed 10,000-fold, leading to a massive if transient increase in MR signal (Ardenkjaer-Larsen et al., 2003). This gain provides sufficient signal to introduce hyperpolarized materials into a biological system, observe the labeled nucleus, and—if metabolism of the substrate is rapid enough—observe real-time transfer of the hyperpolarized nucleus to new molecules through enzyme-catalyzed metabolic reactions.

A large and growing number of metabolites from central carbon metabolism have been hyperpolarized for real-time metabolic studies (Gallagher, Kettunen, Day, Hu, et al., 2008; Gallagher, Kettunen, Day, Lerche, & Brindle, 2008; Gallagher et al., 2009; Golman, Zandt, Lerche, Pehrson, & Ardenkjaer-Larsen, 2006; Moreno et al., 2014; Rodrigues et al., 2014). However, [1-^{13}C]pyruvate has received the most attention to date. Carbon-1 of pyruvate has an unusually long T_1 (approximately 45 s), providing ample opportunity to observe the transfer of this carbon to metabolites of pyruvate. Furthermore, pyruvate is positioned at the interface between anaerobic and aerobic metabolism, a key metabolic node. Pyruvate can be reduced to lactate, transaminated to alanine, carboxylated to oxaloacetate, or decarboxylated to acetyl-CoA, and in the right tissue, all of these reactions can occur rapidly enough to observe by NMR (Fig. 1).
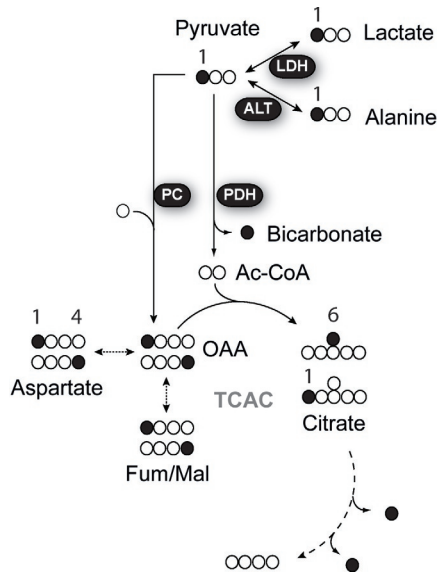
Figure 1 Pyruvate is a substrate for several reactions that may be monitored by hyperpolarized ^{13}C. The strengths of [1-^{13}C]pyruvate as a probe for hyperpolarization experiments are demonstrated in this illustration. The ^{13}C nuclei are in black, with nonenriched carbons in white. Pyruvate exchanges rapidly with the large lactate and alanine pools via the enzymes lactate dehydrogenase (LDH) and alanine amino-transferase (ALT), respectively. These exchange reactions result in the production of [1-^{13}C]lactate and [1-^{13}C]alanine, both of which are readily visible in hyperpolarization experiments in many systems. Depending on the tissue type, it may also be possible to observe flux through pyruvate dehydrogenase (PDH), which releases ^{13}C as bicarbonate and produces unlabeled acetyl-CoA (Ac-CoA). Ac-CoA may then enter the TCA cycle (TCAC). Pyruvate may also be carboxylated by pyruvate carboxylase (PC), generating labeled oxaloacetate (OAA). OAA may be transaminated to aspartate, condensed with Ac-CoA to produce citrate, or equilibrate with other 4-carbon TCAC intermediates (e.g., fumarate and malate, Fum/Mal). Thus, carbon-1 of pyruvate is positioned to probe multiple aspects of aerobic and anaerobic metabolism simultaneously.

Hyperpolarized [1–^{13}C]pyruvate has been used extensively in mouse models of cancer because the rapid interconversion of pyruvate and lactate is readily detected by NMR and has been demonstrated to differentiate benign from malignant tissue (Golman et al., 2006; Hu et al., 2011). Hyperpolarized [1–^{13}C]pyruvate has also been used in human studies to detect malignant tissue in the prostate, where its integration with magnetic resonance imaging has great potential as a clinical tool to diagnose and monitor cancer in patients (Nelson et al., 2013).

In addition to its use for *in vivo* studies, hyperpolarized [1-^{13}C]pyruvate has been used in a number of other applications, including cell culture studies and perfused organs (Harrison et al., 2012; Merritt, Harrison, Sherry, Malloy, & Burgess, 2011; Merritt et al., 2007; Moreno et al., 2014; Yang, Harrison, et al., 2014; Yang, Ko, et al., 2014). These studies capitalize on the extremely fine temporal resolution afforded by hyperpolarization (up to one data point per second) to directly observe, and in some cases quantify, flux through one or more metabolic reactions. Here, we discuss our experiences using hyperpolarization as an analytical approach to understand metabolism in *ex vivo* systems. We describe methods to achieve high levels of polarization in [1-^{13}C]pyruvate using dynamic nuclear polarization (DNP), maximize the efficiency and information yield of cell culture experiments, and analyze metabolism in the perfused heart and liver. We also discuss future directions and challenges for hyperpolarization, including roles for substrates other than pyruvate, and prospects for deriving quantitative flux information from *in vivo* experiments.
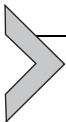
2. HYPERPOLARIZATION METHODS AND SAMPLE PREPARATION

2.1 Hyperpolarization via Dissolution DNP

Among different techniques of resolving the problem of low sensitivity of NMR signals, hyperpolarization via dissolution DNP is regarded as one of the most versatile and effective for increasing the amplitude of NMR signals (Ardenkjaer-Larsen et al., 2003). The underlying principle of DNP is the transfer of high electron spin polarization to the nuclear spins via microwaves, hence creating a larger spin population difference in the Zeeman energy levels of the system, resulting in significant enhancements of NMR signal. Originally used in particle and nuclear physics, the microwave-driven polarization transfer process in nonconducting solids occurs at cryogenic temperatures close to 1 K and at magnetic fields greater than 1 T (Abragam & Goldman, 1978). The NMR signal-amplifying power of DNP has recently been harnessed for biomedical and metabolic research via rapid dissolution, which converts the frozen polarized ^{13}C sample at cryogenic temperature into hyperpolarized ^{13}C liquid solution at physiologically tolerable temperatures (Ardenkjaer-Larsen et al., 2003). In this case, the lifetime of the hyperpolarized ^{13}C NMR signal is dictated by the ^{13}C spin–lattice relaxation time T_1.

2.2 ^{13}C DNP Sample Components and Preparation

Optimized DNP sample preparation is crucial to the success of the hyperpolarized ^{13}C NMR or MRI experiments because it can significantly affect the maximum ^{13}C NMR signal enhancement levels. Typically, a ^{13}C DNP sample is a solution with 10–100 μL volume consisting of:

(a) *^{13}C-enriched substrates.* With the superb ^{13}C NMR signal sensitivity afforded by dissolution DNP, real-time assessment of cellular metabolism is now feasible. Some of the commonly used ^{13}C-enriched biomolecules for metabolic research via hyperpolarized ^{13}C NMR are ^{13}C glucose, ^{13}C pyruvate, ^{13}C acetate, ^{13}C glutamine, ^{13}C fumarate, ^{13}C ascorbic acid, and numerous others (Keshari & Wilson, 2014). Most of these ^{13}C-enriched compounds are in powder form and thus need to be dissolved in a glassing matrix prior to DNP. In special cases, neat liquids such as ^{13}C pyruvic acid are self-glassing and thus, one only needs to add and mix trace amounts of free radicals to complete the DNP sample preparation. As mentioned above, [1-^{13}C]pyruvate is the most commonly used agent, in part because the position of ^{13}C on the carbonyl is associated with a fairly long T_1 relaxation time. The long T_1 of this carbon is related to the fact that its nearest intramolecular contact with protons is with pyruvate's methyl group (carbon 3). Long ^{13}C T_1s are highly advantageous for DNP because they translate to a long lifetime of the hyperpolarized ^{13}C NMR signal and therefore provide greater opportunity to observe metabolic activities. The intrinsic biochemistry of intermediary metabolites drastically limits the number of compounds suitable for hyperpolarization studies because the presence of protons directly bonded to the carbon nucleus reduces the T_1 to 2–10 s. A list of some of the commonly used ^{13}C-enriched compounds and their corresponding liquid-state T_1 relaxation times is given in Table 1.

(b) *Glassing solvents.* The choice of glassing solvents or matrix depends mainly on the criterion of maximum solubility of the ^{13}C substrates. Equally important is the requirement that these solutions form amorphous or noncrystalline solids when subjected to cryogenic temperatures (Kurdzesau et al., 2008; Lumata, Jindal, et al., 2011). Amorphous conditions are also required to evenly distribute the ^{13}C nuclear spins and the free radical electrons across the sample volumes. Common examples of glassing matrices used for ^{13}C DNP are composed of two solvents mixed in 1:1 vol/vol ratio such as glycerol/water,

Table 1 List of Some of the ^{13}C-Enriched Compounds Discussed in This Text and Their Corresponding Liquid-State ^{13}C Spin–Lattice T_1 Relaxation Times at 9.4 T and Ambient Temperature

^{13}C-Enriched Compound	^{13}C T_1 (s)	References
[1–^{13}C]pyruvate	42	Lumata, Ratnakar, et al. (2011)
[2–^{13}C]dihydroxyacetone	32	Moreno et al. (2014)
[U–^{13}C, U–^{2}H]glucose	10	Rodrigues et al. (2014)
[1,4–^{13}C$_2$]fumarate	24	Gallagher et al. (2009)
[1–^{13}C]glutamine	25	Jensen, Karlsson, Meier, Duus, and Lerche (2009)
[1–^{13}C]ascorbic acid	16	Bohndiek et al. (2011)
[1–^{13}C]alanine	29	Jensen et al. (2009)

DMSO/water, ethanol/water, methanol/water, sulfolane/DMSO, and ethyl acetate/DMSO among others. The volume components may be adjusted when higher solubility of a hydrophilic ^{13}C substrate is needed; for example, increasing the ratio of water:glycerol to 4:1 has been used to accommodate some substrates (Lumata, Jindal, et al., 2011). Concentrations of ^{13}C-enriched biomolecules in glassing matrices are typically on the order of a few moles per liter.

(c) *Free radicals*. The next step is the addition of trace amounts of free radicals to the ^{13}C substrate solutions. The following stable, organic free radicals were proven to be effective polarizing agents for dissolution DNP (Lumata, Merritt, Khemtong, et al., 2012; Lumata, Merritt, Malloy, et al., 2013; Lumata, Ratnakar, et al., 2011) as well as their experimentally determined optimal concentrations for DNP: tris{8-carboxyl–2,2,6,6-benzo(1,2-d:4,5-d)–bis(1,3)dithiole–4–yl} methyl sodium salt (trityl OX063, 15 m*M*); 1,3-bisdiphenylene-2-phenylallyl (BDPA, 20 or 40 m*M*); 2,6-di-*tert*-butyl-α-(3,5-di-*tert*-butyl-4-oxo-2,5-cyclohexadien-1-ylidene)-*p*-tolyloxy (galvinoxyl, 20 m*M*); 2,2-diphenyl-1-picrylhydrazyl (DPPH, 40 m*M*); and 4-Oxo-2,2,6,6-tetramethyl-1-piperidinyloxy (4-oxo-TEMPO, 30–50 m*M*). Of these five free radicals, the most commonly used are the water-soluble polarizing agents trityl OX063 and TEMPO, since most ^{13}C-enriched substrates used in DNP are hydrophilic. The other

three free radicals—BDPA, galvinoxyl, and DPPH—can be dissolved in special solvents such as sulfolane/DMSO and sulfolane/ethyl acetate. Generally, the narrow electron spin resonance (ESR) linewidth free radicals trityl OX063 and BDPA were shown to be better polarizing agents for DNP of low-gamma nuclei such as ^{13}C spins (Lumata et al., 2015; Lumata, Merritt, Malloy, Sherry, & Kovacs, 2012a). This is due to the fact that their ESR linewidths match the ^{13}C Larmor frequencies, leading to more efficient hyperpolarization.

A typical sample preparation procedure is outlined below:

- Weigh out the desired amounts of ^{13}C substrate and free radical using analytical balance. Use 1.5-mL microcentrifuge tubes as containers.
- Prepare the glassing solvent solution. Dissolve the ^{13}C substrate in the glassing solvents using a vortex mixer.
- Transfer the ^{13}C substrate solution into the tube containing the free radical. Use the vortex mixer to dissolve the free radical in solution. In some cases, a sonicator bath may be used to completely dissolve the substrate and/or free radical (Lumata, Merritt, Hashami, Ratnakar, & Kovacs, 2012; Lumata, Ratnakar, et al., 2011).

2.3 Other DNP Sample Optimization Tips

2.3.1 Gadolinium Doping

Inclusion of trace amounts (1–2 mM) of Gd^{3+} complexes such as Gd-DOTA into the ^{13}C DNP sample was shown to increase the ^{13}C DNP-enhanced polarization level by as much as 300% in the commercial 3.35 T HyperSense polarizer (Lumata, Jindal, et al., 2011; Lumata, Merritt, Malloy, Sherry, & Kovacs, 2012b). However, this sample preparation practice is so far only recommended for ^{13}C DNP samples that are doped with trityl OX063 free radical. Inclusion of the Gd-complex in ^{13}C samples doped with the other free radicals led to negligible increases in ^{13}C polarization levels. In addition to Gd^{3+} complexes, other lanthanides such as Holmium-DOTA have shown similar beneficial effects on trityl OX063-doped ^{13}C samples. This DNP-enhancing phenomenon is ascribed to the shortening the T_1 relaxation time of the free radical electrons, leading to a more efficient DNP (Lumata, Kovacs, et al., 2013).

2.3.2 Deuteration of the Glassing Matrix: Do's and Don'ts

Using deuterated glassing solvents could be beneficial in some cases leading to large increases in hyperpolarized ^{13}C NMR signal. In other instances,

however, this method may negatively impact the ^{13}C DNP–NMR signal enhancement (Lumata, Merritt, & Kovacs, 2013). For example:

- *Do's: ^{13}C DNP samples doped with large ESR linewidth free radicals.* Use deuterated glassing solvents for ^{13}C samples doped with large ESR linewidth free radicals galvinoxyl, DPPH, and TEMPO. This sample preparation method was shown to double or triple the DNP-enhanced ^{13}C NMR signal in the frozen sample state. The idea is that deuterons in the glassing matrix are lesser heat loads than protons due to their smaller magnetic moments; thus, the former would lead to more efficient ^{13}C hyperpolarization (Kurdzesau et al., 2008; Lumata, Merritt, & Kovacs, 2013).

- *Don'ts: ^{13}C DNP samples doped with narrow-ESR linewidth free radicals.* Do not use deuterated glassing solvents for ^{13}C samples doped with narrow ESR linewidth free radicals such as trityl OX063 and BDPA. Doing so would lead to decreases in ^{13}C DNP levels by as much as 50%. Protons do not effectively couple to the electron dipolar system of trityl and BDPA, rendering them effectively absent from the DNP process. With glassing matrix deuteration, the narrow ESR linewidth free radical electrons have to polarize not only ^{13}C spins but also the deuterons, leading to less efficient ^{13}C DNP (Goertz, 2004; Lumata, Merritt, & Kovacs, 2013).

2.3.3 ^{13}C Enrichment of the Glassing Matrix

This technique is employed to expedite the ^{13}C hyperpolarization process, while the sample is inside the polarizer at cryogenic temperatures. For a typical ^{13}C DNP sample such as sodium [1-^{13}C]pyruvate in 1:1 vol/vol DMSO:water doped with trityl OX063, the microwave irradiation time needed to achieve the maximum DNP-enhanced ^{13}C polarization is about 2–3 h. By using ^{13}C-enriched DMSO in the glassing matrix, the hyperpolarization time can be two to three times faster, thus saving time and cost of cryogens. This phenomenon can be explained by a faster nuclear spin diffusion process as ^{13}C internuclear distance is decreased with the increasing ^{13}C concentration in the system. This is analogous to a domino effect in terms of nuclear polarization transfer (Lumata, Kovacs, Malloy, Sherry, & Merritt, 2011).

2.3.4 Frozen Pellets

This sample preparation practice is especially useful for preparing large DNP sample volumes where amorphous formation of the frozen sample is

sometimes compromised. Normally, small aliquots (10–100 μL) of ^{13}C DNP samples are pipetted into a sample cup (made of polyetheretherketone or Teflon) with approximately 200 μL volume capacity. To ensure glass formation, these small sample aliquots are flash-frozen by dipping the sample cup into liquid nitrogen (LN$_2$). Difficulties arise with large samples (e.g., 200 μL) because of the time necessary to freeze the entire volume. This may allow a fraction of the sample to crystallize. Small droplets of the sample may be prepared by pipetting out small volumes (~10 μL) of ^{13}C sample solution into a styrofoam container with LN$_2$. These small volumes are flash-frozen immediately, then transferred using plastic tweezers into the sample cup, which is also kept in LN$_2$. Once filled with frozen droplets, the sample cup is immediately inserted into the polarizer at cryogenic temperature.

2.4 Operational Steps of ^{13}C Hyperpolarizer

2.4.1 HyperSense Commercial Polarizer

The HyperSense polarizer (Oxford Instruments, UK) is a highly automated commercial polarizer that operates at 3.35 T and at 1–1.6 K with a W-band (94 GHz) microwave source. The following are the experimental steps that we typically follow to polarize ^{13}C DNP samples:

- Prepare cooldown and filling of liquid Helium (LHe) into the cryostat sample space of the polarizer. This can be done by clicking "cooldown" on the software displace on the PC. This step will turn on the rotary vane pump connected to the polarizer as well as adjust the needle valve opening for LHe. Once the LHe level in the polarizer reaches 65% and the temperature is close to 1.4 K, the insert sample button on the PC is activated.

- Pipette out the desired ^{13}C DNP sample volume into the cup (typically 10–100 μL). Flash-freeze the sample cup into LN$_2$. Attach the sample cup snugly at the bottom of the insertion stick. When ready, press "insert sample" on the computer.

- The HyperSense polarizer will then automatically block the pump connection to the polarizer and overpressure the sample space of the cryostat close to 1 Atmosphere. The upper entry of cryostat will then open for sample insertion. Open the upper polarizer door for sample insertion.

- Quickly insert the sample stick into the bottom of the cryostat. Dislodge the sample cup inside the cryostat immediately by simultaneously holding the outer tube and pulling the inner tube of the sample insertion wand.

- Close the polarizer door immediately and click "finish" on the computer. Allow the polarizer to get back to the base temperature for a couple of minutes.
- Click "polarize" to start the ^{13}C hyperpolarization process. This will turn on the microwave source to irradiate the sample at 3.35 T and 1.4 K. Make sure that the optimum microwave irradiation frequency for ^{13}C with the relevant free radical is established before the experiment. It is also recommended to monitor the ^{13}C solid–state polarization buildup curve of the ^{13}C DNP sample for documentation purposes and to ensure that the sample is being properly hyperpolarized.
- Wait until the ^{13}C solid–state polarization buildup curve reaches a plateau or maximum value. The ^{13}C buildup curves are typically exponential with a waiting time of 1–3 h.
- Once the ^{13}C DNP sample reaches the maximum solid–state polarization, click the dissolution button on the computer.
- Open the polarizer door. Inject 4 mL of water or other approved solvent into the top of the automated dissolution wand. Close the upper valve of the dissolution wand.
- Align the bottom of the dissolution wand with the center opening of the cryostat. Close the polarizer door.
- Click "Start dissolution" for the process to start. The water or solvent in the small cylinder container of the dissolution wand will begin to heat and pressurize. This process takes about 3.5 min before the dissolution process begins.
- Once the temperature reaches 200 °C and pressure is at 10 bars, the microwave source is turned off, the pump is blocked from the polarizer, and the sample space of the cryostat is overpressured with He gas.
- The dissolution wand is automatically inserted in the cryostat, acquiring the sample cup and injecting superheated water or solvent into the sample via high pressure He gas.
- A diluted liquid solution containing hyperpolarized ^{13}C biomolecules comes out of the polarizer via a PTFE or Teflon tubing. In 8–10 s, approximately 4 mL of hyperpolarized liquid will be collected into a beaker. This hyperpolarized liquid is then ready for immediate administration into cells, perfused organs or *in vivo* into living subjects for dynamic assessment of metabolism.

Other notes:

- The frequency of microwave irradiation varies among different radicals and is dependent on the magnetic field. The optimal frequency of irradiation must be determined for each radical experimentally.
- The polarization times are specific to the sample being hyperpolarized. The glassing matrix and presence or absence of Gd^{3+} also influence the polarization time. For new analytes, several experiments optimizing the sample conditions such as glassing matrix and radical concentration should be performed to achieve the highest possible solid–state enhancement in the shortest possible time.

2.4.2 Homebuilt DNP Hyperpolarizer

The general operational steps for polarizing ^{13}C samples in our homebuilt 129 GHz DNP hyperpolarizer (Lumata et al., 2015) are very similar to that of the automated HyperSense commercial polarizer, although ours is operated manually. The sample cup in the homebuilt polarizer is optimized to handle up to 600 μL of ^{13}C DNP sample volume. This is advantageous for hyperpolarized ^{13}C NMR or MRI studies of animals larger than small rodents, due to requirement of higher concentration and/or volume of hyperpolarized liquids.

3. DYNAMIC ASSESSMENT OF METABOLISM IN CELLS

While a major advantage of hyperpolarized ^{13}C magnetic resonance is its ability to enable noninvasive monitoring of metabolism in intact tissues, there are several reasons to perform hyperpolarization experiments in cultured cell models as well. First, hyperpolarized substrates allow kinetic assessment of discrete metabolic reactions on a time scale that would be impractical using other methods. Second, cancer cells or other cell lines may provide convenient and affordable systems to assess candidate hyperpolarized substrates prior to deploying these molecules into more cumbersome biological models, including perfused organs and live animals.

The methods described below outline approaches to observe metabolism of hyperpolarized molecules in fresh suspensions of adherent cancer cells. We have demonstrated that some of the metabolic rates observed using hyperpolarized [1-^{13}C]pyruvate were maintained during short periods of suspension (Yang, Harrison, et al., 2014). It should be noted that bioreactor systems have also been used to observe metabolism of encapsulated

adherent cells, providing an alternative to the simple suspension method outlined here (Keshari et al., 2010).

3.1 Preparation of Cultures for Hyperpolarization Experiments

3.1.1 Scale and Quality of Cells Used

- As metabolic rates vary substantially among established cell lines, pilot experiments may be required to optimize conditions for each cell line. The procedure described here has been applied successfully to multiple rapidly proliferating, highly glycolytic cancer cell lines.
- In a typical *in vitro* analysis using hyperpolarized [1-^{13}C]pyruvate, we use 40–80 million cells harvested during exponential growth. This has provided good reproducibility of metabolic rates among individual experiments.

3.1.2 Details of Cell Culture and Harvesting

- Specific plating protocols should be optimized for each cell line, but plating 5×10^6 to 8×10^6 cells into each of several 150-mm dish works well for most adherent cancer cell lines. These cultures can be expected to reach 80–90% confluency—the target for cell harvest—approximately 36–48 h after plating.
- Harvest $75–150 \times 10^6$ cells from three to five 150-mm dishes by using trypsin–EDTA (0.05% for most cell lines) to disengage from the dish. Inactivate the trypsin by diluting in serum-containing culture medium, centrifuge to pellet the cells, then briefly rinse once in 10 mL prewarmed phosphate buffered saline (PBS). Resuspend the culture at a concentration of $50–100 \times 10^6$ cells/mL in fresh medium lacking glucose and pyruvate, but containing 10% dialyzed fetal calf serum, 4 mM glutamine, and standard concentrations of other amino acids.
- Time the preparation of the cell suspension to minimize the time in suspension prior to the hyperpolarization experiment, typically no more than 15 min. In the interim, keep the cells in a conical tube in a 37 °C water bath with frequent mixing to protect against depletion of oxygen from the medium. Trypan blue staining can be performed on a small aliquot of cells right before the hyperpolarization experiment to ensure high viability.
- In the moments preceding dissolution of the hyperpolarized material, transfer the cell suspension into a 10-mL syringe connected with a long teflon tube which goes through a free cap which will later be fitted to a 5-mm NMR tube (see Fig. 2).
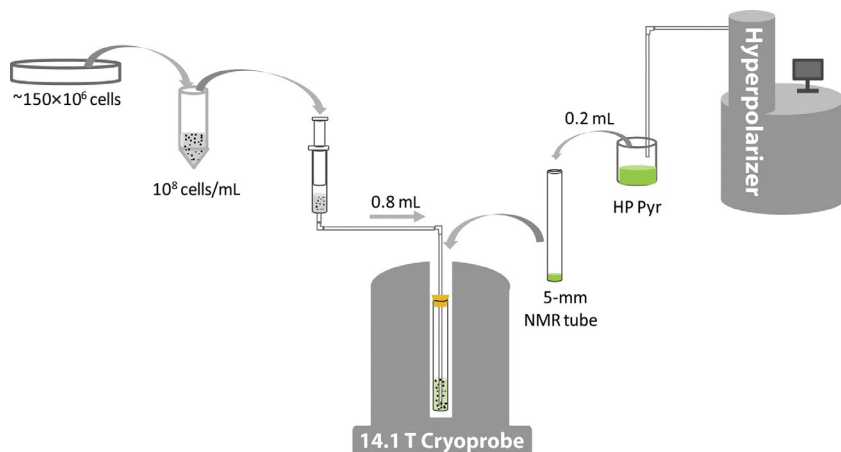
Figure 2 Schematic of a highly efficient system to perform hyperpolarized ^{13}C NMR experiments in cultured cells. The cells must be rapidly harvested for the experiment without changing their metabolism. Mixing of the cells with the hyperpolarized agent is obviously essential. The preferred method is placing a small volume of the HP solution into the bottom of the tube and subsequently injecting a large volume of cells into it to cause turbulent mixing. Injecting a small volume of HP solution into a large volume of cells does not accomplish this goal. To record the initial kinetics, mixing of the cells and the imaging agent should take place inside the magnet with the experiment already queued.

3.2 Administration of Hyperpolarized ^{13}C Substrate and Data Acquisition

- Dissolve hyperpolarized samples using an automated process like the one described above. For cell-based experiments, we use 4 mL of 15.3 mM sodium bicarbonate at 190 °C. Approximately 4 mL of hyperpolarized liquid (pH ~7) should be evacuated from the hyperpolarization chamber and collected in a beaker.
- Using a handheld p1000 pipettor, immediately transfer 0.2 mL of the hyperpolarized solution into the bottom of a 5-mm NMR tube.
- Affix the cap fitted with the Teflon tube connected to the syringe containing the cell suspension, as described above.
- Center the tube into a Varian 10-mm broadband probe tuned to ^{13}C in a 14.1-T magnet.
- Initiate acquisition of ^{13}C NMR spectra immediately after the NMR tube settles into the magnet.
- As the acquisition is initiated, transfer 0.8 mL of the cell suspension into the NMR tube using the syringe fitted with tubing. This produces a final

volume of 1 mL, with 6 mM pyruvate and a cell density of 0.4–0.8 × 10^8 cells/mL. Note that the rationale for this method is to enable observation of the initial period of metabolism as the cells first encounter the hyperpolarized material, as the initial rate of ^{13}C transfer is highly informative.

- Maximizing reproducibility of transfer may require some modifications, particularly for cell lines that become viscous when suspended at the concentrations used here. Following the cell suspension with 0.2–0.5 mL of air bubbling may improve the homogenization of the mixture. Alternatively, the cell suspension can be mixed thoroughly and precisely with the hyperpolarized material in the NMR tube outside the magnet, although this requires some sacrifice of acquiring NMR spectra over the initial phase of ^{13}C transfer.

- At the end of the ^{13}C NMR acquisition (usually no more than 3–4 min after mixing the cells with hyperpolarized material), pellet the cells by centrifugation, save the culture medium, and flash-freeze the pellet in LN$_2$. This enables complementary analysis using mass spectrometry or other methods to validate or aid in the interpretation of data acquired in the hyperpolarization experiment.

3.3 Techniques to Maximize Detection of Products

Our group has successfully combined hyperpolarization with two other techniques aimed to enhance ^{13}C NMR signals. These are described briefly below.

3.3.1 Selective Pulses

Shaped pulses are especially helpful in cases where the NMR signals emanating from products of interest are small compared to the ^{13}C signal of the parent compound. For instance, in *in vitro* hyperpolarized ^{13}C NMR experiments on cancer cell suspensions, the LDH-catalyzed product [1-^{13}C]lactate signal is dwarfed by the hyperpolarized ^{13}C signal from the parent compound, [1-^{13}C]pyruvate. Signal from hyperpolarized bicarbonate arising from decarboxylation of [1-^{13}C]pyruvate is typically much smaller than [1-^{13}C]lactate. To enhance the ^{13}C lactate signal, we applied a Gaussian-shaped selective radiofrequency (RF) excitation pulse at the frequency where [1-^{13}C]lactate is expected. For Varian or Agilent NMR spectrometers, we create the selective shaped pulses using the VNMRJ PBox software (Harrison et al., 2012). This shaped pulse will only excite [1-^{13}C]lactate spins with no or minimal RF excitation effect on the

[1-^{13}C]pyruvate spins. In cases where there are two or more tiny NMR signals of metabolic products of interest, double- or multiple Gaussian selective pulses can be generated to simultaneously interrogate the kinetics of the metabolic products in real time. An important consideration in using shaped pulses is that the NMR signal of the metabolic product should be located at a distinct distance from NMR signal of the parent compound, otherwise there will be substantial RF excitation of the ^{13}C spins from the parent compound. Moreover, the use of selective pulses prolongs the availability of hyperpolarized ^{13}C magnetization of the parent compound since the latter is not or only minimally excited by the selective shaped RF pulse.

3.3.2 Cryogenic Probes

In addition to hyperpolarization, the invention of cryogenically cooled probes (cryoprobes) for NMR is considered to be another important advancement in terms of sensitivity enhancement. This NMR technology is based on the fact that cooling the NMR coil and its tuning and matching components substantially reduces the random thermal motions of electrons termed as the Johnson–Nyquist noise. In addition, the preamplifier, filters, and transceiver electronics are also cooled to reduce the noise originating from the electronics (Kovacs, Moskau, & Spraul, 2005). The use of an NMR cryoprobe results in an immediate improvement of signal-to-noise ratio (SNR) by a factor of 3–5 relative to the SNR obtained in a conventional NMR probe. Unlike dissolution DNP, the improvement in NMR sensitivity produced by an NMR cryoprobe is persistent, provided that the cryogenic conditions of NMR electronics are maintained. We use a 10 mm [1]H-[13]C Bruker CryoProbe system (Bruker Biospin, Billerica, MA) installed in a 600 MHz NMR magnet. This Cryoprobe system is located adjacent to the commercial HyperSense polarizer and a homebuilt DNP polarizer. When hyperpolarization is combined with the cryoprobe, the high ^{13}C SNR that we normally obtain for ^{13}C DNP is further improved by a factor of 4. To our knowledge, combining these two NMR technologies provides the highest ^{13}C NMR sensitivity currently achievable. Consistent with this idea, we have been able to use a hyperpolarization/cryoprobe combination to observe time-resolved signals previously achievable only using selective pulses (Yang, Ko, et al., 2014). Furthermore, the cryoprobe allows straightforward studies of the perfused mouse heart, an organ of such small size that only the combination of hyperpolarization and the cryoprobe has produced published results (Purmal et al., 2014).
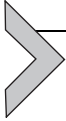
4. DYNAMIC ASSESSMENT OF METABOLISM IN PERFUSED ORGANS

Perfused organs, particularly the heart and liver, have long been used as models to analyze intermediary metabolism, particularly with mass spectrometry and conventional ^{13}C NMR spectroscopy. We have applied hyperpolarization approaches to the perfused heart and liver from mice to observe dynamic metabolism of ^{13}C-labeled probes. Basic experimental setup for these experiments is described below.

4.1 Hyperpolarized ^{13}C NMR of Perfused Heart

4.1.1 Preparation of the Perfused Heart

Animals are anesthetized and a transabdominal incision is then performed to expose the thoracic cavity. The heart is removed from the chest cavity by excising the pulmonary artery, vena cavae, and aorta. Animal death occurs within seconds by exsanguination. The blood vessels are cut as close to the heart as possible without causing any damage to the heart. The excised heart is transferred to ice-cold saline to rinse off the blood and arrest the beating heart. All subsequent procedures prior to the start of perfusion are carried out on ice-cold saline.

Fat deposits and other contaminant tissue on the heart are removed surgically. After sufficient cleaning, a plastic cannula is inserted into the aorta. To provide robust cannulation and avoid any leaks, a surgical suture is used to tie the tissue around the cannula. Care must be taken to avoid any rupture of the tissue during the insertion of the cannula and subsequent application of the suture.

Special concerns
- After excising the heart, it is important to transfer the heart to ice-cold saline rapidly to prevent ischemic injury.
- Insertion of the cannula into the aorta must be performed carefully so that no air bubbles are introduced into the heart. This can typically be accomplished by leaving the cannula submerged in the ice-cold saline as the heart is being cleaned.
- Leaving the heart in ice-cold saline more than a few minutes often results in poor function. The time taken between the excision of the heart and start of perfusion should be minimized as much as practically possible.

4.1.2 Preparation of the Perfusion Rig

A straightforward setup to perfuse the hearts in constant pressure Langendorff mode is to utilize a vertical column providing the appropriate hydrostatic pressure (see Fig. 3). Although portable perfusion systems exist (with electronic pressure and flow rate control), the glass columns are more directly amenable to studying perfused hearts inside an NMR magnet. The perfusate of interest is maintained at a fixed height (in order to provide constant hydrostatic pressure) in the column using peristaltic pumps.
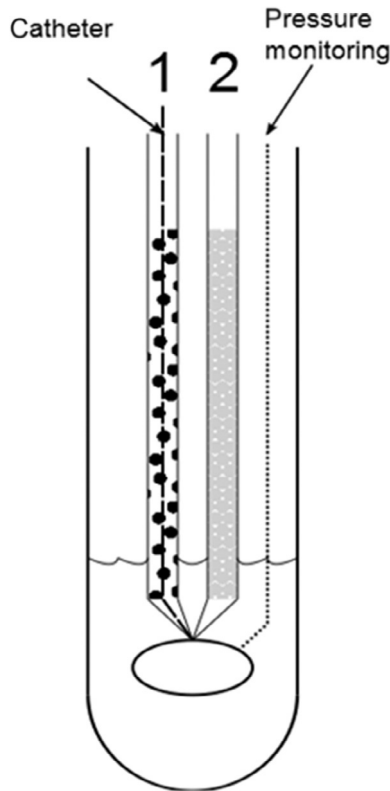
Figure 3 Schematic of a perfused organ inside an NMR tube. In this case, the perfusion rig contains two separate cannula that supply perfusate for either the heart or the liver. The presence of two cannula (1 or 2, or both) allows switching of perfusates to maintain a constant concentration of substrate when the hyperpolarized media is injected through a catheter placed inside the cannula. In the case of the heart, the developed pressure can be measured using tubing placed inside the aorta. The column height of the perfusate is set to provide the correct hydrostatic pressure for a heart. In the case of the liver, flow of the perfusate is set at 8 mL/min using a peristaltic pump distal from the MR magnet.

Continuous supply of oxygen is maintained by aerating the perfusate constantly with a mixture of 95% oxygen/5% carbon dioxide, while temperature is regulated using a heated water jacket. A simple balloon catheter is typically used as a valve to turn the flow of perfusate on or off in this setup.

Special concerns

- Depending on the perfusate, additional equipment may be needed. For example, a thin film oxygenator effectively oxygenates perfusates containing long-chain fatty acids and bovine serum albumin. Bubbling gas directly into such a perfusate will introduce excessive foaming in the perfusion column.
- With the dissolution of CO_2, pH of the perfusate is likely to be altered slightly. Hence, pH should be adjusted prior to attaching the heart to the perfusion rig.

4.1.3 Heart Perfusion and Setting Up the NMR Spectrometer

Once a bubble-free connection is established, perfusate flow is established by deflating the balloon catheter. The heart typically starts beating within a few seconds (typically less than 30). Heart function is monitored in either a continuous mode or at discrete intervals as the instrumentation permits. Heart function can be typically monitored by recording the heart rate and oxygen consumption.

For NMR experiments, an attachment comprised of an NMR tube is connected to the bottom of the perfusion rig and is lowered into the NMR magnet for acquisition of spectra (Fig. 3). By utilizing a sodium-free flush, the effluent from the beating heart is continuously removed. The flush is accomplished by inserting independent tubing to the bottom of the NMR tube. A sodium-free solution that is otherwise osmotically balanced is pumped into the region below the heart at a high rate to force the removal of the perfusate exiting the heart. In this setup, shimming can be accomplished by optimizing the linewidth of ^{23}Na signal from the heart itself. ^{23}Na linewidth of less than 12 Hz (corresponding to ^{13}C linewidth of ~10 Hz) can be routinely obtained with mouse hearts at a field strength of 14.1 T.

Special concerns

- It is critical to ensure that the position of the heart in the NMR tube corresponds to the center of the RF coil of the NMR probe.
- Shimming the magnet prior to the experiment is optimal when carried out as a two-step procedure. In the first step, shimming of the magnet is accomplished using the strong ^{23}Na signal from both the perfusate and

the heart. Once a satisfactory peak shape and width is achieved, the sodium-free flush is utilized, and further shimming is carried out directly using the sodium signal from the heart.

- Shimming on the ^{23}Na signal is often sensitive to abnormalities in the heart function. For example, irregular heart beat can be correlated with fluctuations in the random and rapid variations in the signal which can be correlated with the changes in heart rate (if measured continuously).

For the dissolution, the hyperpolarized sample is usually dissolved using 4 mL of heated phosphate buffered saline and transferred into a beaker where it mixes with a predetermined volume of perfusate. This sample is injected gently, close to the heart, using a catheter that is inserted into the cannula immediately above the heart. Pyruvate metabolism is observed by measuring a series of time-resolved ^{13}C spectra with small flip angle RF pulses. Alternatively, variable flip angle schemes may be utilized if necessary (Xing, Reed, Pauly, Kerr, & Larson, 2013).

Special concerns

- Mixing with perfusate ensures that the osmolarity of the hyperpolarized sample is similar to that of the perfusate and that the sample is adequately oxygenated.
- The injection of the sample should be smooth and constant. Rapid injection can generate turbulence and uneven mixing of the injected substrate with the solution present in the perfusion rig proper.

4.2 Hyperpolarized ^{13}C NMR of Perfused Liver

4.2.1 Hepatectomy

- Heparinize the mouse with about 0.07 mL heparin injected intraperitoneally and anesthetize with 0.09 mL ketamine/xylocaine, also administered intraperitoneally.
- Weigh the mouse and transfer to a prep station. There will be blood and runoff perfusate. It helps to have a mini work table lined with plastic cling wrap.
- Tape the feet of the mouse to the cling wrap while allowing the head and shoulders to fall over the edge of the work table. This allows the liver to rest upward on the tissue lining the thoracic cavity, while the cannulation is performed.
- Pinch the skin above the abdomen with forceps. Lift up and make a wide incision along the midline of the abdomen, taking care not to puncture any organs.

- Fold the skin up over the sternum to expose the abdominal cavity. Slide the fat and intestines with your middle finger to the right and outside of the body cavity, exposing the portal vein.
- Create a path underneath the portal vein close to the liver with a pair of forceps. Feed two 3″ pieces of 4–0 silk suture under the vein and begin a "left–over–right" knot. Taking care not to close the knot, tie them down close to the vein and lay the ends of the piece closer to the head up between the arms.
- Cannulate the portal vein by inserting a 22G × 1″ Terumo Surflo IV Catheter. Use your left hand to move the fatty tissue and create tension on the vessel if needed. Take care not to advance the needle too far for risk of puncturing the vein. An assistant can pull on the two ends of suture closest to the head of the mouse to also create more tension for ease of catheter insertion.
- Once inside the vessel, hold the needle still and use your index finger to advance the catheter off of the needle further into the vein, about ¼″. Do not push the catheter as far as it will go inside the vessel as this may also puncture or create a stoppage of flow and induce ischemia.
- While holding the needle and catheter in place, have an assistant to tie the suture closest to the head of the animal down as tight as possible ensuring that the vein does not slip off the end of the catheter. Ideally, there will be about 5 mm between the end of the catheter tip and first suture knot.
- Let the needle lay in place, while you tie down the second suture. Double knot both sutures and cut off any excess suture material.
- Carefully remove the needle by holding the catheter hub in place and pulling the needle back. Blood should travel back into the hub. Very little to no blood should seep into the body cavity at this point.
- Displace any air in the hub with perfusate and insert your perfusion line while holding the hub firmly. Start your perfusion of the liver by starting the pump connected to the perfusate.
- Cut open the vena cava. The mouse should expire within seconds from exsanguination, and the liver should flush all of the blood out and turn from a red/maroon color to an off–yellow/mustard or tannish color.
- Livers are very delicate. Minimal time should elapse from cannulation to starting the perfusion pump.
- Dissect out the liver by removing first the kidneys followed by intestines and the stomach/pancreas.

- Carefully cut underneath the liver near the spine to separate from connective tissue.
- Switch to the head of the mouse and have an assistant hold the perfusate line in place.
- Cradle the head between your left thumb resting on the chin of the mouse and your index finger curled underneath the shoulders. Lift gently and roll the liver back down over itself toward its natural position.
- Start cutting away the connective tissues, beginning with the thoracic cavity tissue. The liver will slide freely on the plastic cling wrap once more tissue gets cut away.
- As you cut more connective tissues away from the liver, use your left hand to slide the carcass out and away from the liver. Take care in keeping the liver and perfusion line as still as possible. Quick movements with the liver will damage it and induce ischemia.
- Transfer the liver to experimental setup. Use a small cup for transport and take care not to introduce air while moving the catheter hub from setup to setup.

Once the liver has been successfully attached to the perfusion rig, the experimental procedure mirrors the heart protocol. The perfused mouse liver is of course larger than the heart, and as such, a minimum NMR tube size of ~18 mm must be used to accommodate the mouse liver in the NMR magnet. Due to its larger size, the use of a sodium-free flush can be more problematic, as excessively high flow rates can cause the liver to move, making shimming extremely difficult. However, with the proper flow rate for the flush, the two-step ^{23}Na shimming procedure used for the heart will produce similar results for the liver. In addition to oxygen consumption measurements, metabolic viability of the liver is also easily assessed by inspection. If the liver is turning white, it is likely not being perfused correctly and should be discarded.
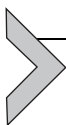
5. CHALLENGES AND FUTURE DIRECTIONS

5.1 Hyperpolarized Substrates in Addition to [1-^{13}C]Pyruvate

Multiple qualities define the utility of new hyperpolarized substrates (Comment & Merritt, 2014). A primary condition is the solubility of the compound in the matrix which carries the radical used for the DNP process. If a solvent mixture is necessary for production of the combined substrate and radical, it must be thoroughly miscible, as partitioning of the sample into

separate phases precludes the process of nuclear spin diffusion necessary for DNP to be effective throughout the sample (Lumata, Kovacs, et al., 2011). Connected to the sample preparation is a phenomenological observation that absolute enhancement of the sample must be high to allow kinetic data to be collected. A good rule of thumb is that enhancements of ∼10,000 will provide an initial signal amplitude suitable for acquisition of time course data. Another primary limitation is the nuclear T_1 of the substrate and its metabolites, as discussed above. Interestingly, if metabolic flux is highly upregulated, as for glucose metabolism in cancer, even agents with short T_1s can yield important metabolic data and potentially biological insights; see the following discussion of hyperpolarized glucose as an imaging agent in cancer. It is most beneficial if the compound in question is either transported or rapidly diffuses into the same space where metabolism occurs. Finally, a multiplicity of metabolic fates will enhance the information yield of the experiment. For example, pyruvate can produce up to four different compounds in single enzyme-catalyzed reactions, enabling simultaneous analysis of multiple pathways, including some that are redox dependent and some that are not.

Another important consideration is the pool sizes of the metabolite derived from the hyperpolarized–imaging agent. Pyruvate again has unique qualifications, as its circulating concentration is fairly low but the size of the alanine and lactate pools are ∼3 and ∼10 times as large. The signal amplitude in hyperpolarization experiments is intimately connected to the pool sizes. This phenomenon is exacerbated in the case of exchange. When exogenous lactate was added to cells studied with hyperpolarized pyruvate, a nearly linear increase in hyperpolarized lactate signal intensity was observed (Day et al., 2007). The kinetics of isotope transport from the small intracellular pyruvate pool into the larger lactate pool is limited only by the amount of ^{13}C label in the lactate pool that is subject to the reverse reaction. In cases where hyperpolarized [1-^{13}C]lactate or [1-^{13}C]alanine has been used, the resulting hyperpolarized [1-^{13}C]pyruvate signal has been relatively small, confirming that fast enzyme kinetics is not sufficient for the production of a large hyperpolarized signal (Chen et al., 2008; Jensen et al., 2009). A large absolute number of HP nuclear spins associated with the detected metabolite is also necessary.

The preceding discussion explains the paucity of data collected with hyperpolarized lactate or alanine, though examples do exist (Bastiaansen, Yoshihara, Takado, Gruetter, & Comment, 2014). From the standpoint of a metabolic perturbation, lactate and alanine should both have fewer

consequences than a bolus injection of the highly oxidized substrate pyruvate. However, due to the pool size effect, hyperpolarized [1-^{13}C]lactate produces only a small amount of [1-^{13}C]pyruvate and consequently a less intense hyperpolarized [^{13}C]bicarbonate signal (Chen et al., 2008). Alanine is confronted with even more difficult circumstances, as its transport does not occur through the high-capacity monocarboxylate transporters that enable lactate and pyruvate import but is electrogenic in nature. The attendant lactate and pyruvate signals generated by injection of hyperpolarized alanine are therefore quite small.

5.1.1 Dihydroxyacetone

Recently, [2-^{13}C]dihydroxyacetone (DHA) has been demonstrated for hyperpolarized imaging of the liver (Moreno et al., 2014). DHA has many qualities similar to pyruvate that suggest it may be successfully used as an HP imaging agent. First, it polarizes to an outstanding level in a water–glycerol matrix, exceeding even the standard sample of trityl radical solubilized directly into pyruvic acid. Second, it has a long nuclear T_1, c.a. 32 s at 9.4 T, which facilitates its delivery and subsequent metabolism while a large signal remains. Third, DHA produces a variety of metabolic products after its initial phosphorylation to dihydroxyacetone phosphate (DHAP). Unfortunately, DHAP has a chemical shift that is unresolvable from the parent compound. DHA metabolism has not yet been observed in organs other than the liver, indicating that an as yet unidentified transporter may be responsible for its uptake. Alternatively, other tissues may lack the ability to phosphorylate DHA to DHAP, which would prevent its subsequent metabolism.

The initial report on DHA as a contrast agent produced new insights into glycolysis, glycogenolysis, and gluconeogenesis in the liver. The traditional model of regulation in the Embden–Meyerhof pathway identifies the three most important regulatory nodes as phosphoenolpyruvate carboxykinase/pyruvate kinase, fructose 1,6-bisphosphatase/6-phosphofructo-1-kinase, and glucose-6-phosphatase/glucokinase. It is difficult to observe kinetics at each separate point of control in an intact system. However, due to the chemical selectivity of MR, almost all the upstream (toward glucose) and downstream (toward pyruvate) metabolites can be detected with a 2 s time resolution using hyperpolarized [2-^{13}C]DHA. In glycogenolytic versus gluconeogenic conditions, only pyruvate kinase produced an observable delay in the production of its product pyruvate and subsequent metabolites, while fructose-1,6-bisphosphatase and glucose-6-phosphatase did not. Prior to the introduction of hyperpolarization methods, insights like this were

nearly impossible to generate, as the only option for generating kinetic measurements with this degree of time resolution would necessitate the serial, destructive acquisition of samples at each time point.

5.1.2 Glucose

Glucose itself is also a suitable hyperpolarized imaging agent, but only when deuteration of the ^{13}C-enriched carbon sites has been used to increase the T_1. The first hint of the power of hyperpolarized [U-^{13}C, U-^{2}H]glucose for studying metabolism was in the work of Meier et al. studying yeast metabolism (Meier, Karlsson, Jensen, Lerche, & Duus, 2011). Nearly, the entire glycolytic pathway from glucose to ethanol formation was observed. In addition, ^{13}CO$_2$ and [^{13}C]bicarbonate were detected and taken as a marker of pyruvate dehydrogenase (PDH) flux. This implies that more than 12 separate enzymatic fluxes can be simultaneously observed. The same substrate was subsequently used to study tumor metabolism *in vivo* where lactate was the primary product observed (Rodrigues et al., 2014). In summary, the authors believe that hyperpolarization technology offers a tremendous opportunity to study enzyme kinetics in intact systems, increasing the likelihood that the insights generated could inform on metabolic control and flux in a variety of tissues and model systems.

5.2 Specific Challenges Associated with Using HP Substrates to Quantify Fluxes *In Vivo*

One of the potentially impactful deliverables of hyperpolarization research is the development of methods to extract quantitative flux data from *in vivo* experiments, ultimately in human patients. Here, we discuss some of the specific challenges associated with using hyperpolarization to definitively quantify metabolic fluxes. In the case of cell culture or isolated systems, this process is dramatically simplified because delivery of the hyperpolarized substrate and its initial concentration can be rigorously controlled. Knowledge of the substrate concentration is obviously a necessary precondition for absolute flux measurements, but extraction of simple rate constants might also provide metrics sensitive to metabolic changes. Estimates of rate constants or actual fluxes *in vivo* have been obtained by many labs using disparate methods. The first method introduced below has obvious counterparts in the biochemical literature. The other studies rely upon magnetic resonance phenomena to facilitate estimates of flux and exchange.

Michaelis–Menten kinetics is typically used to describe single substrate enzyme-catalyzed reactions. Seminal work by Zierhut et al. measured

dose–response curves for hyperpolarized [1-^{13}C]pyruvate in mice and rats in normal tissue and in a model of prostate cancer (Zierhut et al., 2010). Using doses ranging from 50 to 725 μmol/kg, V_{max} and K_m values were measured using the appearance of hyperpolarized [1-^{13}C]alanine and [1-^{13}C]lactate. Tumors were shown to have larger k values (initial rates for forward flux) for lactate production as predicted by the Warburg description of aerobic glycolysis in cancer (Warburg, 1956a). Modeling of the kinetic curves was accomplished using equations that describe only flux from pyruvate into the lactate and alanine pools. While this is an important assumption, other experiments subsequently showed that due to the finite lifetime of the hyperpolarized substrate and its metabolites, the kinetic curves are largely insensitive to exchange, when simple, constant repeat time, and small flip angle experimental protocols are used for data collection (Harrison et al., 2012). The straightforward experimental design of this study produced estimates of values that are readily understood by the larger research community, and as such, this paper served an important place in communicating how HP substrates could give insights into *in vivo* kinetics.

Shortly after this study, Xu et al. reported an alternative method for producing estimates of K_m and V_{max} that used incrementally higher excitation angles for the MR experiment (Xu et al., 2011). Hyperpolarized nuclei are not in thermal equilibrium with surrounding spins in the system being studied. As such, the hyperpolarization state is in a constant state of decay back to the thermal equilibrium value. Also, the detection pulses used for observation of the magnetic resonance signal perturb the spin state in such a way that the hyperpolarization is not recoverable. This latter phenomenon allows specific insights to be generated by starting with low flip angles and incrementing them to a maximum value of 90° at each time point. Using this protocol, K_m and V_{max} can be estimated from a single injection of the hyperpolarized substrate. Intuitively, this experimental design can be explained by analogy to standard dose–response experiments. Since a 90° pulse consumes all the polarization in the region of interest, the subsequent delay before the protocol is repeated allows new hyperpolarized material to flow in. Since the imaging experiment is queued upon injection, each time point reflects the initial delivery and kinetics of metabolite formation as a function of [pyruvate] in the observed tissue. Due to the specifics of the modified Michaelis–Menten equations used for this study, estimates of K_m are subject to effects derived from reverse flux from either alanine or lactate back to the exogenous pyruvate pool. However, quantification of the exchange is still problematic. Paired with the fast chemical shift imaging

protocol used for detection of the metabolites, this progressive excitation method could have tremendous utility in cases where the researcher anticipates large differences in K_m and V_{max}, such as in malignant tissues.

In an effort to gain better insights into the exchange phenomena between pyruvate, lactate, and alanine as measured by hyperpolarized pyruvate, alternative MR protocols have been proposed. Larson et al. demonstrated that a stimulated echo acquisition mode (STEAM) excitation sequence could be tuned to make quantitative estimates of both forward and reverse flux *in vivo* while at the same time producing localized spectra (Swisher et al., 2014). The underlying phenomenon that allows exchange to be monitored is the frequency difference between pyruvate and its metabolites in the MR spectrum. This difference in frequency will manifest as a phase change in the spectra, when the delays of the STEAM sequence are chosen appropriately. While the method is incredibly powerful, deconvolution of the effects of exchange between multiple pools is not straightforward.

Experimentally, a more challenging protocol that is based upon more traditional methods of measuring flux by MR is the inversion transfer method proposed by Kettunen et al. (2010). Selective inversion of either pyruvate or lactate signals produces modulation of the exchanging metabolite that can be modeled according to the modified Bloch equations. This method relies upon mathematical fitting of the exchange curves generated from the time-dependent spectra. The magnetization inversion preparation phase of the sequence can be placed in front of any imaging sequence desired and is therefore at least as flexible as the method proposed by Xu. The primary drawback of these methods is insuring the inversion pulse is properly setup and calibrated. A potentially more robust method of extracting the same kinetic information about pyruvate–lactate exchange was proposed by the same group (Kennedy, Kettunen, Hu, & Brindle, 2012). In this case, [U-^{2}H]lactate is the hyperpolarized substrate. Due to the exchange of protons that is inherent when lactate transits lactate dehydrogenase to for pyruvate, a simple spin echo method can be used to modulate the directly detected ^{13}C MR signals. The modulation again can be modeled using the Bloch equations, yielding accurate estimates of the rate constants describing the pyruvate–lactate equilibrium.

A fundamental challenge for the field of HP applications has been establishing methods for independently verifying the kinetic data observed. Steady-state isotope tracer methods for measuring metabolic flux are extremely well established, and with proper experimental design, they

can be used to not only confirm HP results but also, when integrated with the HP data, produce a powerful tool for assessing global energy metabolism. The combination of HP and steady-state tracer methods was first used to rigorously prove that HP [^{13}C]bicarbonate produced by the heart arose exclusively from PDH flux (Merritt et al., 2007). By monitoring the ^{13}C enrichment of glutamate extracted from the perfused heart, it was established that the addition of a competing fatty acid to the perfusate effectively quenched pyruvate oxidation and hence the production of HP [^{13}C]bicarbonate by PDH flux. Further development of this approach led to the demonstration that HP [^{13}C]bicarbonate production could be quantitatively modeled in cell culture (Yang, Harrison, et al., 2014). This single absolute flux measurement could then be used to normalize a complete set of relative flux measurements obtained by tracer NMR methods. The result was a global, quantitative picture of Krebs cycle turnover. The juxtaposition of oxidative versus anaplerotic handling of pyruvate illustrated just how powerful this new method could be for establishing metabolic phenotypes in cancer cells. Future work marrying hyperpolarization with other quantitative methods should significantly enhance the interpretation of *in vivo* HP data as well as produce new insights into intermediary metabolism.
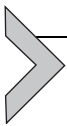
6. CONCLUSION

Hyperpolarization has vastly expanded the applicability of MR-based methods for assessing metabolism due to the $\sim 10^4$ gain in sensitivity. Combined with the traditionally understood strengths of MR, i.e., the chemical selectivity and its applicability to living, functioning systems, powerful new insights into the kinetics of metabolic processes are being routinely generated. We believe that as the technology becomes more widely disseminated, it will find an increasing number of applications in basic science as well as in medical research.

REFERENCES

Abragam, A., & Goldman, M. (1978). Principles of dynamic nuclear polarisation. *Reports on Progress in Physics*, *41*, 395.

Andronesi, O. C., Kim, G. S., Gerstner, E., Batchelor, T., Tzika, A. A., Fantin, V. R., et al. (2012). Detection of 2-hydroxyglutarate in IDH-mutated glioma patients by in vivo spectral-editing and 2D correlation magnetic resonance spectroscopy. *Science Translational Medicine*, *4*, 116ra4.

Ardenkjaer-Larsen, J. H., Fridlund, B., Gram, A., Hansson, G., Hansson, L., Lerche, M. H., et al. (2003). Increase in signal-to-noise ratio of >10,000 times in liquid-state NMR. *Proceedings of the National Academy of Sciences of the United States of America*, *100*, 10158–10163.

Bastiaansen, J. M., Yoshihara, H. I., Takado, Y., Gruetter, R., & Comment, A. (2014). Hyperpolarized ^{13}C lactate as a substrate for in vivo metabolic studies in skeletal muscle. *Metabolomics*, *10*, 986–994.

Bohndiek, S. E., Kettunen, M. I., Hu, D.-e., Kennedy, B. W. C., Boren, J., Gallagher, F. A., et al. (2011). Hyperpolarized [1-^{13}C]-ascorbic and dehydroascorbic acid: Vitamin C as a probe for imaging redox status in vivo. *Journal of the American Chemical Society*, *133*, 11795–11801.

Busch, R., Neese, R. A., Awada, M., Hayes, G. M., & Hellerstein, M. K. (2007). Measurement of cell proliferation by heavy water labeling. *Nature Protocols*, *2*, 3045–3057.

Chen, A. P., Kurhanewicz, J., Bok, R., Xu, D., Joun, D., Zhang, V., et al. (2008). Feasibility of using hyperpolarized [1-^{13}C] lactate as a substrate for in vivo metabolic ^{13}C MRSI studies. *Magnetic Resonance Imaging*, *26*, 721–726.

Choi, C., Ganji, S. K., DeBerardinis, R. J., Hatanpaa, K. J., Rakheja, D., Kovacs, Z., et al. (2012). 2-hydroxyglutarate detection by magnetic resonance spectroscopy in IDH-mutated patients with gliomas. *Nature Medicine*, *18*, 624–629.

Choudhary, C., Weinert, B. T., Nishida, Y., Verdin, E., & Mann, M. (2014). The growing landscape of lysine acetylation links metabolism and cell signalling. *Nature Reviews Molecular Cell Biology*, *15*, 536–550.

Comment, A., & Merritt, M. E. (2014). Hyperpolarized magnetic resonance as a sensitive detector of metabolic function. *Biochemistry*, *53*, 7333–7357.

Day, S. E., Kettunen, M. I., Gallagher, F. A., De-En, H., Lerche, M., Wolber, J., et al. (2007). Detecting tumor response to treatment using hyperpolarized ^{13}C magnetic resonance imaging and spectroscopy. *Nature Medicine*, *13*, 1382–1387.

DeBerardinis, R. J., & Thompson, C. B. (2012). Cellular metabolism and disease: What do metabolic outliers teach us? *Cell*, *148*, 1132–1144.

Elkhaled, A., Jalbert, L. E., Phillips, J. J., Yoshihara, H. A., Parvataneni, R., Srinivasan, R., et al. (2012). Magnetic resonance of 2-hydroxyglutarate in IDH1-mutated low-grade gliomas. *Science Translational Medicine*, *4*, 116ra5.

Gallagher, F. A., Kettunen, M. I., Day, S. E., Hu, D. E., Ardenkjaer-Larsen, J. H., Zandt, R., et al. (2008). Magnetic resonance imaging of pH in vivo using hyperpolarized ^{13}C-labelled bicarbonate. *Nature*, *453*, 940–943.

Gallagher, F. A., Kettunen, M. I., Day, S. E., Lerche, M., & Brindle, K. M. (2008). ^{13}C MR spectroscopy measurements of glutaminase activity in human hepatocellular carcinoma cells using hyperpolarized ^{13}C-labeled glutamine. *Magnetic Resonance in Medicine*, *60*, 253–257.

Gallagher, F. A., Kettunen, M. I., Hu, D. E., Jensen, P. R., Zandt, R. I., Karlsson, M., et al. (2009). Production of hyperpolarized [1,4-$^{13}C_2$]malate from [1,4-$^{13}C_2$]fumarate is a marker of cell necrosis and treatment response in tumors. *Proceedings of the National Academy of Sciences of the United States of America*, *106*, 19801–19806.

Gallamini, A., Zwarthoed, C., & Borra, A. (2014). Positron emission tomography (PET) in oncology. *Cancers*, *6*, 1821–1889.

Gerriets, V. A., Kishton, R. J., Nichols, A. G., Macintyre, A. N., Inoue, M., Ilkayeva, O., et al. (2015). Metabolic programming and PDHK1 control CD4+ T cell subsets and inflammation. *The Journal of Clinical Investigation*, *125*, 194–207.

Goertz, S. T. (2004). The dynamic nuclear polarization process. *Nuclear Instruments and Methods in Physics Research Section A: Accelerators, Spectrometers, Detectors and Associated Equipment*, *526*, 28–42.

Golman, K., Zandt, R. I., Lerche, M., Pehrson, R., & Ardenkjaer-Larsen, J. H. (2006). Metabolic imaging by hyperpolarized ^{13}C magnetic resonance imaging for in vivo tumor diagnosis. *Cancer Research*, *66*, 10855–10860.

Hanahan, D., & Weinberg, R. A. (2011). Hallmarks of cancer: The next generation. *Cell*, *144*, 646–674.

Harrison, C., Yang, C., Jindal, A., DeBerardinis, R. J., Hooshyar, M. A., Merritt, M., et al. (2012). Comparison of kinetic models for analysis of pyruvate-to-lactate exchange by hyperpolarized ^{13}C NMR. *NMR in Biomedicine*, *25*, 1286–1294.

Hu, S., Balakrishnan, A., Bok, R. A., Anderton, B., Larson, P. E., Nelson, S. J., et al. (2011). ^{13}C-pyruvate imaging reveals alterations in glycolysis that precede c-Myc-induced tumor formation and regression. *Cell Metabolism*, *14*, 131–142.

Jensen, P. R., Karlsson, M., Meier, S., Duus, J. Ø., & Lerche, M. H. (2009). Hyperpolarized amino acids for in vivo assays of transaminase activity. *Chemistry: A European Journal*, *15*, 10010–10012.

Kaelin, W. G., Jr., & McKnight, S. L. (2013). Influence of metabolism on epigenetics and disease. *Cell*, *153*, 56–69.

Kennedy, B. W. C., Kettunen, M. I., Hu, D.-E., & Brindle, K. M. (2012). Probing lactate dehydrogenase activity in tumors by measuring hydrogen/deuterium exchange in hyperpolarized l-[1-^{13}C, U-^{2}H]lactate. *Journal of the American Chemical Society*, *134*, 4969–4977.

Keshari, K. R., Kurhanewicz, J., Jeffries, R. E., Wilson, D. M., Dewar, B. J., Van Criekinge, M., et al. (2010). Hyperpolarized ^{13}C spectroscopy and an NMR-compatible bioreactor system for the investigation of real-time cellular metabolism. *Magnetic Resonance in Medicine*, *63*, 322–329.

Keshari, K. R., & Wilson, D. M. (2014). Chemistry and biochemistry of ^{13}C hyperpolarized magnetic resonance using dynamic nuclear polarization. *Chemical Society Reviews*, *43*, 1627–1659.

Kettunen, M. I., Hu, D. E., Witney, T. H., McLaughlin, R., Gallagher, F. A., Bohndiek, S. E., et al. (2010). Magnetization transfer measurements of exchange between hyperpolarized [1-^{13}C]pyruvate and [1-^{13}C]lactate in a murine lymphoma. *Magnetic Resonance in Medicine*, *63*, 872–880.

Kovacs, H., Moskau, D., & Spraul, M. (2005). Cryogenically cooled probes—A leap in NMR technology. *Progress in Nuclear Magnetic Resonance Spectroscopy*, *46*, 131–155.

Kurdzesau, F., van den Brandt, B., Comment, A., Hautle, P., Jannin, S., van den Klink, J. J., et al. (2008). Dynamic nuclear polarization of small labelled molecules in frozen water–alcohol solutions. *Journal of Physics D: Applied Physics*, *41*, 155506.

Kurhanewicz, J., Vigneron, D. B., Brindle, K., Chekmenev, E. Y., Comment, A., Cunningham, C. H., et al. (2011). Analysis of cancer metabolism by imaging hyperpolarized nuclei: Prospects for translation to clinical research. *Neoplasia*, *13*, 81–97.

Lumata, L., Jindal, A. K., Merritt, M. E., Malloy, C. R., Sherry, A. D., & Kovacs, Z. (2011). DNP by thermal mixing under optimized conditions yields >60,000-fold enhancement of 89Y NMR signal. *Journal of the American Chemical Society*, *133*, 8673–8680.

Lumata, L., Kovacs, Z., Malloy, C., Sherry, A. D., & Merritt, M. (2011). The effect of ^{13}C enrichment in the glassing matrix on dynamic nuclear polarization of [1-^{13}C]pyruvate. *Physics in Medicine and Biology*, *56*, N85.

Lumata, L., Kovacs, Z., Sherry, A. D., Malloy, C., Hill, S., van Tol, J., et al. (2013). Electron spin resonance studies of trityl OX063 at a concentration optimal for DNP. *Physical Chemistry Chemical Physics, 15*, 9800–9807.

Lumata, L. L., Martin, R., Jindal, A. K., Kovacs, Z., Conradi, M. S., & Merritt, M. E. (2015). Development and performance of a 129-GHz dynamic nuclear polarizer in an ultra-wide bore superconducting magnet. *Magnetic Resonance Materials in Physics, Biology and Medicine, 28*, 195–205.

Lumata, L., Merritt, M. E., Hashami, Z., Ratnakar, S. J., & Kovacs, Z. (2012). Production and NMR characterization of hyperpolarized 107,109Ag complexes. *Angewandte Chemie, International Edition, 51*, 525–527.

Lumata, L., Merritt, M., Khemtong, C., Ratnakar, S. J., van Tol, J., Yu, L., et al. (2012). The efficiency of DPPH as a polarising agent for DNP-NMR spectroscopy. *RSC Advances, 2*, 12812–12817.

Lumata, L., Merritt, M. E., & Kovacs, Z. (2013). Influence of deuteration in the glassing matrix on ^{13}C dynamic nuclear polarization. *Physical Chemistry Chemical Physics, 15*, 7032–7035.

Lumata, L., Merritt, M., Malloy, C., Sherry, A. D., & Kovacs, Z. (2012a). Fast dissolution dynamic nuclear polarization NMR of ^{13}C-enriched 89Y-DOTA complex: Experimental and theoretical considerations. *Applied Magnetic Resonance, 43*, 69–79.

Lumata, L., Merritt, M. E., Malloy, C. R., Sherry, A. D., & Kovacs, Z. (2012b). Impact of Gd^{3+} on DNP of $[1-^{13}C]$pyruvate doped with trityl OX063, BDPA, or 4-oxo-TEMPO. *The Journal of Physical Chemistry A, 116*, 5129–5138.

Lumata, L. L., Merritt, M. E., Malloy, C. R., Sherry, A. D., van Tol, J., Song, L., et al. (2013). Dissolution DNP-NMR spectroscopy using galvinoxyl as a polarizing agent. *Journal of Magnetic Resonance, 227*, 14–19.

Lumata, L., Ratnakar, S. J., Jindal, A., Merritt, M., Comment, A., Malloy, C., et al. (2011). BDPA: An efficient polarizing agent for fast dissolution dynamic nuclear polarization NMR spectroscopy. *Chemistry: A European Journal, 17*, 10825–10827.

Maher, E. A., Marin-Valencia, I., Bachoo, R. M., Mashimo, T., Raisanen, J., Hatanpaa, K. J., et al. (2012). Metabolism of $[U-^{13}C]$glucose in human brain tumors in vivo. *NMR in Biomedicine, 25*, 1234–1244.

Marin-Valencia, I., Yang, C., Mashimo, T., Cho, S., Baek, H., Yang, X. L., et al. (2012). Analysis of tumor metabolism reveals mitochondrial glucose oxidation in genetically diverse human glioblastomas in the mouse brain in vivo. *Cell Metabolism, 15*, 827–837.

Meier, S., Karlsson, M., Jensen, P. R., Lerche, M. H., & Duus, J. Ø. (2011). Metabolic pathway visualization in living yeast by DNP-NMR. *Molecular BioSystems, 7*, 2834–2836.

Merritt, M. E., Harrison, C., Sherry, A. D., Malloy, C. R., & Burgess, S. C. (2011). Flux through hepatic pyruvate carboxylase and phosphoenolpyruvate carboxykinase detected by hyperpolarized ^{13}C magnetic resonance. *Proceedings of the National Academy of Sciences of the United States of America, 108*, 19084–19089.

Merritt, M. E., Harrison, C., Storey, C., Jeffrey, F. M., Sherry, A. D., & Malloy, C. R. (2007). Hyperpolarized ^{13}C allows a direct measure of flux through a single enzyme-catalyzed step by NMR. *Proceedings of the National Academy of Sciences of the United States of America, 104*, 19773–19777.

Metallo, C. M., & Vander Heiden, M. G. (2013). Understanding metabolic regulation and its influence on cell physiology. *Molecular Cell, 49*, 388–398.

Moreno, K. X., Satapati, S., DeBerardinis, R. J., Burgess, S. C., Malloy, C. R., & Merritt, M. E. (2014). Real-time detection of hepatic gluconeogenic and glycogenolytic states using hyperpolarized $[2-^{13}C]$dihydroxyacetone. *The Journal of Biological Chemistry, 289*, 35859–35867.

Nelson, S. J., Kurhanewicz, J., Vigneron, D. B., Larson, P. E., Harzstark, A. L., Ferrone, M., et al. (2013). Metabolic imaging of patients with prostate cancer using hyperpolarized $[1-^{13}C]$pyruvate. *Science Translational Medicine, 5*, 198ra108.

Oz, G., Alger, J. R., Barker, P. B., Bartha, R., Bizzi, A., Boesch, C., et al. (2014). Clinical proton MR spectroscopy in central nervous system disorders. *Radiology*, *270*, 658–679.

Plas, D. R., & Thompson, C. B. (2005). Akt-dependent transformation: There is more to growth than just surviving. *Oncogene*, *24*, 7435–7442.

Pope, W. B., Prins, R. M., Albert Thomas, M., Nagarajan, R., Yen, K. E., Bittinger, M. A., et al. (2012). Non-invasive detection of 2-hydroxyglutarate and other metabolites in IDH1 mutant glioma patients using magnetic resonance spectroscopy. *Journal of Neuro-Oncology*, *107*, 197–205.

Purmal, C., Kucejova, B., Sherry, A. D., Burgess, S. C., Malloy, C. R., & Merritt, M. E. (2014). Propionate stimulates pyruvate oxidation in the presence of acetate. *American Journal of Physiology Heart and Circulatory Physiology*, *307*, H1134–H1141.

Rodrigues, T. B., Serrao, E. M., Kennedy, B. W., Hu, D. E., Kettunen, M. I., & Brindle, K. M. (2014). Magnetic resonance imaging of tumor glycolysis using hyperpolarized ^{13}C-labeled glucose. *Nature Medicine*, *20*, 93–97.

Sunny, N. E., Parks, E. J., Browning, J. D., & Burgess, S. C. (2011). Excessive hepatic mitochondrial TCA cycle and gluconeogenesis in humans with nonalcoholic fatty liver disease. *Cell Metabolism*, *14*, 804–810.

Swisher, C. L., Larson, P. E., Kruttwig, K., Kerr, A. B., Hu, S., Bok, R. A., et al. (2014). Quantitative measurement of cancer metabolism using stimulated echo hyperpolarized carbon-13 MRS. *Magnetic Resonance in Medicine*, *71*, 1–11.

Warburg, O. (1956a). On respiratory impairment in cancer cells. *Science*, *124*, 269–270.

Warburg, O. (1956b). On the origin of cancer cells. *Science*, *123*, 309–314.

Ward, P. S., & Thompson, C. B. (2012). Metabolic reprogramming: A cancer hallmark even warburg did not anticipate. *Cancer Cell*, *21*, 297–308.

Xing, Y., Reed, G. D., Pauly, J. M., Kerr, A. B., & Larson, P. E. (2013). Optimal variable flip angle schemes for dynamic acquisition of exchanging hyperpolarized substrates. *Journal of Magnetic Resonance*, *234*, 75–81.

Xu, T., Mayer, D., Gu, M., Yen, Y. F., Josan, S., Tropp, J., et al. (2011). Quantification of in vivo metabolic kinetics of hyperpolarized pyruvate in rat kidneys using dynamic ^{13}C MRSI. *NMR in Biomedicine*, *24*, 997–1005.

Yang, C., Harrison, C., Jin, E. S., Chuang, D. T., Sherry, A. D., Malloy, C. R., et al. (2014). Simultaneous steady-state and dynamic ^{13}C NMR can differentiate alternative routes of pyruvate metabolism in living cancer cells. *The Journal of Biological Chemistry*, *289*, 6212–6224.

Yang, C., Ko, B., Hensley, C. T., Jiang, L., Wasti, A. T., Kim, J., et al. (2014). Glutamine oxidation maintains the TCA cycle and cell survival during impaired mitochondrial pyruvate transport. *Molecular Cell*, *56*, 414–424.

Ying, H., Kimmelman, A. C., Lyssiotis, C. A., Hua, S., Chu, G. C., Fletcher-Sananikone, E., et al. (2012). Oncogenic Kras maintains pancreatic tumors through regulation of anabolic glucose metabolism. *Cell*, *149*, 656–670.

Yuneva, M. O., Fan, T. W., Allen, T. D., Higashi, R. M., Ferraris, D. V., Tsukamoto, T., et al. (2012). The metabolic profile of tumors depends on both the responsible genetic lesion and tissue type. *Cell Metabolism*, *15*, 157–170.

Zierhut, M. L., Yen, Y. F., Chen, A. P., Bok, R., Albers, M. J., Zhang, V., et al. (2010). Kinetic modeling of hyperpolarized ^{13}C1-pyruvate metabolism in normal rats and TRAMP mice. *Journal of Magnetic Resonance*, *202*, 85–92.

Impact of Gd^{3+} doping and glassing solvent deuteration on ^{13}C DNP at 5 Tesla[1] ANDHIKA KISWANDHI, Univ of Texas, Dallas, BIMALA LAMA, AMRIS/NHMFL, Univ of Florida, PETER NIEDBALSKI, MUDREKH GODERYA, Univ of Texas, Dallas, JOANNA LONG, AMRIS/NHMFL, Univ of Florida, LLOYD LUMATA, Univ of Texas, Dallas — Dynamic nuclear polarization (DNP) is a technique which can be used to amplify signals in nuclear magnetic resonance (NMR) and magnetic resonance imaging (MRI) by several thousand-fold. The most commonly available DNP system typically operates at the W-band field or 3.35 T, at which it has been shown that ^{13}C NMR signal can be enhanced by deuteration and Gd^{3+} doping. In this work, we have investigated the applicability of these procedures at 5 T. Our results indicate that the deuteration of the glassing matrix still yields an enhancement of ^{13}C DNP when 4-oxo-TEMPO free radical is used. The effect is attributed to the lower heat load of the deuterons compared to protons. An addition of a trace amount of Gd^{3+} gives a modest enhancement of the signal when trityl OX063 is used, albeit with a less pronounced relative enhancement compared to the results obtained at 3.35 T. The results suggest that the enhancement obtained via Gd^{3+} doping may become saturated at higher field. These results will be discussed using a thermodynamic model of DNP.

Andhika Kiswandhi
Univ of Texas, Dallas

Date submitted: 05 Nov 2015   Electronic form version 1.4

Hyperpolarized 13C NMR lifetimes in the liquid-state: relating structures and T1 relaxation times[1] CHRISTOPHER PARISH, PETER NIEDBALSKI, University of Texas at Dallas, ZOHREH HASHAMI, LEILA FIDELINO, ZOLTAN KOVACS, Advanced Imaging Research Center, University of Texas Southwestern Medical Center, LLOYD LUMATA, University of Texas at Dallas — Among the various attempts to solve the insensitivity problem in nuclear magnetic resonance (NMR), the physics-based technique dissolution dynamic nuclear polarization (DNP) is probably the most successful method of hyperpolarization or amplifying NMR signals. Using this technique, liquid-state NMR signal enhancements of several thousand-fold are expected for low-gamma nuclei such as carbon-13. The lifetimes of these hyperpolarized 13C NMR signals are directly related to their 13C spin-lattice relaxation times T1. Depending upon the 13C isotopic location, the lifetimes of hyperpolarized 13C compounds can range from a few seconds to minutes. In this study, we have investigated the hyperpolarized 13C NMR lifetimes of several 13C compounds with various chemical structures from glucose, acetate, citric acid, naphthalene to tetramethylallene and their deuterated analogs at 9.4 T and 25 deg C. Our results show that the 13C T1s of these compounds can range from a few seconds to more than 60 s at this field. Correlations between the chemical structures and T1 relaxation times will be discussed and corresponding implications of these results on 13C DNP experiments will be revealed.

Christopher Parish
University of Texas at Dallas

Date submitted: 04 Nov 2015   Electronic form version 1.4

Construction and ^{13}C NMR signal-amplification efficiency of a dynamic nuclear polarizer at 6.4 T and 1.4 K[1] ANDHIKA KISWANDHI, PETER NIEDBALSKI, CHRISTOPHER PARISH, SARAH FERGUSON, DAVID TAYLOR, GEORGE MCDONALD, LLOYD LUMATA, Univ of Texas, Dallas —

Dissolution dynamic nuclear polarization (DNP) is a rapidly emerging technique in biomedical and metabolic imaging since it amplifies the liquid-state nuclear magnetic resonance (NMR) and imaging (MRI) signals by >10,000-fold. Originally used in nuclear scattering experiments, DNP works by creating a non-Boltzmann nuclear spin distribution by transferring the high electron ($\gamma = 28,000$ MHz/T) thermal polarization to the nuclear spins via microwave irradiation of the sample at high magnetic field and low temperature. A dissolution device is used to rapidly dissolve the frozen sample and consequently produces an injectable hyperpolarized liquid at physiologically-tolerable temperature. Here we report the construction and performance evaluation of a dissolution DNP hyperpolarizer at 6.4 T and 1.4 K using a continuous-flow cryostat. The solid and liquid-state ^{13}C NMR signal enhancement levels of ^{13}C acetate samples doped with trityl OX063 and 4-oxo-TEMPO free radicals will be discussed and compared with the results from the 3.35 T commercial hyperpolarizer.

Andhika Kiswandhi
Univ of Texas, Dallas

Date submitted: 04 Nov 2015

Electronic form version 1.4

Optimization of ^{13}C dynamic nuclear polarization: isotopic labeling of free radicals[1] PETER NIEDBALSKI, CHRISTOPHER PARISH, ANDHIKA KISWANDI, LLOYD LUMATA, University of Texas at Dallas — Dynamic nuclear polarization (DNP) is a physics technique that amplifies the nuclear magnetic resonance (NMR) signals by transferring the high polarization of the electrons to the nuclear spins. Thus, the choice of free radical is crucial in DNP as it can directly affect the NMR signal enhancement levels, typically on the order of several thousand-fold in the liquid-state. In this study, we have investigated the efficiency of four variants of the well-known 4-oxo-TEMPO radical (normal 4-oxo-TEMPO plus its ^{15}N-enriched and/or perdeuterated variants) for use in DNP of an important metabolic tracer [1-^{13}C]acetate. Though the variants have significant differences in electron paramagnetic resonance (EPR) spectra, we have found that changing the composition of the TEMPO radical through deuteration or ^{15}N doping yields no significant difference in ^{13}C DNP efficiency at 3.35 T and 1.2 K. On the other hand, deuteration of the solvent causes a significant increase of ^{13}C polarization that is consistent over all the 4-oxo-TEMPO variants. These findings are consistent with the thermal mixing model of DNP.

Peter Niedbalski
University of Texas at Dallas

Date submitted: 06 Nov 2015   Electronic form version 1.4

Production and NMR signal optimization of hyperpolarized 13C-labeled amino acids CHRISTOPHER PARISH, PETER NIEDBALSKI, SARAH FERGUSON, ANDHIKA KISWANDHI, LLOYD LUMATA, University of Texas at Dallas — Amino acids are targeted nutrients for consumption by cancers to sustain their rapid growth and proliferation. 13C-enriched amino acids are important metabolic tracers for cancer diagnostics using nuclear magnetic resonance (NMR) spectroscopy. Despite this diagnostic potential, 13C NMR of amino acids however is hampered by the inherently low NMR sensitivity of the 13C nuclei. In this work, we have employed a physics technique known as dynamic nuclear polarization (DNP) to enhance the NMR signals of 13C-enriched amino acids. DNP works by transferring the high polarization of electrons to the nuclear spins via microwave irradiation at low temperature and high magnetic field. Using a fast dissolution method in which the frozen polarized samples are dissolved rapidly with superheated water, injectable solutions of 13C-amino acids with highly enhanced NMR signals (by at least 5,000-fold) were produced at room temperature. Factors that affect the NMR signal enhancement levels such as the choice of free radical polarizing agents and sample preparation will be discussed along with the thermal mixing physics model of DNP. The authors would like to acknowledge the support by US Dept of Defense award no. W81XWH-14-1-0048 and Robert A. Welch Foundation grant no. AT-1877.

Christopher Parish
University of Texas at Dallas

Temperature dependence of proton NMR relaxation times at earth's magnetic field[1] PETER NIEDBALSKI, ANDHIKA KISWANDHI, CHRISTOPHER PARISH, SARAH FERGUSON, EDUARDO CERVANTES, ANISHA OOMEN, ANAGHA KRISHNAN, AAYUSH GOYAL, LLOYD LUMATA, University of Texas at Dallas — The theoretical description of relaxation processes for protons, well established and experimentally verified at conventional nuclear magnetic resonance (NMR) fields, has remained untested at low fields despite significant advances in low field NMR technology. In this study, proton spin-lattice relaxation (T_1) times in pure water and water doped with varying concentrations of the paramagnetic agent copper chloride have been measured from 6 to 92^oC at earth's magnetic field (1700 Hz). Results show a linear increase of T_1 with temperature for each of the samples studied. Increasing the concentration of the copper chloride greatly reduced T_1 and reduced dependence on temperature. The consistency of the results with theory is an important confirmation of past results, while the ability of an ultra-low field NMR system to do contrast-enhanced magnetic resonance imaging (MRI) is promising for future applicability to low-cost medical imaging and chemical identification.

Peter Niedbalski
University of Texas at Dallas

Electronic form version 1.4

Hyperpolarized ^{89}Y NMR spectroscopic detection of yttrium ion and DOTA macrocyclic ligand complexation: pH dependence and Y-DOTA intermediates[1] SARAH FERGUSON, ANDHIKA KISWANDHI, PETER NIEDBALSKI, CHRISTOPHER PARISH, University of Texas at Dallas, ZOLTAN KOVACS, University of Texas Southwestern Medical Center, LLOYD LUMATA, University of Texas at Dallas — Dissolution dynamic nuclear polarization (DNP) is a rapidly emerging physics technique used to enhance the signal strength in nuclear magnetic resonance (NMR) and imaging (MRI) experiments for nuclear spins such as yttrium-89 by >10,000-fold. One of the most common and stable MRI contrast agents used in the clinic is Gd-DOTA. In this work, we have investigated the binding of the yttrium and DOTA ligand as a model for complexation of Gd ion and DOTA ligand. The macrocyclic ligand DOTA is special because its complexation with lanthanide ions such as Gd^{3+} or Y^{3+} is highly pH dependent. Using this physics technology, we have tracked the complexation kinetics of hyperpolarized Y-triflate and DOTA ligand in real-time and detected the Y-DOTA intermediates. Different kinds of buffers were used (lactate, acetate, citrate, oxalate) and the pseudo-first order complexation kinetic calculations will be discussed.

Sarah Ferguson
University of Texas at Dallas

Date submitted: 04 Nov 2015   Electronic form version 1.4

Real-time tracking of dissociation of hyperpolarized ^{89}Y-DTPA: a model for degradation of open-chain Gd^{3+} MRI contrast agents[1]

SARAH FERGUSON, PETER NIEDBALSKI, CHRISTOPHER PARISH, ANDHIKA KISWANDHI, University of Texas at Dallas, ZOLTAN KOVACS, University of Texas Southwestern Medical Center, LLOYD LUMATA, University of Texas at Dallas
— Gadolinium (Gd) complexes are widely used relaxation-based clinical contrast agents in magnetic resonance imaging (MRI). Gd-based MRI contrast agents with open-chain ligand such as Gd-DTPA, commercially known as magnevist, are less stable compared to Gd complexes with macrocyclic ligands such as GdDOTA (Dotarem). The dissociation of Gd-DPTA into Gd ion and DTPA ligand under certain biological conditions such as high zinc levels can potentially cause kidney damage. Since Gd is paramagnetic, direct NMR detection of the Gd-DTPA dissociation is quite challenging due to ultra-short relaxation times. In this work, we have investigated Y-DTPA as a model for Gd-DPTA dissociation under high zinc content solutions. Using dissolution dynamic nuclear polarization (DNP), the ^{89}Y NMR signal is amplified by several thousand-fold. Due to the the relatively long T_1 relaxation time of ^{89}Y which translates to hyperpolarization lifetime of several minutes, the dissociation of Y-DTPA can be tracked in real-time by hyperpolarized ^{89}Y NMR spectroscopy. Dissociation kinetic rates and implications on the degradation of open-chain Gd^{3+} MRI contrast agents will be discussed.

Sarah Ferguson
University of Texas at Dallas

Date submitted: 05 Nov 2015   Electronic form version 1.4

Influence of Ho^{3+}-doping on ^{13}C dynamic nuclear polarization[1]

ANDHIKA KISWANDHI, PETER NIEDBALSKI, CHRISTOPHER PARISH, University of Texas at Dallas, PAVANJEET KAUR, National High Magnetic Field Laboratory, ANDRE MARTINS, University of Texas at Dallas, LEILA FIDELINO, CHALERMCHAI KHEMTONG, University of Texas Southwestern Medical Center, LIKAI SONG, National High Magnetic Field Laboratory, ALAN SHERRY, LLOYD LUMATA, University of Texas at Dallas
— We report the effects of the addition of trace Ho-DOTA on the ^{13}C dynamic nuclear polarization and the relaxation time of [1-^{13}C] acetate doped with trityl OX063 free radical. Our result shows that the polarization can be improved by a factor of 2.7 fold using Ho-DOTA doping, compared to the undoped samples, similar to the effect of Gd-HP-DO3A doping. In contrast to Gd-HP-DO3A doping, the ^{13}C relaxation rate is only minimally affected by Ho-DOTA. The W-band electron spin resonance studies revealed a considerable reduction of the electron spin-lattice relaxation time T_1 of trityl OX063 at low temperatures, which corresponds to the ^{13}C polarization enhancement, in agreement with the thermodynamic picture of DNP.

Andhika Kiswandhi
University of Texas at Dallas

Date submitted: 27 Sep 2016   Electronic form version 1.4

Hyperpolarized Magnetic Resonance: Enhancing MRI Signals by >10,000-fold for Non-Invasive Metabolic Assessment of Cancer[1]

LLOYD LUMATA, University of Texas at Dallas

In vivo or in vitro nuclear magnetic resonance (NMR) spectroscopy and imaging (MRI) of nuclei other than proton is hampered by inherently low signal sensitivity. This insensitivity problem emanates from the minute differences in spin populations between the nuclear Zeeman energy levels. Dynamic nuclear polarization (DNP) or hyperpolarization, an offshoot of a particle physics/nuclear scattering technology, has recently solved this insensitivity problem by amplifying the NMR signals of insensitive nuclei such as carbon-13 by 10,000-fold or higher. The trick is to transfer the high electron thermal polarization to the nuclear spins via microwave irradiation at low temperature (close to 1 K) and high magnetic field (>1 T), then rapidly dissolve the frozen polarized samples into hyperpolarized liquids at physiologically tolerable temperature. In this talk, I will present the physics, instrumentation and engineering aspects, optimization methods, and biomedical applications of the DNP technology. This cutting-edge physics technology is currently revolutionizing cancer diagnostics by providing biochemical and metabolic information at the molecular level with superb sensitivity and excellent specificity.

Hyperpolarization: Enhancing Magnetic Resonance Signals by >10,000-fold for Metabolic Assessment of Cancer

Lloyd L. Lumata

Department of Physics, University of Texas at Dallas, Richardson, TX 75080

Due to its specificity and use of non-destructive radiofrequency waves, *nuclear magnetic resonance* (NMR) is a widely-used analytical and structural elucidation technique in chemistry, biology and materials science. However, in spite of its numerous applications, *in vitro* or *in vivo* NMR spectroscopy (MRS) and imaging (MRI), especially of nuclei with low gyromagnetic ratio γ such as ^{13}C, suffer from inherently low signal sensitivity due to the relatively weak magnetic moments of the nuclear spins. The nuclear polarization P, a parameter related to the strength of the NMR or MRI signal, is only on the order of a few parts per million (ppm) at ambient conditions as dictated by Boltzmann statistics.[1]

Figure 1: A schematic and photo of the homebuilt dynamic nuclear polarizer built by the PI that can enhance the ^{13}C NMR and MRI signals by >10,000-fold.[2]

An elegant solution to this sensitivity problem is "hyperpolarization" via dissolution dynamic nuclear polarization (DNP). DNP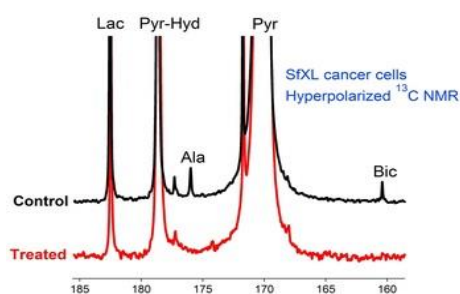 is a physics technique that creates a non-Boltzmann nuclear spin distribution by transferring the high electron thermal polarization to the nuclear spins via microwave irradiation at high magnetic field and low temperature. The frozen sample typically consists of stable-isotope enriched biomolecules dissolved in a glassing matrix and doped with trace amounts of free radicals. A dissolution device is used to rapidly dissolve the frozen sample inside the DNP machine (see Fig. 1) and consequently produces

Figure 2: *Left*: Photo a 10-mm NMR tube containing 100 million SfXL glioblastoma cancer cells in 1 mL cell suspension prior to NMR measurement. *Right*: real-time ^{13}C NMR metabolic assessment of SfXL cells after administration of hyperpolarized ^{13}C-pyruvate in living cancer cells.

an injectable "hyperpolarized" liquid at physiologically-tolerable temperature.[1] As depicted in Fig. 2, *this means that the NMR and MRI signals of reporter molecules (MRS/MRI molecular probes that can detect pH, metabolism, and other important biological activities) are enhanced by at least 10,000-fold*.[3]

In this talk, *I will delve into the discussion of the physics, instrumentation and engineering aspects, optimization methods, and biomedical applications of the DNP technology*. This cutting-edge physics technology is currently revolutionizing cancer diagnostics by providing biochemical and metabolic information at the molecular level with superb sensitivity and excellent specificity. *This research is supported in part by the U.S. Department of Defense grant no. W81XWH-14-1-0048 and the Welch Foundation grant no. AT-1877.*

References:
1. J. H. Ardenkjaer-Larsen et al., Increase in signal-to-noise ratio of >10,000 times in liquid-state NMR, *Proc. Natl. Acad. Sci. U.S.A.* **100**, 10158-10163 (2003).
2. L. Lumata, et al., Development and performance of a 129 GHz dynamic nuclear polarizer in an ultra-wide bore superconducting magnet, *Magnetic Resonance Materials in Physics, Biology and Medicine* **98**, 195-205 (2015).
3. L. Lumata et al., Hyperpolarized ^{13}C magnetic resonance and its use in metabolic assessment of cultured cells and perfus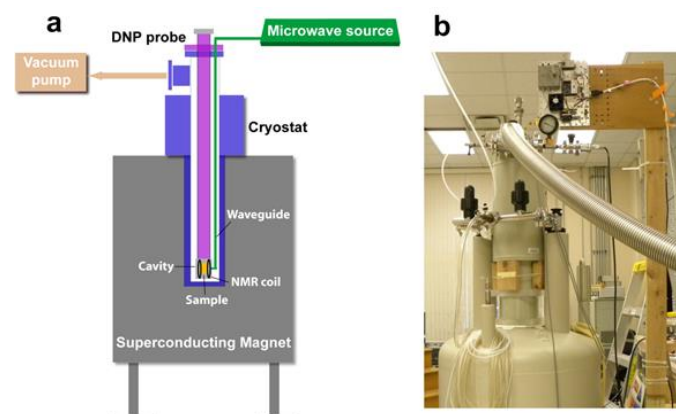ed tissues, *Methods in Enzymology* **561**, 73-106 (2015).